Final Report

DETERMINATION OF AXIAL PILE CAPACITY OF PRESTRESSED CONCRETE CYLINDER PILES

UF Project No.: 4910450487712

Contract No.: BC 354 RPWO-60

By:

M. C. McVay, D. Badri and Z. Hu
University of Florida
Civil and Coastal Engineering Dept.

Submitted to:

Mr. Richard Long
Research Center
Florida Department of Transportation
605 Suwannee Street, MS 30
Tallahassee, FL 32399-0450
(904) 488-8572

and

Mr. Peter Lai, PE
Florida Department of Transportation
605 Suwannee Street, MS 5L
Tallahassee, FL 32399
(904) 488-8911

UNIVERSITY OF FLORIDA

Department of Civil and Coastal Engineering, College of Engineering
365 Weil Hall, P.O. Box 116580, Gainesville, FL 32611-6580
Tel: (352) 392-8697 SunCom: 622-8697 Fax: (352) 392-3394

April 2004

Technical Report Documentation Page

1. Report No.	2. Government Accession No.	3. Recipient's Catalog No.

4. Title and Subtitle	5. Report Date
Determination of Axial Pile Capacity of Prestressed Concrete Cylinder Piles	April 2004
	6. Performing Organization Code
7. Author(s) M. C. McVay, D. Badri, Z. Hu	8. Performing Organization Report No. 4910-4504-877-12
9. Performing Organization Name and Address University of Florida Department of Civil and Coastal Engineering 365 Weil Hall / P.O. Box 116580 Gainesville, FL 32611-6580	10. Work Unit No. (TRAIS) 11. Contract or Grant No. BC 354 RPWO-60
12. Sponsoring Agency Name and Address Florida Department of Transportation Research Management Center 605 Suwannee Street, MS 30 Tallahassee, FL 32301-8064	13. Type of Report and Period Covered Final Report November 2001 – February 2004 14. Sponsoring Agency Code

15. Supplementary Notes

Prepared in cooperation with the Federal Highway Administration

16. Abstract

This study focused on determining unit skin and tip resistance of large diameter open-ended steel and concrete cylinder piles in different soil types using insitu SPT data. A total of 35 piles with pile diameters ranging from 36” to 84” (most common 54”) were collected from Florida, California, Virginia, Maryland, etc. Each had a static load test, with a few (9) instrumented with strain gauges along their length. Twenty-one of the static load tests reached Davisson’s capacity used to assess failure.

Using the database of piles, which reached failure, equations of unit skin friction and end bearing vs. SPT N values were developed. For those piles that didn’t have strain gauges to differentiate skin from tip resistance, DeBeer’s method of plotting load vs. displacement on log-log plot was used to differentiate skin from tip resistance. In determining end bearing, the use of pile cylinder area or total cross-sectional area was studied. It was found from dynamic analysis of large open-ended piles that the unit skin friction inside the pile did not generally overcome the inertia force acting on the soil plug (i.e., pile was unplugged during driving). However, FEM studies on static or slow rates of loading (i.e., no inertia forces) suggested that many cylinder piles acted plugged during static loading. LRFD resistance factor, ϕ, analysis suggested that the pile’s total end area gave better prediction than the pile’s cylinder area (% of Davisson capacity available for design, ϕ/λ_R =0.65 vs. 0.60). A range of LRFD resistance factors versus reliability values were determined for design.

17. Key Words	18. Distribution Statement
Cylinder Piles, Axial Capacity, Insitu SPT, LRFD Resistance Factors	No restrictions. This document is available to the public through the National Technical Information Service, Springfield, VA, 22161

19. Security Classif. (of this report)	20. Security Classif. (of this page)	21. No. of Pages	22. Price
Unclassified	Unclassified	125	

Form DOT F 1700.7 (8-72)

TABLE OF CONTENTS

LIST OF TABLES

TABLE Page

LIST OF FIGURES

CHAPTER 1

INTRODUCTION

1.1 BACKGROUND

There are numerous advantages of using a large diameter cylinder piles compared to smaller solid piles, or drilled shafts. For instance, the moment of inertia of a round pipe increases by D^4 and is capable of resisting large lateral loads (i.e., ship impacts), i.e., moment capacities, versus smaller piles/shafts. In the case of large diameter piles vs. drilled shafts, cylinder piles provide larger skin and tip resistance in sands, and clays, as compared to drilled shafts, as a result of installation technique. In addition, cylinder piles do not require the use of a steel casing when the ground surface (i.e., mud line) is located below mean sea level. Moreover, quality control issues are not as significant with cylinder piles as compared to drilled shafts. Unfortunately, the axial capacities of cylinder piles are not as well understood as drilled shafts. The latter is the focus of this study.

1.2 RESEARCH SCOPE

The scope of the research was to develop unit skin friction and end bearing resistance vs. Standard Penetration Test (SPT) "N" curves for large diameter (>36") prestressed concrete and steel cylinder piles in various soil types (sands, silts and clays). As with smaller diameter piles, separation of steel from prestressed concrete skin friction and end bearing was considered. To assist with design, Load and Resistance Factor Design (LRFD) resistance factors, ϕ, were also established for the proposed methods.

1.3 PROJECT TASKS

To accomplish the research, the following tasks were identified and completed:

1. A database of static load tests on cylinder piles along with soil stratigraphy and insitu SPT data was collected. A total of thirty-six load test data on large diameter cylinder piles was collected. A list of organizations/agencies contacted, and data obtained are provided in the forthcoming chapters.

2. The data in the database was classified on the soil type, pile material, outer diameter of the pile, shell thickness of the pile, and the state of plug within the pile (i.e., plugged/unplugged). An online database was then built to store and share data with other researchers. The knowledge of Microsoft Access, ASP (i.e., Active Server Protocol), SQL (i.e., Structured Query Language) and JavaScript was used in the design of this database.

3. Each cylinder pile's static load test results were separated into unit skin friction, and unit tip resistance. The latter was accomplished from either strain gages data, or a combination of Davisson's and DeBeer's method. These results were then correlated against uncorrected SPT blow counts (N), for different soil types and pile material. The results were compared with unit skin friction and end bearing values in SPT97 for small diameter piles.

4. Impacting the unit bearing calculation (i.e., use of total base area or ring area) was the identification of the cylinder pile's end condition, i.e., was it "unplugged" or "plugged?" To accomplish the latter, 1) a finite element (ADINA) fluid study of soil flowing into and around an open pile was undertaken; as well as 2) a dynamic finite difference study of forces (inertia, and skin friction) on the soil plug was performed. The dynamic study revealed for typical Florida soils, large diameter cylinder piles (i.e., 54" or larger) would remain unplugged due to the large inertia forces on the plug. However, in the case of static loading, the inertia forces are zero, and the soil within the pile could plug (i.e., ADINA FEM study). Consequently, the study considered both scenarios.

5. Using the unit skin and end bearing curves vs. SPT N values, the 36-load test piles were predicted and compared to FDOT failure criterion. The bias (i.e., measured over predicted ratio), COV (i.e., coefficient of standard deviation) and LRFD resistance factors, ϕ were determined vs. different reliability values.

CHAPTER 2

DATA COLLECTION

In order to collect static load test data on large diameter cylinder piles over eighty Geotechnical consulting companies, federal and state department transportation (DOTs) agencies were contacted throughout the US and around the world. In the case of DOTs, FDOT (i.e., Florida Department of Transportation), CALTRANS (i.e., California Department of Transportation), VDOT (i.e., Virginia Department of Transportation), NCDOT (i.e., North Carolina Department of Transportation) and MSHA (i.e., Maryland State Highway Administration) were each contacted. Each contributed one or more sites with single or multiple static load test information on cylinder pile tests. All had conducted the axial load test in general conformance with ASTM D 1143-81 (1994). A total of 35 load tests were collected from either the DOTs or their consultants. A discussion of the data follows.

2.1 COLLECTED CYLINDER PILE INFORMATION

To obtain the unit skin friction and end bearing curves vs. SPT "N" values, the following information was needed:

1. Static load test to failure with cast insitu instrumentation (strain gauges) to assist with the differentiate of skin and tip resistance;
2. Description of soil stratigraphy, and insitu SPT N values in load test vicinity;
3. Physical description of the pile: outer diameter, shell thickness, pile length, and Young's Modulus of pile material;
4. Information on soil within the pipe, i.e., "plugged," or "unplugged."

A description of each follows.

2.1.1 Classification Based on Soil Type

For later integration into FDOT's pile capacity program, SPT97, the soil was classified into four general types: plastic clay, clay-silt-sand mixtures, clean sands, and soft limestone or very shelly sands. Generally, the soil stratigraphy for each of the cylinder piles consisted of more than one layer. Table 2-1 gives a breakdown by soil type in which the piles were placed.

Table 2-1 Soil Type and Description

Soil Type	Description	Number of Piles
1	Plastic Clay	13
2	Clay-silt-sand mixtures, very silty sand, silts and marls	11
3	Clean Sands	18
4	Soft Limestone, very shelly sands	2

2.1.2 Classification Based on Pile Material

Based on pile material type, the piles were classified into either concrete or steel piles. Table 2-2, lists the number of piles of each type, in the database. All of the piles were open ended.

Table 2-2 Pile Type Classification

Material Type	Description	Number
1	Concrete	26
2	Steel	9

2.1.3 Classification Based on Pile Outer Diameter and Shell Thickness

Piles were also analyzed (i.e., skin friction, etc.) as a function of diameter (outer), as well as shell thickness. Shell thickness and outer diameter were also used in pile plugging analysis. Table 2-3, lists the number of piles with various diameters, and shell thickness.

Table 2-3 Classification Based on Pile Outer Diameter and Shell Thickness

Outer Diameter	Number	Shell Thickness	Number
84-inch	1	8-inch	4
72-inch	2	6.9-inch	2
66-inch	3	6-inch	7
54-inch	19	5-inch	9
42-inch	10	2-inch to 1-inch	5
36-inch	1	>1-inch	8

2.1.4 Classification Based on Plug Status

Of interest is the status of the soil within the cylinder of the pile during driving. If it were "plugged," i.e., moves downward with the pile during driving, then it would also remain "plugged" during the static load test. For such piles, i.e., "plugged," the end bearing would be computed from the unit end bearing times the total cross-sectional areas. In the case of "unplugged" piles during driving, the pile may act "plugged" during static load test, since the inertia forces prevalent during driving are no longer present. A discussion of the latter is given in Chapter five.

For this study, a plugged pile was defined as one in which, the soil within the pile had no relative movement with respect to the pile during driving. Table 2-4, lists the number of plugged piles, and unplugged piles in the database.

Table 2-4 Plugged and Unplugged Piles in the Database

Plug Status	Number
Plugged	10
Unplugged	25

2.2 CURRENT UF/FDOT CYLINDER PILE DATABASE PROJECTS, AND BRIEF DESCRIPTION

Table 2-5 lists the thirty-five piles, from eleven different projects, in the current UF/FDOT database, along with a brief description of diameter, shell thickness, pile material, major soil type, and the number of static load test data available for each project.

Table 2-5 Current Pile Database

	Project Name	Pile Description			Major Soil Type	Number of Tests
		Outer Diameter	Shell Thickness	Pile Material		
1	St. Georges Island Bridge Replacement Project, FL	54-inch	8-inch	Post Tensioned Concrete	Silty Sands over Limestone	4
2	Chesapeake Bay Bridge and Tunnel Project, VA	54-inch, 66-inch	6-inch	Prestressed Concrete	Dense sands	6
3	San-Mateo Hayward Bridge, CA	42-inch	6.9-inch	Concrete	Silty Clays	2
4	Oregon Inlet, NC	66-inch	6-inch	Concrete	Silty Fine Sands	1
5	Woodrow-Wilson Bridge, MD	54-inch, 42-inch and 36-inch	1-inch	Steel	Silty Sands	3
6	North and South Trestle, I-664 Bridge, VA	54-inch	5-inch	Concrete	Silts and Sands	9
7	Salinas River Bridge, CA	72-inch	.75-inch	Steel	Mixed	1
8	Port of Oakland, CA	42-inch	.625-inch, .75-inch	Steel	Clays	4
9	I-880 Oakland, CA	42-inch	.75-inch	Steel	Clays	2
10	Santa Clara River Bridge, CA	84-inch, 72-inch	1.5-inch, 1.74-inch	Steel	Sands	2
11	Berenda Slough Br, CA	42-inch	.625-inch	Steel	Sands	1
					Total	35

The predominate soil type at the side and tip of each pile are given Table 2-6 based on the SPT boring data. The latter will be used in differentiating unit skin and end bearing resistance as a function of SPT N values. A brief description of each project follows.

Table 2-6 Soil Type Classification for Side and Tip for Various Projects

No.	Project Name	Soil Type For		Insitu Test
		Skin Friction	End Bearing	
1	St. Georges Island Project	Sand	Limestone	SPT/CPT
2	St. Georges Island Project	Sand	Limestone	SPT/CPT
3	St. Georges Island Project	Sand	Limestone	SPT/CPT
4	St. Georges Island Project	Sand	Limestone	SPT/CPT
5	Chesapeake Bay Bridge	Silt	Silt	CPT/SPT
6	Chesapeake Bay Bridge	Silt	Silt	CPT/SPT
7	Chesapeake Bay Bridge	Silt	Silt	CPT/SPT
8	Chesapeake Bay Bridge	Sand	Sand	CPT/SPT
9	Chesapeake Bay Bridge	Sand	Sand	CPT/SPT
10	Chesapeake Bay Bridge	Sand	Sand	SPT
11	San Mateo Hayward Bridge	Silt	Silt	SPT
12	San Mateo Hayward Bridge	Silt	Silt	SPT
13	Oregon Inlet	Silt	Silt	CPT/SPT
14	I-664 Bridge North	Clay	Clay	SPT
15	South Test-4	Sands	Sands	SPT
16	South Test-5	Sands	Sands	SPT
17	South Test-6	Sands	Sands	SPT
18	South Test-10	Sands	Sands	SPT
19	South Test-11	Sands	Sands	SPT
20	South Test-12	Sands	Sands	SPT
21	South Test-13	Sands	Sands	SPT
22	South Test-14	Sands	Sands	SPT
23	Woodrow Wilson Bridge	Sands	Clays	SPT
24	Woodrow Wilson Bridge	Sands	Clays	SPT
25	Woodrow Wilson Bridge	Sands	Clays	SPT
26	Salinas River Bridge	Clays	Clays	SPT
27	Port Of Oakland 27NC	Clay	Clays	SPT
28	Port Of Oakland 17NC1	Clay	Clays	SPT
29	Port Of Oakland 10NC1	Clay	Clays	SPT
30	Port Of Oakland 31NC	Clay	Clays	SPT
31	I-880 Oakland Site 3C	Clay	Clays	SPT
32	I-880 Oakland Site 3H	Clay	Clay	SPT
33	Santa Clara River Bridge 13	Sand	Sands	SPT
34	Santa Clara River Bridge 7	Sand	Sands	SPT
35	Berenda Slough Br 4	Silts	Silts	SPT

2.2.1 St. Georges Island Bridge Replacement Project

The St Georges Bridge was built for the F.D.O.T (i.e., Florida Department of Transportation) by the team of Boh Brothers Construction, and Jacob Civil, Inc.; in Apalachicola Bay over intercoastal waters. Applied Foundation Testing, Inc. performed the load test. The piles tested were spun-cast post tensioned concrete cylinder piles with an outer diameter of 54-inches, shell thickness of 8-inches and lengths of 80-ft.

The prevailing soil type at the location was very loose silty sand, above a layer of dense to very dense silty sand, underlain by a layer of limestone. The piles were driven to refusal in the limestone layer. Additional details on the soils, pile, and installation were available from the Geotechnical records of Williams Earth Sciences, Inc. (WES). Insitu data from both CPT (i.e., Cone Penetration Test) and SPT (i.e., Standard Penetration Test) were available for this project.

Data for four compression load test were reported for this project. Reaction load was applied through frame-supported barges filled with water. Four pipe piles supported the barges. Jack pumping rate controlled the rate of loading. All the test piles were instrumented with embedded strain gages along their length and with a toe accelerometer. None of the piles at the project formed a soil plug during driving.

2.2.2 Chesapeake Bay Bridge and Tunnel Project

The load-testing program was performed in regards to the construction of an additional bridge adjacent to the existing Chesapeake Bay Bridge. The CBBTD (i.e., Chesapeake Bay Bridge and Tunnel District) contracted with Tidewater Construction Corporation (TCC), to perform the construction, installation, and load testing of the piles. Bayshore Concrete Products, Inc., a subcontractor to TCC, fabricated the piles.

Load test information for six prestressed concrete cylinder piles was available for this project. Fifty-four inch diameter piles were used at TP-1, TP-2, TP-3, and TP-6, whereas 66-inch diameter piles were used at TP-4 and TP-5. All of the piles had 6-inch wall thickness. The lengths of the piles varied from 128-ft at site TP-6 to 204-ft at site TP-5.

The prevailing soil at location TP-1, TP-2 and TP-6 was silt and clay with small amounts of sand; at locations TP-3, TP-4 and TP-5, the prevailing soil was dense gray sand with small amounts of silt and clay. Insitu data from both SPT and CPT were available for this project.

Piles TP-1, TP-4, TP-5 and TP-6 formed soil plugs, the upper surface of the plugs formed in these piles were at depths of 13-ft, 1-ft, 8-ft, and 6-ft below mudline. Piles TP-2 and TP-3 did not form any soil plug.

2.2.3 San-Mateo Hayward Bridge

The San Mateo Bridge, also called the San Mateo-Hayward Bridge, runs roughly east west and crosses the lower part of San Francisco Bay. California State Highway 92 passes over the bridge and joins Haywood, I-580 and I-880 on the east side of the bay with Foster City, San Mateo and US101 on the west side. The scope of the project involved building a new 60-foot trestle on the north side of the already existing trestle.

CALTRANS performed load test on two large diameter prestressed concrete cylinder piles. The piles had an outer diameter of 42-inch, and a shell thickness of 6.9-inch. The length of the pile was 42.25-meters at site A, and 40.8-meters at site B.

SPT data are available for this project. The closest boring to Site A, indicates layers of very soft silty clay down to an elevation of –55-ft, followed by interbedded layers of compact silty clay, and compact sand down to the tip elevation of the pile. The closest boring in the vicinity of Site B indicates very soft silty clay down to an elevation of –20 ft, followed by interbedded layers of stiff silty clay, and compact sand down to the tip elevation of the pile.

2.2.4 Bridge over Oregon Inlet and Approaches on NC-12

The bridge over Oregon Inlet and approaches on NC-12 is located on the south side of Oregon Inlet's Bonner Bridge in Dare County, North Carolina.

The NCDOT (i.e., North Carolina Department of Transportation) contracted with Hardway Company, and S&ME Environmental Services for both Pile and Test Boring work.

The test consisted of Static Axial Compressive load test on a 66-inch diameter concrete cylinder pile with a 6-inch wall thickness, and a length of 131.5-feet.

Insitu data from both SPT, and CPT were available for this project. The soil profile consists of clayey silt to a depth of –12 meters, followed by layers of sand and sandy silt until the tip elevation is reached. No soil plug formed during driving of the pile.

2.2.5 Woodrow Wilson Bridge

The Woodrow Wilson Bridge is located about 6 miles south of Washington DC Metropolitan area; it is approximately at the mid point of I-95, which is one of the busiest east coast interstate highways.

The load testing for the project was planned and implemented by Potomac Crossing Consultants (PCC), a joint venture of URS Corporation, Parsons-Brinkerhoff, and Rummel-Klepper-Kahl, acting as the General Engineering Consultants (GEC). All work was authorized by the Maryland State Highway Administration (MSHA) in conjunction with the Federal Highway Administration (FHWA) and was performed in association with Section Design Consultant (SDC), Parson Transportation Group (PTG) and Mueser Rutledge Consulting Engineers (MRCE).

Three axial static load tests are available from this project and are identified as PL-1, PL-2 and PL-3. PL-1. Test PL-1 occurred near the eastern bascule pier in the main navigation channel of the Potomac River. Test PL-2 was located to the west of the secondary channel near the eastern abutment, and test PL-3 was located on land in Jones Point Park, Virginia.

All of the load tests occur in the Atlantic Coastal Plains soils, which consist of a wide belt of sedimentary deposits overlying the crystalline bedrock of the Piedmont, which outcrops to the northwest. These materials, known collectively as the Potomac Group, consist of dense sands and gravels with variable fractions of fines, and very stiff to hard, highly over-consolidated clays. Although these clays are very stiff, the presence of slickensides often reduces the overall shear strength of the soil mass. The clays vary in mineral composition, and as a consequence have variable potential for expansion. SPT Insitu data was available for this project.

The Potomac River is a tidal river with a mean water elevation of +1 feet above sea level, but fluctuates between Mean Low Water of elevation –1-feet and Mean High Water of elevation +3-feet.

The three steel piles at PL-1, PL-2, and PL-3 had outer diameters of 54-inch, 42-inch, and 36-inch and, lengths of 164-ft, 125-ft, and 96-ft, respectively. All piles had a shell thickness of 1-inch. None of the piles formed a soil plug.

2.2.6 Monitor-Merrimac Memorial Bridge-Tunnel (I-664 Bridge)

The Monitor-Merrimac Memorial Bridge-Tunnel connects I-664 in Hampton to I-664/I-264 in Chesapeake. The VDOT (i.e., Virginia Department of Transportation) contracted with STS Consultants Ltd of Virginia to conduct the load test program.

Static axial load test were performed on 54-inch diameter prestressed concrete cylinder piles with a 5-inch wall thickness and pile lengths varying from 47.9-ft at Test-4 to 145.1-ft at Test-10. A total of nine load test data was available from the project, one on the north side and eight from the south side of the bridge.

The general soil profile at the site indicates interbedded layers of soft black silt, very soft gray silty clay, green-gray sandy silts, and sandy clays. These soils comprise the Yorktown formation, which exhibits a significant amount of soil freeze or setup. Insitu data from SPT are available for this project. None of the piles formed a soil plug during driving.

2.2.7 Salinas River Bridge

The Salinas River Bridge is located on SR101, over the Salinas River near Soledad, California. Data on one 72-inch diameter, 3/4-inch thick steel pipe pile is available for this project. The pile was installed specifically for testing (and not to be incorporated into the bridge structure) by the personnel from the Office of Structural Foundation, Geotechnical Support Branch of Caltrans.

Boring B-13 is the closest boring to the test pile, located about 90 feet away. Boring B-13 shows layers of loose to compact sand from the ground surface elevation of 7-ft to –32-ft. The sand layers are underlain by a layer of soft clay to an elevation –52-ft, and layers of loose silt to an elevation –70 ft. Below these layers to an elevation of –103 ft are layers of soft to stiff clay. From elevation –103 ft to –121 ft is a layer of dense sand. Insitu data from SPT are available for this project.

The pile did not form an internal soil plug during installation. Measurements taken upon completion of driving showed the top of soil plug to be 13 feet below ground surface elevation. The difference in elevation between the top of soil plug and original ground elevation is likely a result of vibration-induced settlement of the soil inside the pile, or as a result of the soft clay being displaced by the denser material inside the pile.

2.2.8 Port of Oakland

Four static axial load tests on 42-inch diameter, cast-in-steel shell concrete piles were conducted at the Port of Oakland Connector Viaduct and Maritime On and Off Ramps. Members of the Geotechnical Support Branch of Caltrans conducted these tests.

Subsurface conditions at the three sites can be estimated based upon fieldwork completed by Caltrans. Soil encountered at all of the test locations consisted of three distinct materials: fill, Young Bay Mud deposit, and Old Bay Mud deposits. Throughout the jobsite the elevations separating these four materials varied considerably.

2.2.9 I-880 Oakland Site

The load test site is located at the west end of the West Grand Avenue aerial structure, approximately 1100 feet east of the San Francisco Oakland Bay Bridge Toll Plaza and north of the existing west bound lanes of I-80, along the margin of the San Francisco Bay. Caltrans carried out the test in an effort to better understand issues associated with the use of large diameter steel piles. The study consisted of installing two 42-inch diameter, 3/4-inch thick steel cylinder piles.

Soils at these various test sites consists of Artificial Fill; Young Bay Mud - an unconsolidated Holocene estuarine deposit; Merritt Sands – a Pleistocene non-marine deposit (member of the San Antonio formation); and Old Bay Mud – an older Pleistocene marine deposit also referred to as Yerba Buena Mud. Depth to bedrock is estimated to vary from –500 ft to –550 ft.

The piles at Site 3 were 120 ft in length. Due to transportation and handling constraints, driving occurred in two phases. The first portion of pile installation consisted of installing a nominal 80 ft long pile spliced together from two 40 ft section in a nearby fabrication yard. The remaining 40 ft section of the pile was suspended vertically, then welded to the portion of the pile previously installed. Piles were then driven to the specified tip elevation.

At the completion of installation, the plug was measured at 3.25 ft below the original ground for Pile 3C and 10 ft below the ground surface for Pile 3H.

2.2.10 Santa Clara River Bridge

The load test program was a part of the Santa Clara River Bridge replacement, on the I-5 and I-5/SR-126 road separation (Magic Mountain Parkway) in Los Angeles County at Santa Clarita. The project included the installation of two large diameter cast-in-steel-shell (CISS) piles at location Pier 13 and Pier 7. The piles at Pier 13 and Pier 7 were 72-inch diameter, 1.5-inch thick and 84-inch diameter and 1.74-inch thick respectively. Personnel from the Foundation Testing Branch (FTB), of the Office of Geotechnical Support (Caltrans) conducted two compressive static axial load tests each at Pier 13 and Pier 7.

The subsurface location at pier 13 as inferred from Boring B1-99 indicates the presence of alternating layers of very stiff clay and dense sand with silt and gravels. At deeper depths, the boring encountered very dense layers of sands and gravels. The subsurface location at Pier 7 location as inferred from Boring 00-3 indicates the presence of alternating layers of medium to very dense silts and sands with very stiff clays. At deeper depth, the boring encountered very dense layers of sands and gravels over cemented silty sands. Insitu data from SPT are available for this project.

2.2.11 Berenda Slough Bridge

The Berenda Slough Bridge is located on Route 220 in Madera County near Chowchilla. The project included the installation of 42-inch diameter, 5/8-inch thick cast-in-steel-shell pile, by the personnel from the Foundation Testing and Instrumentation Branch of the Division of Structural Foundations.

Boring 98-5 indicates layers of sand, silty sand, and silt present at the test pile site. Insitu SPT data was available for this project.

CHAPTER 3

UF/FDOT CYLINDER PILE DATABASE ON INTERNET

The online UF/FDOT large diameter cylinder pile database was developed, as a joint effort with researchers around the world to study large diameter driven piles. The main purpose of the database was to share the existing load test data, and get more data. The database was built on a Microsoft Access, html (i.e., HyperText Markup Language), ASP (i.e., Active Server Pages) and JavaScript platform. A description of the Online database follows.

3.1 MAIN PAGE

The MAIN page (Fig. 3-1), grants the user permission to enter the database. Based on the type of username and password, the user is identified as an administrator, or a regular user, and given permission to access the various pages within the database.

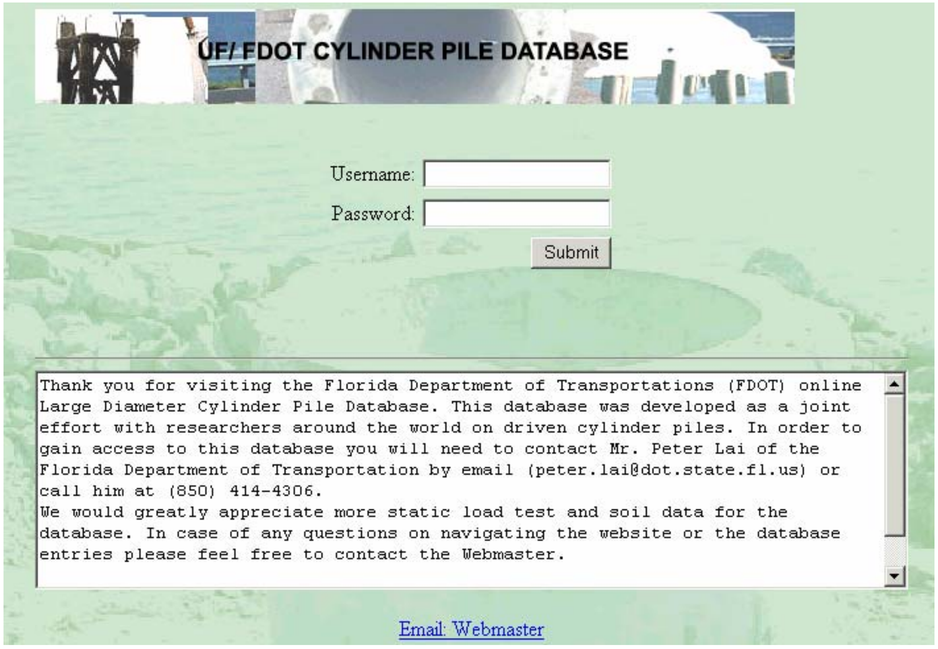

Figure 3-1 Shows the MAIN page with the username and password fields, and a note to new users.

3.1.1 Administrator User

All users are given access from the MAIN page, to the MENU page. Once on the MENU page, administrator users are given access to both data entry, and viewing of existing data, Figure 3-2.

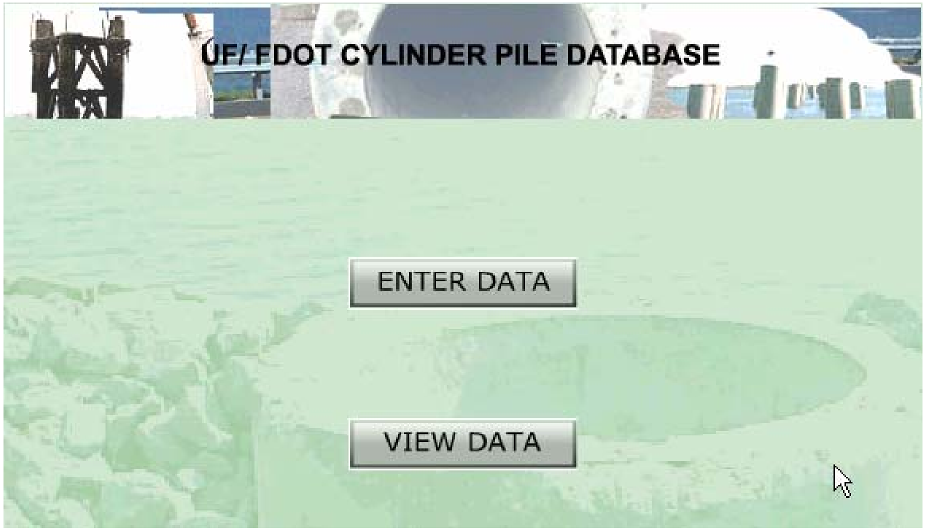

Figure 3-2 Shows the MENU page, with the enter data and view data fields.

3.1.2 Regular User

A regular user has rights only to view the data (i.e., VIEW DATA page), and would be prompted to enter the administrative username and password to enter the ENTER DATA page.

Once the user enters the VIEW DATA page, he/she is taken to the PROJECTS page. The PROJECTS page, lists all the projects in the database, the user can view the details of the listed project from there on.

The various pages within the ENTER DATA and VIEW DATA are discussed simultaneously, as they have the same formats.

3.2 PROJECT PAGE

The PROJECT page, Figure 3-3, lists the names of all the projects in the database, in three columns. The data for each project is presented in six sections (pages). An option of

Berenda Slough Br Pier 4	Bridge Over Oregon Inlet on NC 12	Chesapeake Bay Bridge LT-1
Chesapeake Bay Bridge LT-2	Chesapeake Bay Bridge LT-3	Chesapeake Bay Bridge LT-4
Chesapeake Bay Bridge LT-5	Chesapeake Bay Bridge LT-6	I-664 Bridge, Test-10, VA
I-664 Bridge, Test-11, VA	I-664 Bridge, Test-12, VA	I-664 Bridge, Test-13, VA
I-664 Bridge, Test-14, VA	I-664 Bridge, Test-4, VA	I-664 Bridge, Test-5, VA
I-664 Bridge, Test-6, VA	I-880 Oakland Site 3C	I-880 Oakland Site 3H
Port of Oakland 10NC1	Port of Oakland 17NC1	Port of Oakland 27NC
Port of Oakland 31NC	Salinas River Bridge	Santa Clara River Bridge Pier 13
Santa Clara River Bridge Pier 7	St.Georges Island Bridge Replacement LT-1	St.Georges Island Bridge Replacement LT-2
St.Georges Island Bridge Replacement LT-3	St.Georges Island Bridge Replacement LT-4	Trestle Bent 9, I-664, VA
Woodrow Wilson Bridge PL-1 Pile-C	Woodrow Wilson Bridge PL-2 Pile-F	Woodrow Wilson Bridge PL-3 Pile-I

Figure 3-3 PROJECT page showing a list of projects available on the UF/FDOT online database.

navigating back to the list of projects (PROJECT page) is available from each of these pages. The six pages describing each project are as follows:

1. General page.
2. Load test page.
3. Insitu test and soil page.
4. Soil plug page.
5. Driving page.
6. Analysis and results page.

A brief description of each page follows.

3.2.1 General Page

The GENERAL page, Figure 3-4, summarizes the entire project information, and can be classified into:

1. Project Overview.
2. Pile Description.
3. Insitu Test and Analysis.

3.2.1.1 Project Overview

Information falling under this category includes project name, project number, submitting company, submitting engineer, and comments. The latter gives a general overview of the project.

3.2.1.2 Pile Description

Information describing the describing the pile's diameter, shell thickness, total length, and composition (i.e., material) are recorded here.

3.2.1.3 Insitu Test and Analysis

Types of insitu test available at the project, pile top elevation, pile-tip elevation, water elevation, mudline elevation, embedded length of the pile, major soil type (querying), and plug status are recorded here.

The insitu test data could be from CPT, SPT, or CPT/SPT (both CPT and SPT). In case of CPT/SPT, the insitu test and soil page would be CPT test by default, with an option of viewing or entering SPT data. This is further described in section 3.2.3. The two options for the plug status are plugged, and unplugged; these have been created as drop down window in the data entry page.

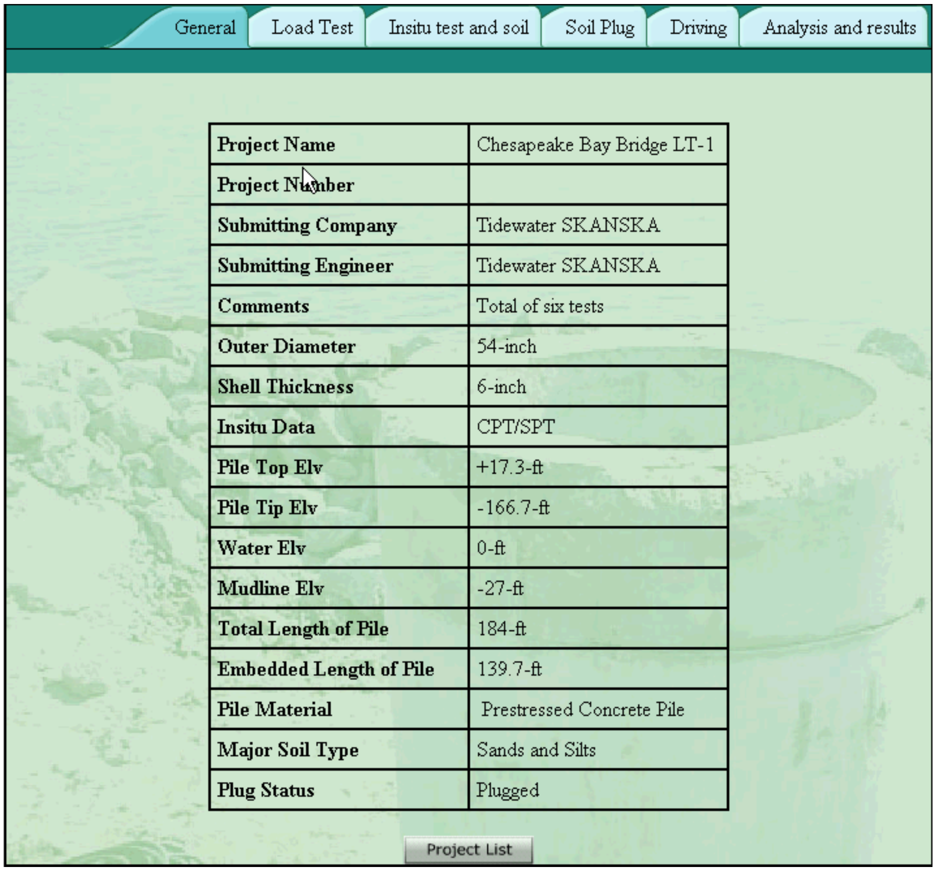

Project Name	Chesapeake Bay Bridge LT-1
Project Number	
Submitting Company	Tidewater SKANSKA
Submitting Engineer	Tidewater SKANSKA
Comments	Total of six tests
Outer Diameter	54-inch
Shell Thickness	6-inch
Insitu Data	CPT/SPT
Pile Top Elv	+17.3-ft
Pile Tip Elv	-166.7-ft
Water Elv	0-ft
Mudline Elv	-27-ft
Total Length of Pile	184-ft
Embedded Length of Pile	139.7-ft
Pile Material	Prestressed Concrete Pile
Major Soil Type	Sands and Silts
Plug Status	Plugged

Figure 3-4 Shows the format of the General page.

3.2.2 Load Test Page

The load test page (Fig. 3-5) consists of the three columns: Time (minutes), Force (tons), and Displacement (inch). The latter is used to construct a load deformation response of the pile. The view graph page uses the JavaScript application in plotting the two columns force and displacement (Fig. 3-6).

The Go to Strain Data link at the top of load test page (Fig. 3-5), tabulates the data from the strain gages. The three columns on the STRAIN DATA page are the Time (min), Depth of the strain gage from the top of the pile (ft), and the force (Tons) transferred to pile at that depth (calculated using strain gage data), Figure 3-7. The view graph option plots the load along the length of the pile. The Go to Main Data link brings the user back to the main load test page.

General | Load Test | Insitu test and soil | Soil Plug | Driving | Analysis and results

Go to Strain Data

Time (min)	Force (Tons)	Displacement (inch)
	50	0.01
	100	0.01
	150	0.015
	200	0.015
	400	2.25
	300	2.24
	200	2.21
	100	2.2
	0	2.2

View Graph

Project List

Records 1 to 43 of 43

Figure 3-5 Shows the format of the Load test page.

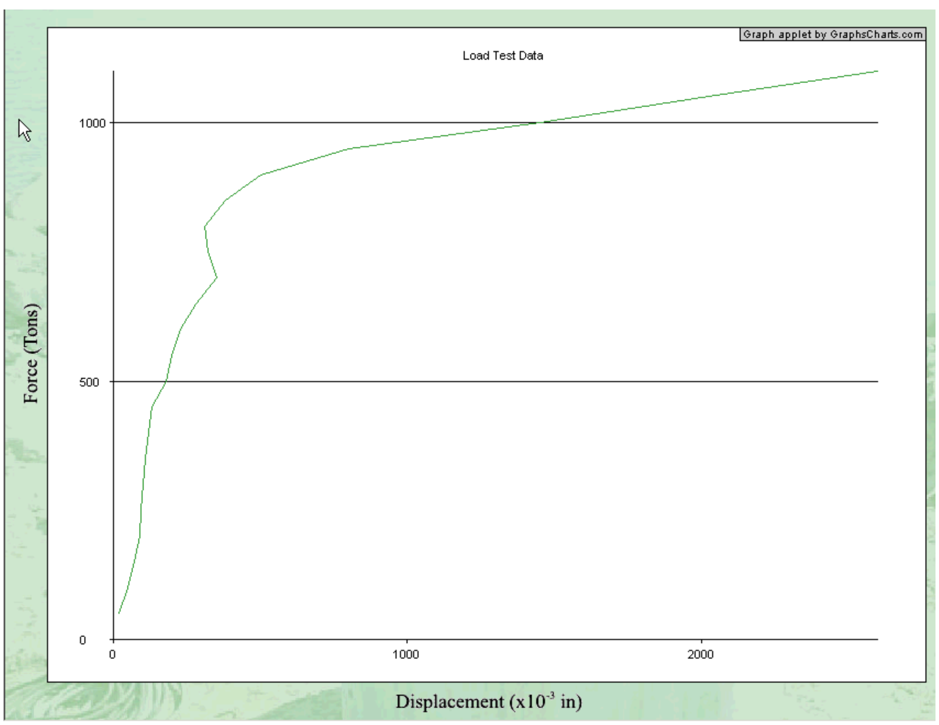

Figure 3-6 Shows a plot of load displacement of the pile.

Time (min)	Depth (ft)	Force (Tons)
5000	-13.5	528.0514596
	-45.5	509.8427886
	-61.5	236.7127233
10000	-13.5	598.5016748
	-45.5	580.3652605
	-61.5	217.6369727
15000	-13.5	658.1133954
	-45.5	658.1133954
	-61.5	292.4948424
20000	-13.5	819.3901959
	-45.5	801.1815249
	-61.5	364.1734204
25000	-13.5	939.3362034
	-45.5	921.2720457
	-61.5	379.3473129
30000	-13.5	1043.530265
	-45.5	1025.538364
	-61.5	359.8380225

Figure 3-7 Screen view of force vs. depth data page.

3.2.3 Insitu Test and Soil Page

Based on the selected type of insitu test information on the General page, different insitu test pages will open (Fig. 3-8). In case of CPT test, the page opens up with six columns namely elevation, depth, soil type, cone resistance, friction resistance, and friction ratio. The page has an option of plotting a graph of cone resistance (Fig. 3-9) vs. elevation, and skin friction vs. resistance at the bottom of the page (Fig. 3-8).

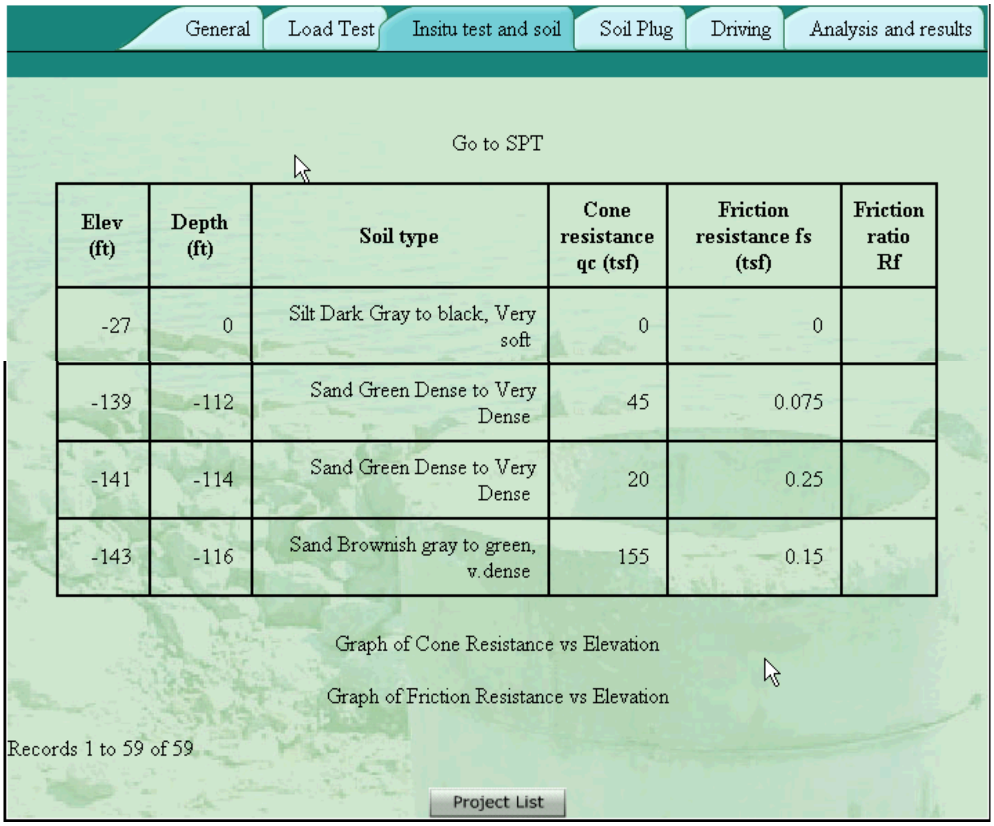

Elev (ft)	Depth (ft)	Soil type	Cone resistance qc (tsf)	Friction resistance fs (tsf)	Friction ratio Rf
-27	0	Silt Dark Gray to black, Very soft	0	0	
-139	-112	Sand Green Dense to Very Dense	45	0.075	
-141	-114	Sand Green Dense to Very Dense	20	0.25	
-143	-116	Sand Brownish gray to green, v.dense	155	0.15	

Figure 3-8 Screen shot showing the insitu test page for CPT data.

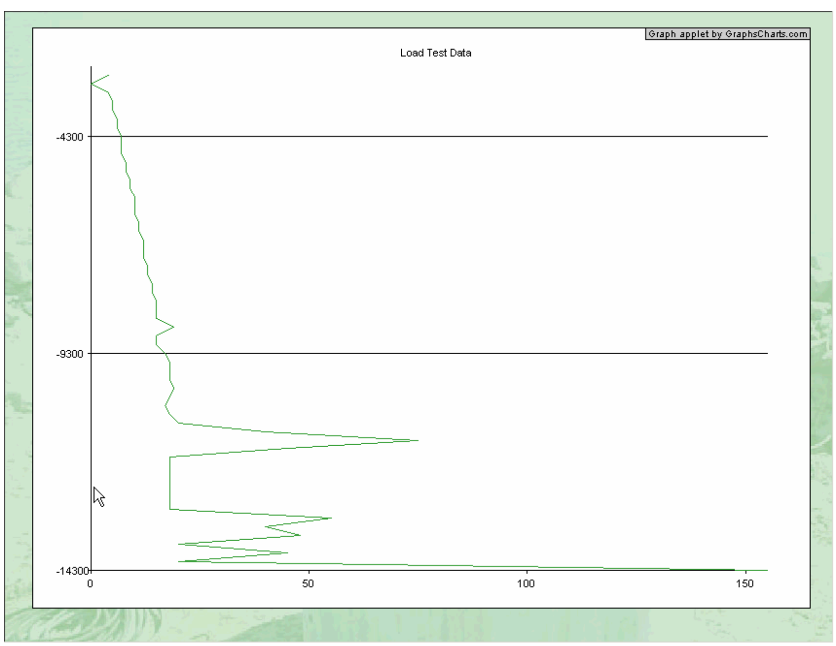

Figure 3-9 Plot of Cone resistance vs. elevation.

If on the General Page (Fig. 3-4), SPT is selected, a page of four columns: elevation, depth, soil type and uncorrected blow count (N), Figure 3-10 is displayed. An option of plotting blow count vs. elevation (Fig. 3-11) is available at the bottom of the page.

In case there are both CPT and SPT data available from the test (Fig. 3-4), the insitu data page opens up with CPT data, and option for SPT data (Fig. 3-8) entry is given at the top of the page.

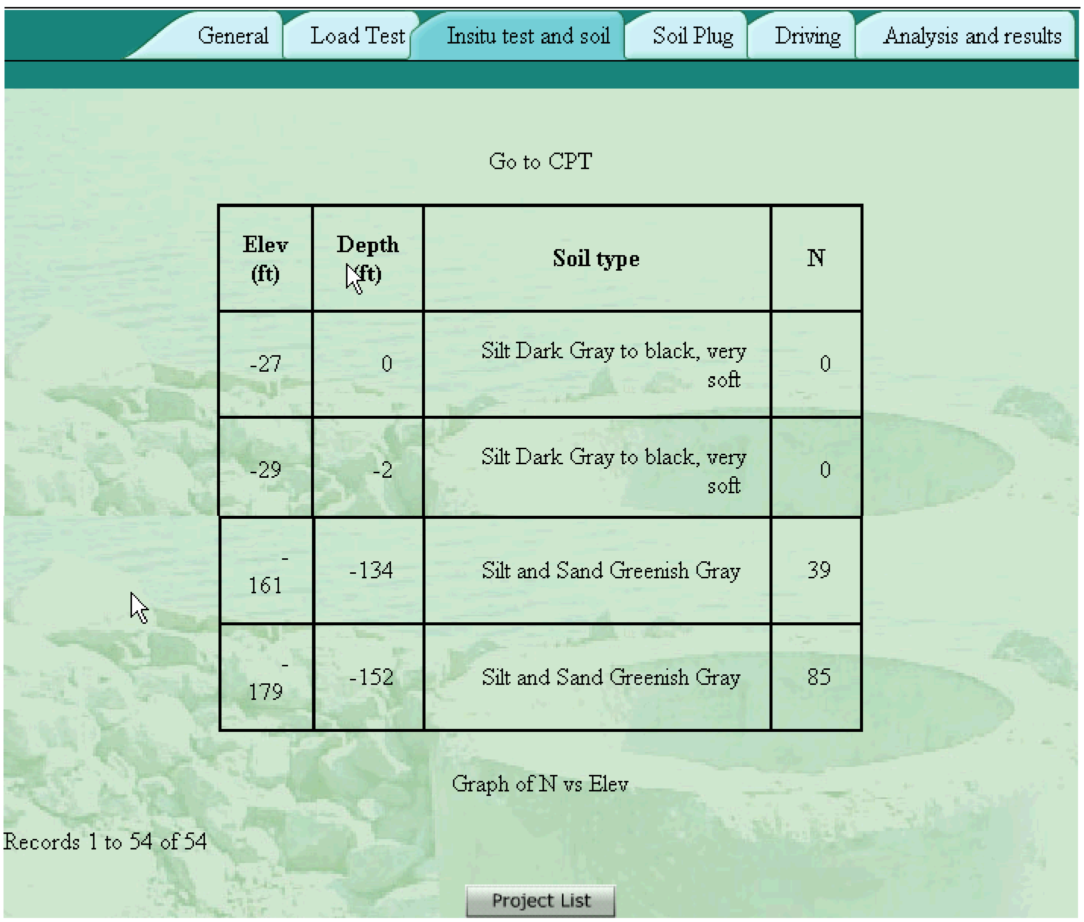

Figure 3-10 Screen shot showing the format for the SPT page.

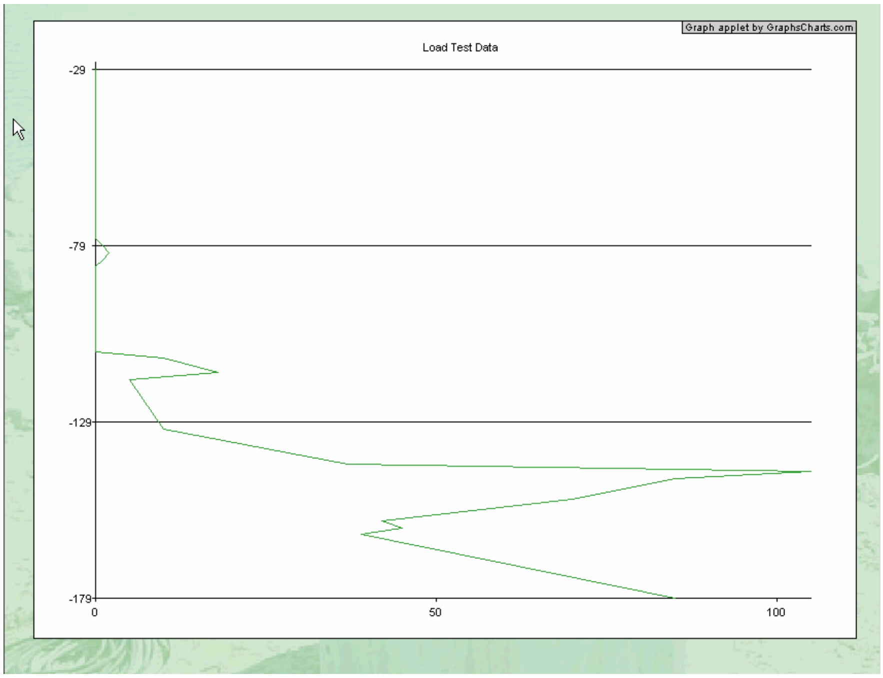

Figure 3-11 Plot of blow count vs. elevation.

3.2.4 Soil Plug Page

The soil plug page has information on the status of the plug (i.e., plugged vs. unplugged), plug height from the mudline (h_m) (Fig. 3-12), plug height from the tip (h_t), type of soil at the tip, as well as soil type at the mudline. Figure 3-13, is a screen picture of the soil plug page.

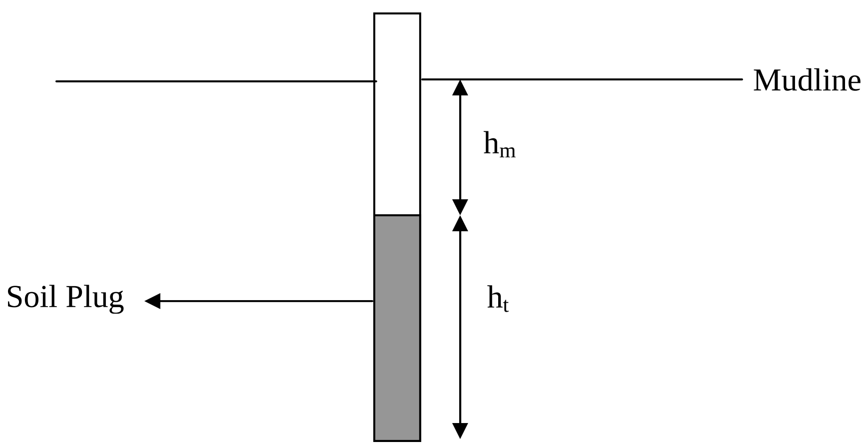

Figure 3-12 Description of the parameters used in defining the soil plug.

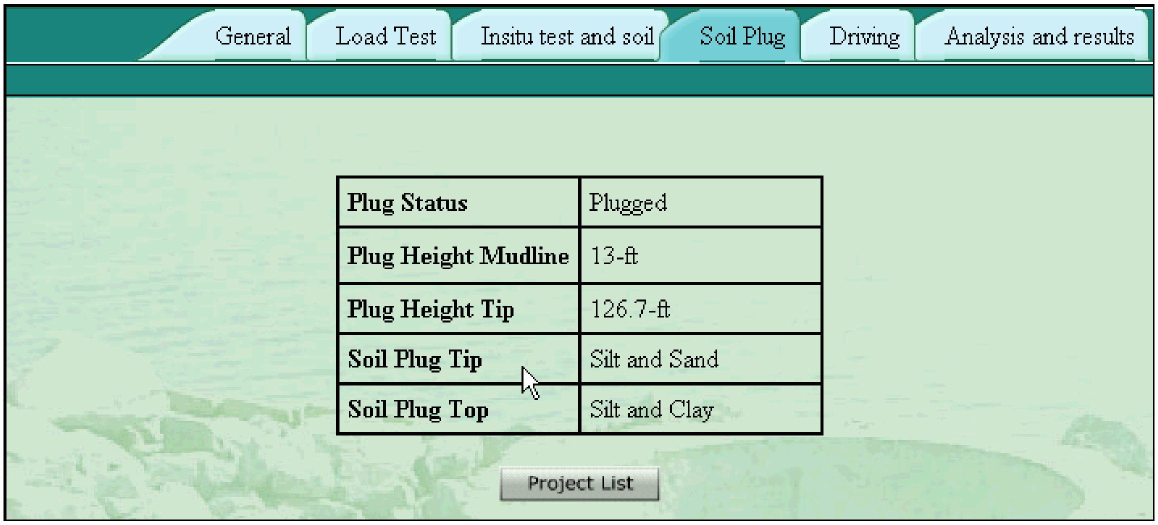

Figure 3-13 Screen shot of the soil plug page.

3.2.5 Driving Page

The driving page (Fig. 3-14) has information such as the type of hammer, weight of hammer, theoretical energy, pre-bored depth, number of blows to drive last ft (last blow), time at end of driving, and start of re-strike.

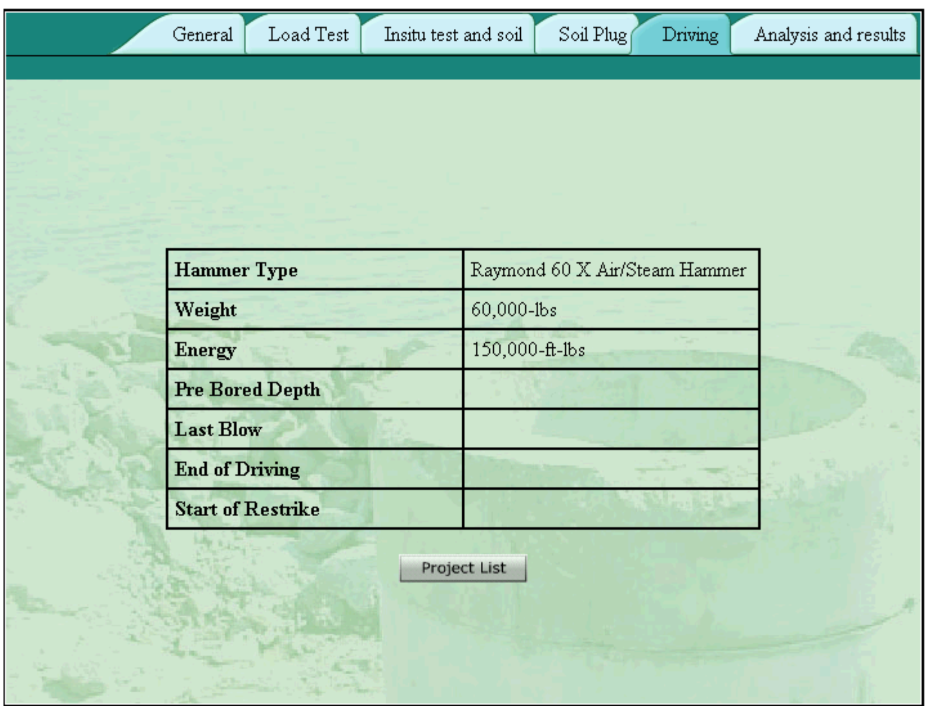

Figure 3-14 Screen shot of the driving page.

3.2.6 Analysis and Results Page

The analysis and results page (Fig. 3-15) has information on method of capacity estimation, Pile Modulus, etc. Results of the analysis such as skin friction, and end bearing are also presented.

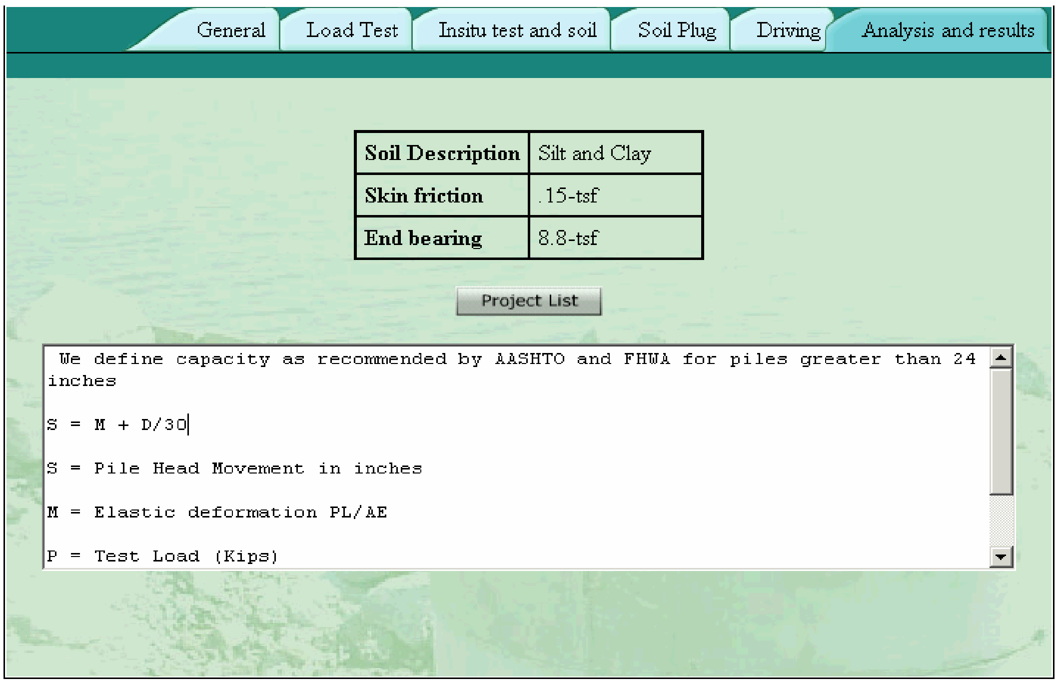

Figure 3-15 Screen shot of the analysis and results page.

CHAPTER 4

DATA REDUCTION

4.1 INTRODUCTION

Data for each cylinder pile load-test in the database had to be separated into total force carried in skin and end bearing respectively. Subsequently, using the surface areas, and tip areas, the unit skin friction (stress) and end bearing (stress) vs. SPT N values had to be established as a function of soil types.

Given the recorded data in the load tests, two different approaches were required to obtain unit skin and end bearing stresses:

1. Direct Method: Strain gage data from the instrumented cylinder piles (separates skin friction from end bearing directly);
2. Indirect Method: Plotting the load vs. deflection data on a arithmetic scale and obtaining Davisson's Capacity (i.e., failure axial load), and subsequently plotting load vs. deflection data in a log-log plot (DeBeer's Method) to give the distribution of skin and tip.

Both methods are discussed in more detail below, after a discussion of failure capacity.

4.2 DAVISSON'S METHOD

Typical, load settlement response (Davisson, 1976) of a pile is shown in Figure 4-1 for end bearing, skin friction or a combination. Evident, from the figure is that as a skin friction pile undergoes failure, large increases in settlements occur at small changes in load. However, in the case of a point bearing pile, the load-settlement response of the pile does not exhibit large increases of settlement at failure load. A pile which develops its resistance from both skin and tip, has load settlement response which transitions between skin friction to end bearing behavior (Fig. 4-1). As consequence, Davisson developed the elastic offset approach to define pile failure or capacity.

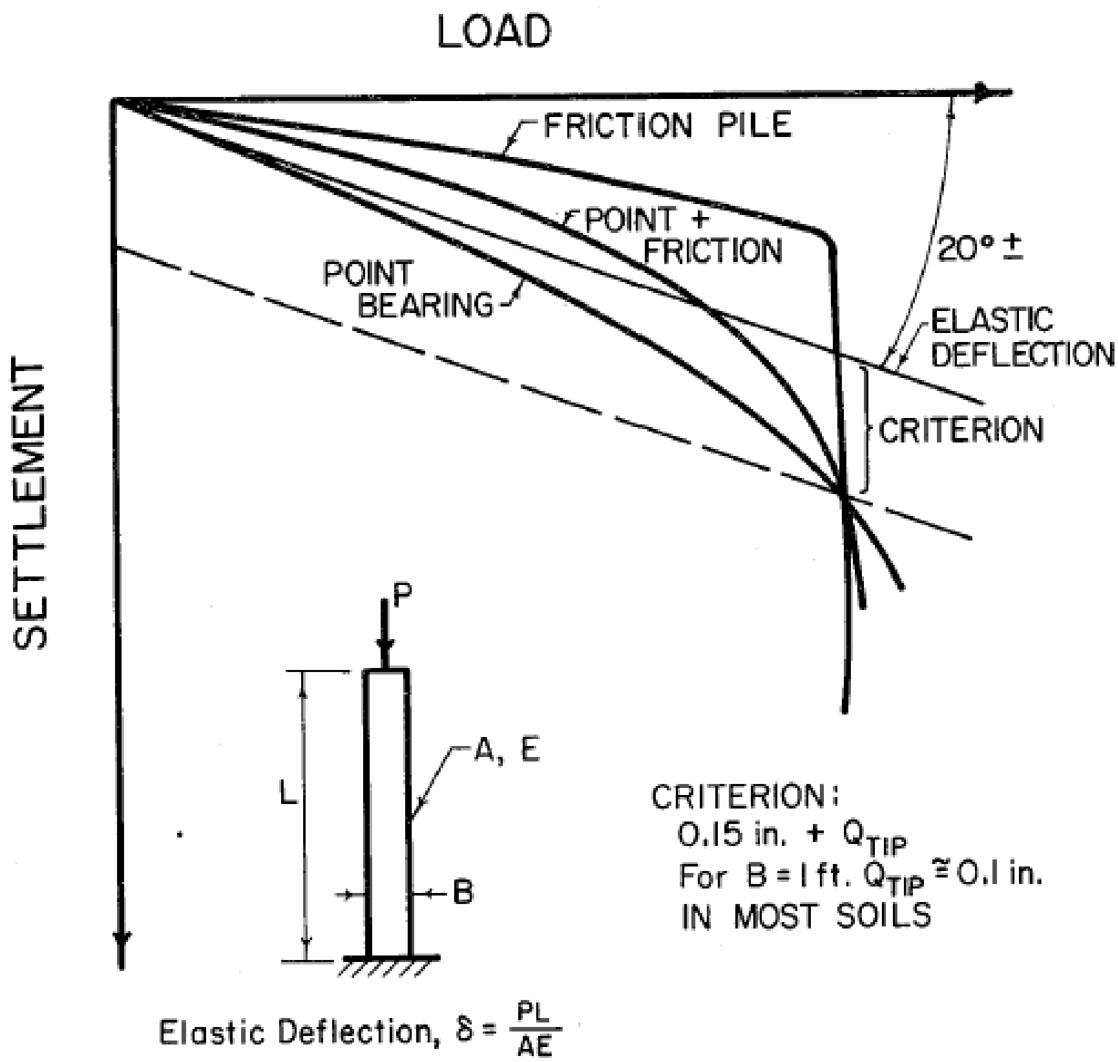

Figure 4-1 Interpretation of pile load test. (High Capacity Piles, M.T. Davisson, 1976)

The FDOT, as well as AASHTO and FHWA, recommends Davisson approach for small diameter piles, however, for piles greater than 24 inches in diameter, the failure load is defined with an offset of:

$$S = \Delta + D / 30 \qquad \text{Eq. 4-1}$$

Where:

S = Pile head movement (inch)

Δ = Elastic deformation or (P * L) / (A * E)

P = Test load (kips)

L = Pile length (inch)

A = Cross-sectional area of the pile

E = Modulus of elasticity of the pile material (ksi)

D = Pile diameter (inch)

Shown in Figure 4-2 is the load settlement response for St. Georges Island concrete cylinder pile, Test-1. The elastic load vs. deformation line was determined first, and then the offset line was drawn to the right of the elastic line at a distance of D/30. The failure capacity is identified at the intersection of the failure line and the load vs. deformation response of the pile (1050 tons). Evident from the shape of the pile's load vs. settlement response, skin friction is significant for this pile.

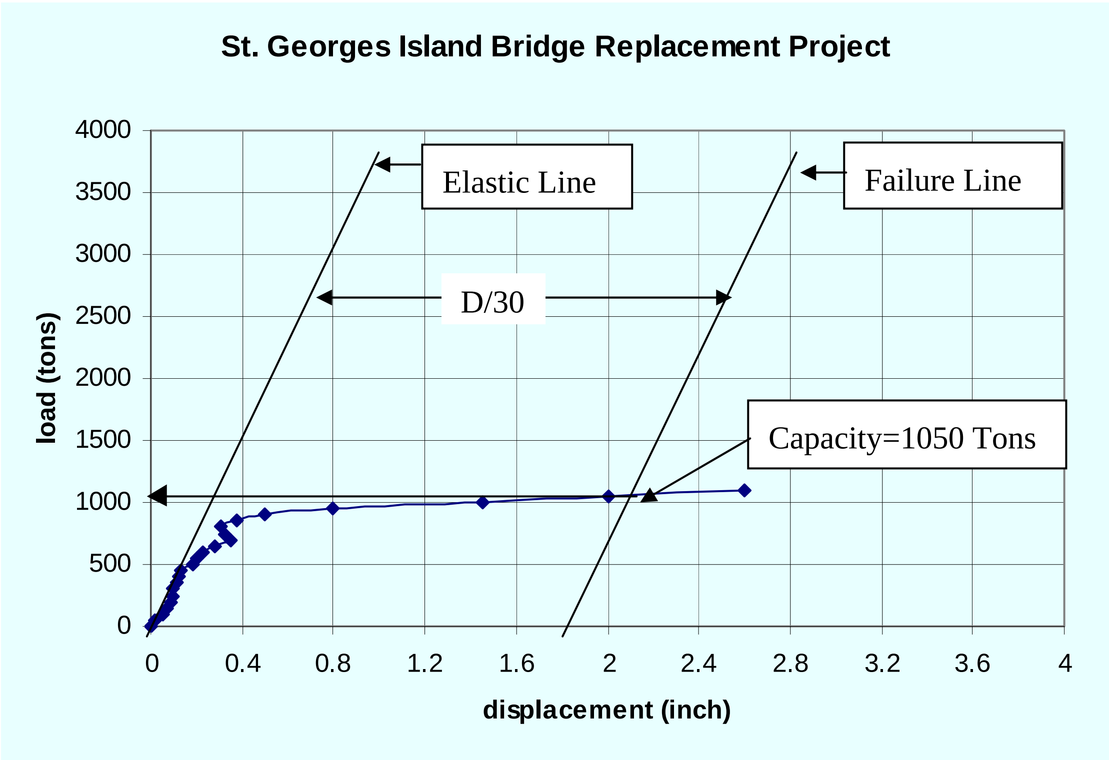

Figure 4-2 Determining capacity of pile, using Davisson's method, for the St. Georges Island Bridge Replacement Project, Load Test-1.

4.3 DIRECT METHOD - DATA REDUCTION FROM STRAIN GAGES

Strain gages, either surface mounted (steel pipe) or embedment type (concrete), are installed in/on the pile, to determine the ultimate skin friction value in each of the soil strata. As an axial load is applied to the pile, some percentage of the load is transferred to the surrounding soil. Generally, the load is transferred initially to the uppermost stratum, and as the loads increase, more of the load is transmitted to the lower stratums, through the stiffer pile. Eventually, any increase in applied load will be transferred directly to the pile tip, since the unit skin friction along the pile is fully mobilized (i.e., ultimate).

The unit skin friction value along any portion of the pile is calculated as the difference in the load between two adjacent strain gages divided by the surface area of the pile between the gages, that is,

$$f = (P_1 - P_2) / (C * L_{1-2}) \qquad \text{Eq. 4-2}$$

f = Unit Skin Friction (tsf)
P_1 = Load from strain gage 1 (Tons)
P_2 = Load from strain gage 2 (Tons)
C = Circumference of the pile (ft)
L_{1-2} = Length between gages (feet)

The calculation of the load from a strain gage is derived from Hooke's law, and algebraic substitution utilizing the basic principals from mechanics of materials,

$$\sigma = E * \varepsilon \qquad \text{Eq. 4-3}$$

σ = Stress (ksi)
E = Modulus of Elasticity (ksi)
ε = strain (in/in)

The stress in a structural member is obtained by dividing the magnitude of the load by the cross sectional area,

$$\sigma = P/A \qquad \text{Eq. 4-4}$$

σ = Stress (ksi)
P = Load (kips)
A = Cross-sectional area (sq-in)

A structural member responds to stress by straining, which is the ratio of total deformation of the member to the total length of the member, or:

$$\varepsilon = \delta/L \qquad \text{Eq. 4-5}$$

ε = Strain (in/in)
δ = Total deformation under load (in)
L = Length of member (in)

Substituting P/A for σ in Hooke's Law (Equation 2) results in:

$$P / A = E * \varepsilon$$

Or,

$$P = E * \varepsilon * A \qquad \text{Eq. 4-6}$$

The elastic modulus and the cross-sectional area of the pile are known, and that the strain is measured in the load tests for various loads applied to the top of the pile.

Using Eq. 4-6 for various strain measures along the pile, and applied loads, load distribution along the pile is plotted in Figure 4-3. Using Eq. 4-2, with the axial forces, (Fig. 4-3), the unit skin friction along the pile for various applied loads may be determined. Of interest, is the ultimate skin friction for various soil layers along the piles, as well as the mobilized end bearing at the FDOT failure load (i.e., Davisson).

Data from instrumented piles, i.e., strain gages, were available from four load tests performed at St. Georges Island Bridge Project, and three load tests at the Woodrow Wilson Bridge Project.

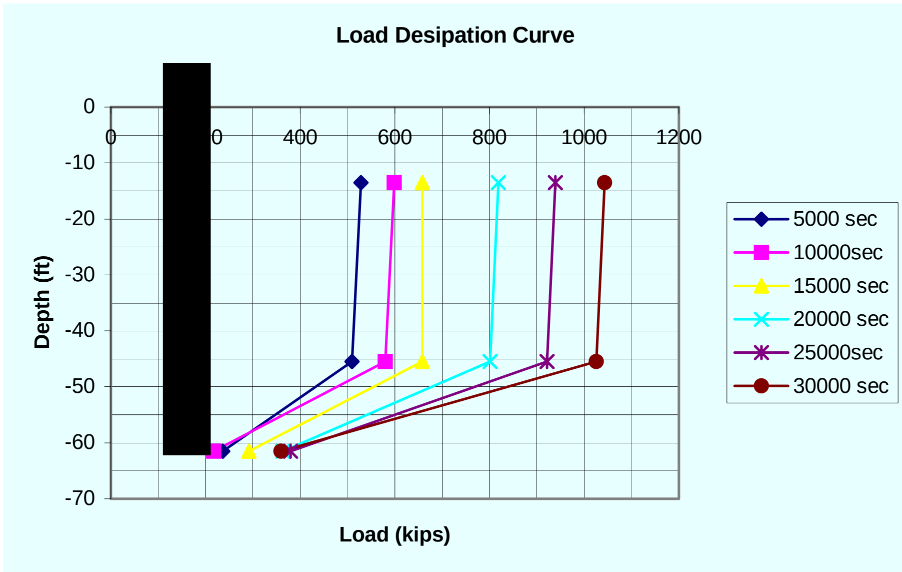

Figure 4-3 A plot of load distribution along the pile vs. strain gage elevation with increment in axial load/time for the St. Georges Island Bridge Replacement project.

4.4 INDIRECT METHOD-DATA REDUCTION USING DEBEER'S METHOD

In the case of no strain gage instrumentation in the pile, the skin and tip resistance was computed using the methods proposed by DeBeer (1967) and DeBeer and Wallays (1972). They suggest that the load transfer from skin friction and end bearing may be separated into two separate distinct curves as shown in Figure 4-4. Evident, is that the skin friction is mobilized very quickly (i.e., small head displacements), whereas, the pile end bearing requires significant displacements. Consequently, if the load deformation curve were to be plotted on a double logarithmic scale, the response would occur along two distinct approximate straight lines (i.e., skin friction, and end bearing), Figure 4-5. That is the polynomial representing the end bearing (Fig. 4-4) would have a different power representation or slope in Figure 4-5 on a logarithmic scale than the skin friction polynomial (Fig. 4-4). Moreover, the intersection of the lines in the logarithmic plot would represent the transition from skin friction to end bearing. The difference between the FDOT failure capacity and the intersection would represent the mobilized end bearing.

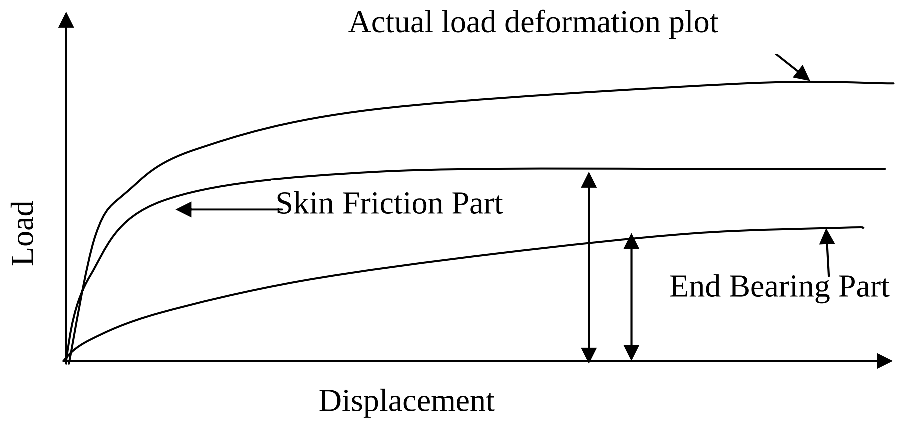

Figure 4-4 Separation of load vs. deformation plot into skin and tip.

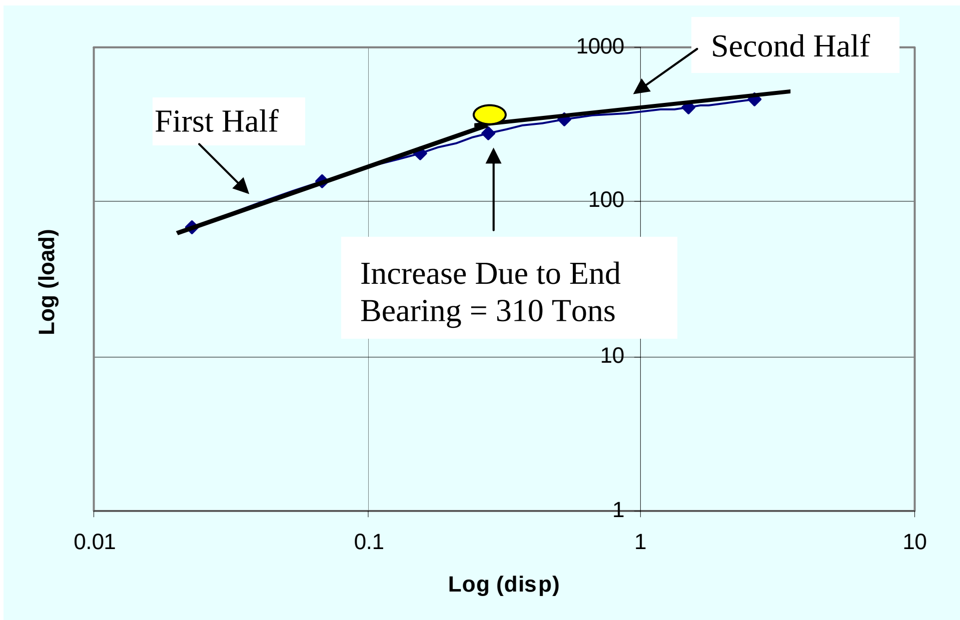

Figure 4-5 Separating skin friction and end bearing using DeBeer's method.

Of concern, are the cases in which there are no two clearly distinct lines or slopes. Either the pile is just end bearing or skin friction. The latter choice is made by information on soil type around the pile tip.

All of the piles, which had strain gage information, were reduced and compared with the indirect method to check DeBeer's approach.

4.5 COMPARISON BETWEEN DIRECT AND INDIRECT METHOD

Data from strain gages were available from seven tests (four from the Georges Island Bridge Replacement, and three from Woodrow Wilson Bridge Project). Both direct and indirect methods were used in reducing skin friction, and tip resistance for the tests. Table 4-1 shows a comparison between the two methods. No strain gage data (NA) the Table indicates that the strain gage at the tip failed to produce reliable data during the static loading process. It was subsequently not considered as identified in the load test report (St. Georges Island Test-2, Woodrow Wilson-C, Woodrow Wilson-I).

No data for DeBeer’s unit skin friction, or end bearing, indicates that the load test was not taken to failure, i.e., Davisson’s capacity. Consequently, the skin and tip resistance could not be computed. For those cases, which did go to failure, the comparison between Strain gauge and DeBeer methods appear to be reasonable.

Table 4-1 Comparison Between Direct and Indirect Methods

Project Name	Unit Skin Friction (tsf)		Unit End Bearing (tsf)	
	Strain Gage	DeBeer's	Strain Gage	DeBeer's Method
St. Georges Island -1	0.99	1.17	38.4	24.9
St. Georges Island -2	0.28	N.A	N.A	N.A
St. Georges Island -3	0.12	N.A	81.69	N.A
St. Georges Island -4	0.85	1.11	48.852	49.822
Woodrow Wilson Bridge-C	0.42	0.53	N.A	N.A
Woodrow Wilson Bridge-F	0.93	0.85	58.8	51.9
Woodrow Wilson Bridge-I	0.81	N.A	N.A	N.A

CHAPTER 5

ESTIMATION OF SOIL PLUG

5.1 INTRODUCTION

Open-ended large diameter cylinder piles have been used for years in the offshore industry. Of interest, for both end-bearing estimates and pile drivability analysis is the behavior of the soil "column" within the pile cylinder. Specifically, during the initial stage of driving, soil will enter the pile at a rate equal to the rate of pile penetration. However, with penetration, the inner soil column develops friction between its sides and the pile. If the side friction builds to an extent to overcome gravity and inertia forces, the soil attaches itself to the inside wall of the pile and both move as one unit. The latter is generally referred to as "plugged" versus "unplugged," i.e., soil moving separately from the pile. It should be noted that the soil mass within the pile cylinder is typically referred to as the "soil plug" (Paikowsky, 1990), even if it moves with or separately from the pile (i.e., plugged or unplugged). Herein, the soil within the pile is referred to as the soil column and if it is attached (i.e., moves with pile) it is called plugged or unplugged if they move separately.

Of interest to this study is if the soil within the pile is in a "plugged" state during the static loading for end bearing considerations. It should be noted, that if the cylinder pile were to plug during driving, it would remain plugged during the static loading. However, if pile was unplugged during driving, it still could behave plugged during static load, since the inertia forces present during driving (see 5.2.1) would be absent. To study the behavior of the cylinder pile under static analysis, a finite element analysis, ADINA (i.e., Automatic Dynamic Incremental Non-Linear Analysis), of a cylinder pile slowly moving through a soil was performed. The properties of this model were based on data from the St. Georges Island Bridge Replacement

Project. A brief discussion of available literature on cylinder pile plugging (arching, and inertial forces on the plug) is presented first.

5.2 SOIL-PILE ARCHING PHENOMENON

As soil moves into the pile during driving, there is an increase in the side resistance in the lower zone of the pile. When the soil skin resistance within the cylinder exceeds the tip bearing resistance, the pile plugs preventing further soil penetration. This increased resistance has been explained by soil arching.

According to Paikowsky (1990), the arching mechanism occurs as a result of a reorientation of the granular soil particles into an arch (Fig. 5-1). The arch has a convex (upward) curvature in the upper zone, attributed to a bulb of reduced stresses during the pile's initial penetration. The arch has a concave (downward) curvature at the tip of the plug, attributed to a bulb of increased vertical stresses due to penetration in a plugged or a semi-plugged mode (Fig. 5-1).

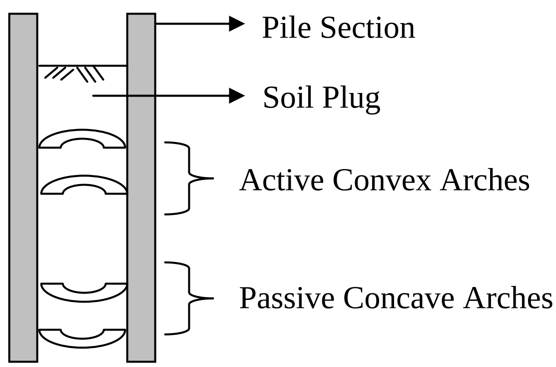

Figure 5-1 Isobars of the vertical stress within the soil plug, showing the transition from active to passive arching.

When subject to loading (static or dynamic), load is transferred through the soil mass to the inner walls of the pile. When the loads exceed the arch capacity, dilation and shear take place along the arch, allowing penetration of additional soil until a new stable arch forms, for which the arch resistance exceeds the upward pushing forces (tip capacity). This process accounts for zones of varying soil densities within the pile cylinder. For all plugged piles, the densest soil zone exists a quarter diameter away from the tip. In case of unplugged piles, the densest zone exists at the pile tip with diminishing density upwards in the soil cylinder. Unfortunately, Paikowsky (1990) does not identify when a cylinder pile will plug, especially as a function of pile size, wall thickness, etc.

5.3 SOIL PLUG FORCES DURING DRIVING

At the beginning of the driving process, soil enters the inside of the pile cylinder from the bottom. As the pile penetrates deeper, the height of the soil column, L increases, and the side friction, Fs (Fig 5-2A), acting between the soil and the inside of the pile walls increases. Acting against the soil-wall friction is the weight of the soil column and the vertical uplift force at the bottom of the soil column from the underlying soil. If the side friction increases to a value greater than the end bearing, the soil column will want to attach itself to the inside of the pile (plug) and subsequently move with the pile. Due to its subsequent downward motion (i.e., moving with the pile), the soil column will develop additional force, inertia, I, equal to the mass of the soil plug times the pile downward acceleration will develop (Fig. 5-2B). The inertia force on the plug acts upward in opposite direction of the pile motion (i.e., downward).

Obviously, if Fs is of sufficient magnitude to overcome inertia, **I,** (Fig. 5-2B), and Q_t ($q_{tip} \cdot A_{cross}$: total cross-sectional pipe area), then the pile behaves plugged and it will have sufficient magnitude to overcome just Q_t under static loading (i.e., Fig. 5-2A). If the pile were to remain unplugged during driving, it still may act plugged (i.e., Fs > Qt) during static loading, and the end bearing calculation, Q_t ($q_{tip} \cdot A_{cross}$) would remain the same, i.e., unit end bearing (stress) would be multiplied by total pipe cross-sectional area. However, if the pile remains unplugged during static loading (i.e., Fs < $Q_t = q_{tip}\ A_{cross}$), then Qt should be computed using the unit end bearing (q_t: stress) times the cross-sectional area of the pipe material alone [i.e., $\Pi\ (D_o^2 - D_i^2)/4$] and not the total pipe cross-sectional area [$\Pi\ (D_o^2)/4$] as with the plugged scenario.

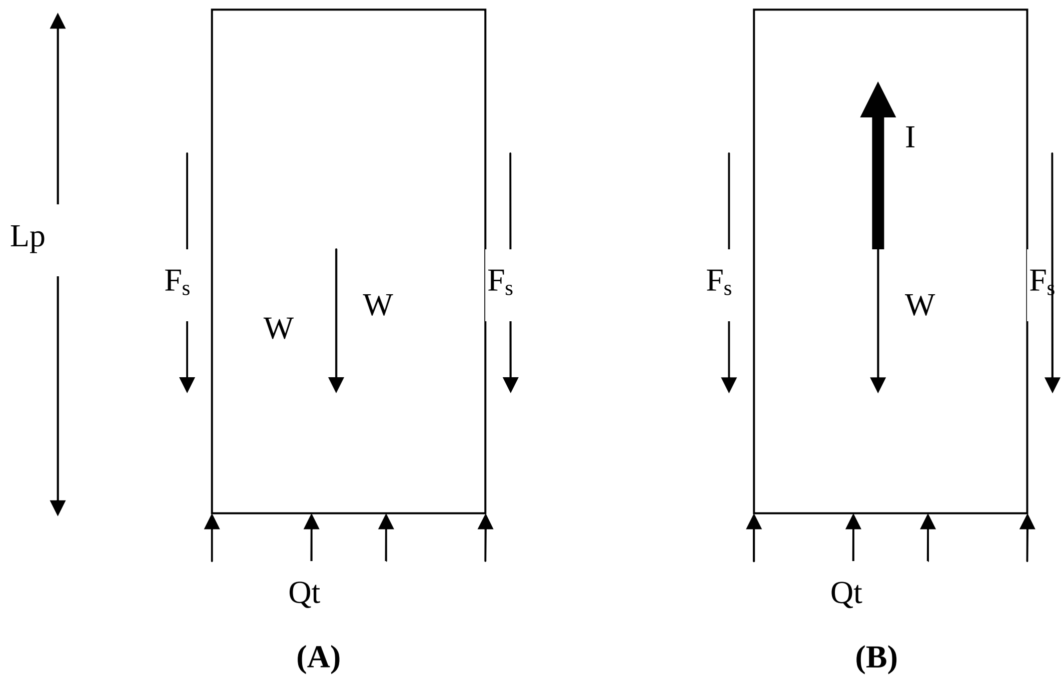

Figure 5-2 Free body diagram of soil column within the pile during driving.

For small diameter pipe piles (e.g., 12 to 18”), the inertia forces on the soil column are generally small and ignored with Fs vs. Qt used for assessing the pile’s plugged or unplugged status. However as the diameter of cylinder piles have become larger, the latter is no longer true. Specifically, the inertia force, I, will become the dominant force that Fs must overcome as the pipe diameter increases. The latter is shown below through the calculation of soil plug height, Lp (Fig. 5-2), required for sufficient Fs to overcome Qt (end bearing) and I (inertia), for a given plug acceleration (i.e., pile acceleration during driving). A discussion of each of the forces and how it was computed is presented first.

1. Frictional Force, **Fs**: The soil column feels this force, in the downward direction, on the pile soil interface. Its magnitude is equal to the product of the soil column surface area, times the unit skin friction at the interface. As this study was carried out to see the effects of soil column diameter, and g-forces on the soil plug mass, the interface frictional coefficient was chosen to be a constant value for the parametric study. (Based on design curves for cylinder pile, discussed in Chapter 6)
2. Weight of the soil column, **W**: The weight of the soil column is the product of the volume of the soil column, times the average total unit weight of soil. This force acts in the downward direction.
3. Tip Resistance, $\mathbf{Q_t}$: The tip resistance acting on the soil column is equal to the product of the soil column cross sectional area times the unit tip resistance. This force, $\mathbf{Q_t}$, acts in the upward direction trying to push the soil column into the pile.
4. Inertia Force, **I**: The inertial force is equal to the product of the soil column mass, and the pile acceleration, and represents the resistance of the soil column weight to the downward acceleration imparted by the hammer to the pile-soil system. The inertial force acts in the upward direction, trying to oppose the motion, and creating a resultant upward force. If the inertial effects are large enough, the pile will continue to core. The inertial force acts only during the driving process.

The assumptions made in these calculations are:

1. The g-forces on the soil column are constant for the full length, and its value equal to the average g-forces on the embedded portion of the pile.
2. The damping forces were ignored; note the radiation soil damping which occurs on the outside of pile (3D effects), does not occur here, i.e., one-dimensional.
3. The shear strength of the soil column is much larger than that of the pil-soil-column interface .

For static loading, i.e., Figure 5-2A, vertical force equilibrium gives:

$$\mathrm{Fs} + \mathrm{W} = \mathrm{Qt} \qquad \text{Eq. 5-1}$$

Substituting in unit skin friction, fs, unit tip resistance, qt, and soil column areas (i.e., surface and cross-sectional) gives:

$$(\pi \mathrm{Dfs})\mathrm{Lp} + \left(\frac{\pi \mathrm{D}^2 \gamma}{4}\right)\mathrm{Lp} = \left(\frac{\pi \mathrm{D}^2}{4}\right) * \mathrm{qt} \qquad \text{Eq. 5-2}$$

Simplifying,

$$\mathrm{Lp}\{\mathrm{fs} + 0.25\gamma \mathrm{D}) = 0.25\,\mathrm{qtD} \qquad \text{Eq. 5-3}$$

and solving for Lp, i.e., the required soil column height for equilibrium between side friction, Fs, and end bearing, Qt (using total cross-sectional area) is

$$L_p = \frac{q_t D}{4 \; fs + \gamma \; D} \qquad \text{Eq. 5-4}$$

Where:

Lp	=	Length of the plug (ft).
D	=	Diameter of the plug/ inner diameter of the pile (inch).
γ	=	Total unit weight of soil (pcf).
fs	=	Unit skin friction between the plug and pile (tsf).
Fs	=	Total skin frictional force (Tons).
qt	=	Unit end bearing at pile toe (tsf).
Qt	=	Total tip resistance on the soil plug (Tons).
W	=	Weight of the soil plug (Tons).

For dynamic loading, i.e., during pile driving, Figure 5-2B, vertical force equilibrium gives:

$$Fs + W = Qt + I \qquad \text{Eq. 5-5}$$

Substituting in unit skin friction, fs, unit tip resistance, qt, mass of soil column (W/g = Volume x unit wt/g), and soil column areas (i.e., surface, and cross-sectional) gives:

$$(\pi D fs)Lp + \left(\frac{\pi D^2 \gamma}{4}\right)Lp = \left(\frac{\pi D^2}{4}\right)qt + \left(\frac{\pi D^2 \gamma}{4}\right)\frac{Lp * ap * g}{g} \qquad \text{Eq. 5-6}$$

simplifying,

$$Lp\,\{fs + 0.25\gamma D - 0.25\gamma D * ap) = 0.25qtD \qquad \text{Eq. 5-7}$$

And solving for Lp, gives

$$L_p = \frac{q_t D}{4 \; fs + \gamma \; D \; (1 - ap)} \qquad \text{Eq. 5-8}$$

where, ap · g = is the soil column acceleration (ft/sec^2) and ap is a dimensionless number identifying the soil column acceleration in terms of gs.

A comparison of Eqs. 5-4 and 5-8 show them to be quite similar with the exception of the average soil column acceleration, ap, in the denominator of Eq. 5-8. The latter will result in a negative term when ap>1 in the denominator which is magnified by the pile diameter, D, and will result in a significant increase in soil column height for equilibrium conditions and plugging.

Using Equation 5-8, a parametric study of pile diameter on inertia Force, I, and required soil column height, Lp, to develop sufficient, Fs, was undertaken for typical Florida soil and pile sizes. To accomplish this, a MathCAD file was developed for Eqs 5-5 to 5-8, as shown in Figure 5-3. The input parameters are the outer diameter of the pile, shell thickness (to calculate the diameter of the soil column), soil type (same classification as SPT97), SPT N values for unit skin friction, and unit end bearing calculations, and submerged unit weight of soil.

A parametric study was carried out on piles with six different diameters (54", 38", 24", 20", 16", and 12"), one soil type (silt), a pile length of 80 ft (St. Georges) with soil column g-forces varying from 0-g (static loading case: Eq. 5-8 reduces to Eq. 5-4) to 45-g. Table 5-1 tabulates the various parameters and their values used in the study.

Figure 5-4, shows the computed soil column heights for soil diameters (inner diameter of the pile) of 54-inch, 38-inch, 24-inch, 20-inch, 16-inch, and 12-inch using equations 5-8 from the Mathcad file (Fig. 5-3) for plugging. For discussion, consider the 54" concrete pile in the figure. For an average pile plug acceleration of 10 gs, a soil column height of approximately 40 ft (Eq. 5-8) is required to develop enough unit skin friction, Qs (fs = 0.586 tsf x surface area), to overcome end bearing, Qt (96.9 tons), and inertia force, I. If the acceleration of the soil column increases to 15 gs, a soil column height equal to the total pile length, 80 ft is required for plugging. If the soil plug acceleration exceeds 15 gs, the soil will not plug. Also of interest, is the soil column height at 0 gs, i.e., static loading, which are according to Figure 5-4 is approximately 25 ft. Evident from the figure, significant soil friction, Fs, is used to overcome Inertia effects, I, for large diameter pipes. Note the required soil column accelerations, for "plugging" of

$OD := 54 \text{ inch} \qquad t := 8 \text{ inch} \qquad ap := 1 \quad g$

$unitweight := 50 \text{ pcf} \qquad unitweigh := \frac{unitweight}{2000}$

$type := 3 \qquad Nskin := 25 \qquad Ntip := 30$

$D := \frac{(OD - 2 \cdot t)}{12} \qquad D = 3.167 \text{ ft}$

Soil Type	Pile Material	Type
clay	concrete	1
clay	steel	2
silt	concrete	3
sand	concrete	4
sand	steel	5

calculates the diameter of the soil plug in terms of pile dimension

$$fs := \left| \begin{array}{l} .62 \cdot \ln(Nskin) - .9922 \text{ if } type = 1 \\ .5211 \cdot \ln(Nskin) - .7989 \text{ if } type = 2 \\ .025 \cdot Nskin - .039 \text{ if } type = 3 \\ .0188 \cdot Nskin - .0296 \text{ if } type = 4 \\ .0152 \cdot Nskin - .016 \text{ if } type = 5 \end{array} \right. \qquad qt := \left| \begin{array}{l} .2226 \cdot Ntip \text{ if } type = 1 \\ .2226 \cdot Ntip \text{ if } type = 2 \\ .4101 \cdot Ntip \text{ if } type = 3 \\ .5676 \cdot Ntip \text{ if } type = 4 \\ .5676 \cdot tsfp \text{ if } type = 5 \end{array} \right.$$

$fs = 0.586 \text{ tsf} \qquad qt = 12.303$

$$PLcalc := \frac{.25 \cdot qt \cdot D}{[fs + unitweight \cdot D \cdot .25 \cdot (1 - ap)]} \qquad PLcalc = 16.621 \text{ ft}$$

$$Qb := fs \cdot \pi \cdot D \cdot PLcalc \qquad W := \frac{\pi \cdot D^2 \cdot PLcalc \cdot unitweight}{4} \qquad Qp := \frac{qt \cdot \pi \cdot D^2}{4} \qquad I := W \cdot ap$$

$Qb = 96.896 \text{ Tons} \qquad W = 6.545 \times 10^3 \text{ Tons} \qquad Qp = 96.896 \text{ Tons} \qquad I = 6.545 \times 10^3 \text{ Tons}$

$NettUpwardForce := I + Qp \qquad NettUpwardForce = 6.642 \times 10^3 \text{ Tons}$

$NettDownwardForce := W + Qb \qquad NettDownwardForce = 6.642 \times 10^3 \text{ Tons}$

Figure 5-3 Screen shot of the MathCAD file showing plug height, upward force, and downward force calculations.

Table 5-1 Fixed Parameters in Study, and Values

Parameter	Value
Soil Type	Silt
Pile Material	Concrete
SPT N Value for Skin	25-blows
SPT N Value for Tip	30-blows
Pile Length	80-ft

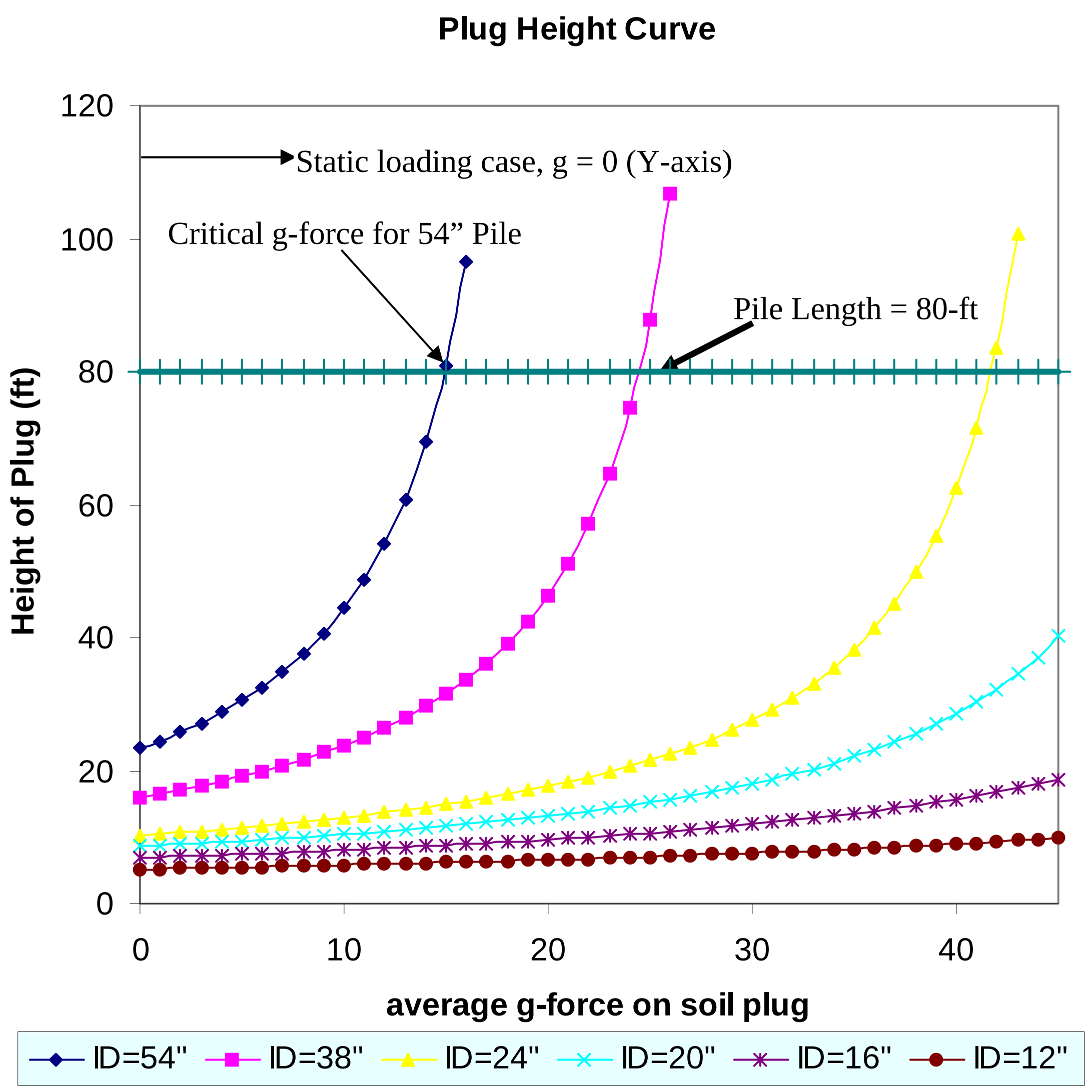

Figure 5-4 Variation of plug height with soil plug diameter and g-forces.

a 38” vs. a 24” diameter pile (below 22 gs vs. below 42 gs). Note, the small difference in pile diameter changes, but the large differences in soil column acceleration levels required for plugging. The latter is due scale effects in the mass computation, i.e., pile diameter is squared.

A line labeled “critical g-force value” in Figure 5-4, identifies if a particular size pile will plug. At g-force values above the critical g-force value there is no “plugging,” or the pile will "cookie cut" into the soil mass. At soil column accelerations level below the critical g-force value, the soil within the pile "plugs," i.e., attaches to the inside of the pile and both move as one mass. The length of the latter plug is directly proportional to the g-force that the soil column experiences during the driving process (Fig. 5-4). Shown in Table 5-2 are the critical soil column accelerations, for various pile diameters, in which the soil will remain "unplugged" during driving.

Table 5-2 Critical g-force Values with Diameter

Soil Plug Diameter	Critical g-force Value
54-inch	15-g
38-inch	24-g
24-inch	42-g
20-inch	<45-g
16-inch	
12-inch	

Of interest, is the typical acceleration levels that the "plugged" soil mass could experience during pile driving. The latter is very much impacted by the type of pile being driven, i.e., concrete vs. steel. Both the allowable stresses and the particle velocities for each are quite different with concrete being much lower than steel. For this research, various diesel and air steam hammers were investigated along with different pile sizes, cushions, and soil descriptions. Generally, in the case of prestressed concrete piles, average pile accelerations from 40 to 60 gs were observed for piles driven with FDOT 455 specifications. However, in the case of steel piles, much higher gs, i.e., over 100 were observed. The latter is in agreement with open literature data reported by Stevens (1988). Stevens (1988) reports measured pile accelerations ranging from 160 to 215g when driving large diameter offshore steel piles.

Evident, large diameter steel pipe piles are far less likely to plug than similar diameter concrete piles during driving even when driven into the same material. Also as shown in Figure 5-4, the required plug heights to mobilize the full static tip resistance, i.e., $Q_t = q_{tip}$ Across, are small (largest is 25 ft, 54”), suggesting the use of total pile area in Qt calculations is reasonable.

To shed more light on the potential for soil “plugging” under static load testing (i.e., not driving), a FEM study of a pile “slowly” penetrating a viscous material (i.e., soil) was undertaken. A brief description of the model is presented before the parametric study (varying soil strength, pile diameter, etc.).

5.4 ADINA MODELING

The pile model was described, including the geometry of the model, material properties, boundary conditions and loads using the pre-processor ADINA-IN and analyzed using the structural analysis program ADINA of the AUI System (i.e., ADINA User Interface).

5.4.1 General Overview of the Pile Model

The pile was modeled with two-dimensional, nine node, axisymmetric Isoparametric solid elements. The axisymmetric element analyzes one radian of the system and assumes there is no variation in the hoop (theta) direction.

A Local Cartesian coordinate system was used in defining the model points. The pile had two degrees of freedom, translation in the yz-plane. The points were then bound together using a vertex surface to define the pile. A vertex surface is one whose geometry is defined by points (unlike a patch surface whose boundary is defined by lines). The sides of the pile coming in contact with the soil were defined as fluid-structure boundaries (section 5.4.3).

5.4.2 Material Model of the Pile

An elastic isotropic material (i.e., Hooke's Law) was used to describe the pile. The two material constants required to define the constitutive relation were E (i.e., Young's Modulus), and ν (i.e., Poisson's Ratio).

5.4.3 Properties of the Pile

The model pile was assigned values based on data from the St. Georges Island project. The average penetration of the pile was taken to be roughly 0.4inch/sec, which is comparable to the soil penetration rate recommended for deep, quasi-static penetration tests of soil (0.4-0.8 inch/sec, ASTM 1979). Further, a range of values was chosen for the pile property as to carry out a parametric study. This study was used to find out the factors impacting the formation of a plug within the pile as a load test is performed. Table 5-3 summarizes the properties of the pile and the variations.

Table 5-3 Pile Properties and Its Variations

Pile Property	Actual Model	Parametric study Model
Pile Length	80 ft	80 ft
Outer Diameter	54 inch	36 inch - 60 inch
Shell Thickness	8 inch	10 inch - 6 inch
Young's Modulus	6300 ksi	6300 ksi
Poisson's Ratio	0.15	0.15
Unit Weight	150 pcf	150pcf
Rate of Penetration	0.5 inch/sec	0.3 inch/sec - 0.5inch/sec

5.4.4 Pile Modeling

For this study, the pile remains stationary, and is represented with a Lagrangian coordinate system. In order to recreate the pile penetration process, the top end of the pile, Figure 5-5,

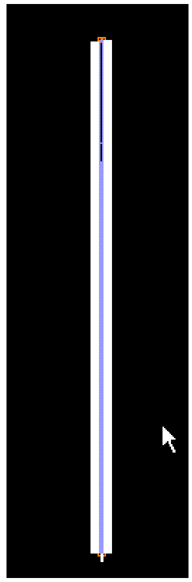

Figure 5-5 ADINA pile input, thick lines indicating contact surface.

was held fixed and the soil was modeled with a viscous fluid flowing past the pile from the bottom up. An upward traction of 100 psf was applied to the viscous fluid to result in a pile-soil relative movement of .5 inch/sec (section 5.3.3).

5.5 ADINA-F THEORY AND MODELING

The soil properties, boundary conditions, and pile loading were modeled using the ADINA-F (i.e., ADINA-Fluid) feature of the AUI system. The soil boundary was chosen larger than 7.5 times the pile diameter so as to avoid boundary effects as suggested by Vipulanandan et al. (1989).

5.5.1 General Overview of the Soil Model

The soil was assumed to be an viscous axisymmetric two-dimensional steady state flow problem, where the soil particles move along streamlines around the pile as modeled by Azzouz and Baligh (1989). A total of five vertex surfaces were used to define the soil mass.

5.5.2 Material Model of the Soil

Initially the "constant property" model was used to define the soil mass. Variations were later made in the properties of the soil so as to carry out a parametric study. For instance, the loose and dense sand behavior of soil was modeled using the compressible and incompressible flow types. 561 nodes were used in defining the entire soil mass.

5.5.3 Boundary Condition

A no slip boundary condition was applied along the pile soil interface so as to introduce shearing action between the pile and soil (surface 1, 2, and 3) in Figure 5-6. A slip surface was also introduced on the boundary surfaces at the edges of the soil mass (labeled 4 and 5) in Figure 5-6.

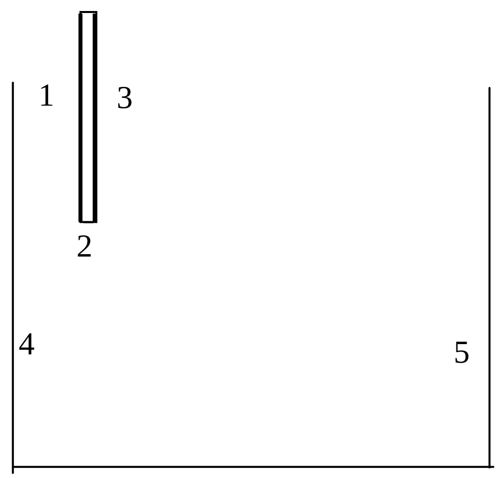

Figure 5-6 Figure showing the slip and no slip surfaces along the various boundaries.

5.5.4 Properties of the Soil

As identified by Chow (1981), the soil was modeled as a viscous fluid and was assigned a range of fluid dynamic shear strengths ranging from 500 pa-sec to 2000 pa-sec, Table 5-4. The latter have mohr-coulomb angles of internal friction of 28 to 35 degrees. Table 5-4 summarizes the properties of the soil and the range of values chosen for carrying out a parametric study.

Table 5-4 Soil Properties and Its Variation

Soil Property	Actual Model	Parametric Model
Unit Weight	100 pcf	80 pcf-120 pcf
Friction Angle/Dynamic Shear Strength	28 degree/ 500 pa-sec	28 degree/500 pa-sec – 35 degrees/2000 pa-sec

5.5.5 Soil Modeling

As identified earlier, the soil particles are flowing by the pile, and undergo large displacements, which are represented by a Eulerian coordinate system, Figure 5-7. In the Eulerian formulation, the mesh points are stationary and the soil particles move through the finite element mesh in the prescribed direction. In this formulation, attention is focused on the motion of the material through a stationary control volume from which equilibrium and mass continuity of the soil particles is maintained.

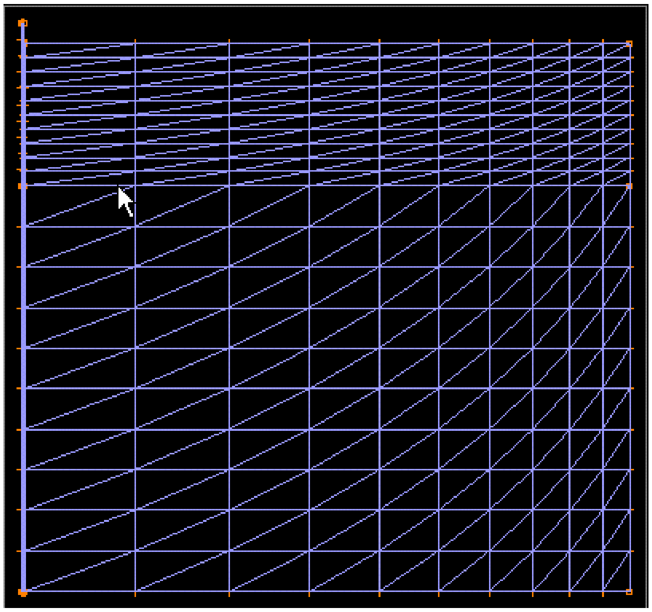

Figure 5-7 Showing an ADINA-F soil mesh.

5.6 ADINA-FSI THEORY AND MODELING

The ADINA pile model and the ADINA-F soil model are merged together using the ADINA-FSI (i.e., Fluid Structure Interaction) feature. In FSI, the fluid forces (soil) are applied onto the solid (pile), and the solid deformation changes the fluid (soil) domain. The pile was based on the Lagrangian coordinate system, and the soil was modeled using the Eulerian coordinate system. For the FSI model, the coupling was brought about based on the arbitrary-Lagrangian-Eulerian (ALE) coordinate system.

5.7 ADINA PLOT

The results of the ADINA-FSI were then viewed using the post processor ADINA-PLOT. Figure 5-8 shows the plot files for both pile (ADINA) and soil (ADINA-F).

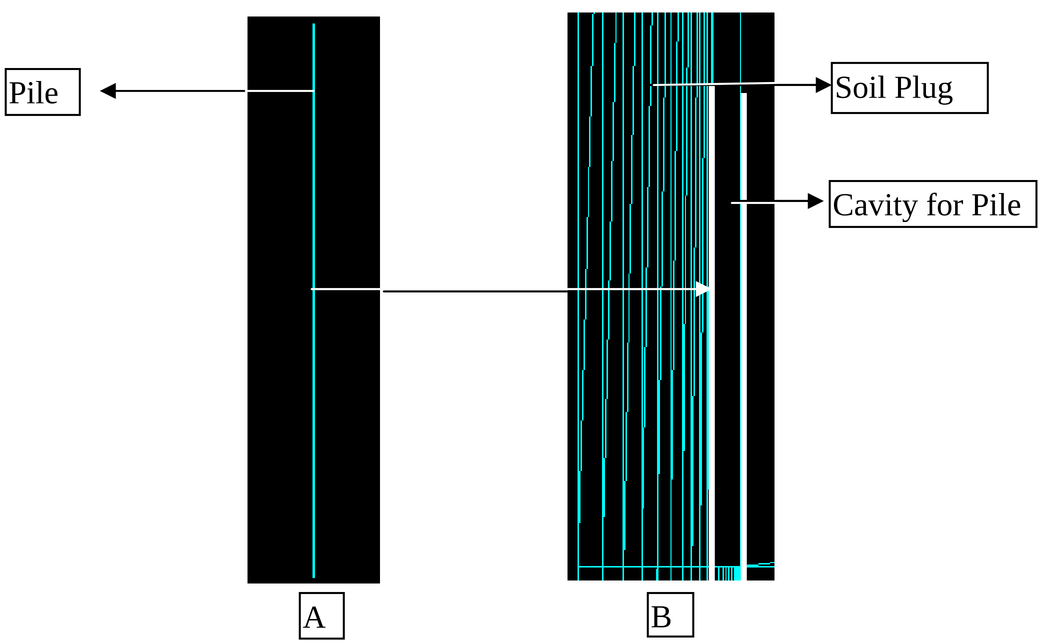

Figure 5-8 A) Plot of the pile as generated by ADINA, B) Plot of the soil mass as generated by ADINA-F, showing the cavity where the pile is placed in the ADINA-FSI model.

In order to perform an analysis, the Preprocessor (ADINA-In) was used to vary model input, ADINA-F (fluids) was run in conjunction with ADINA (pile), by ADINA-FSI and the output was viewed with ADINA-PLOT, as shown in Figure 5-9.

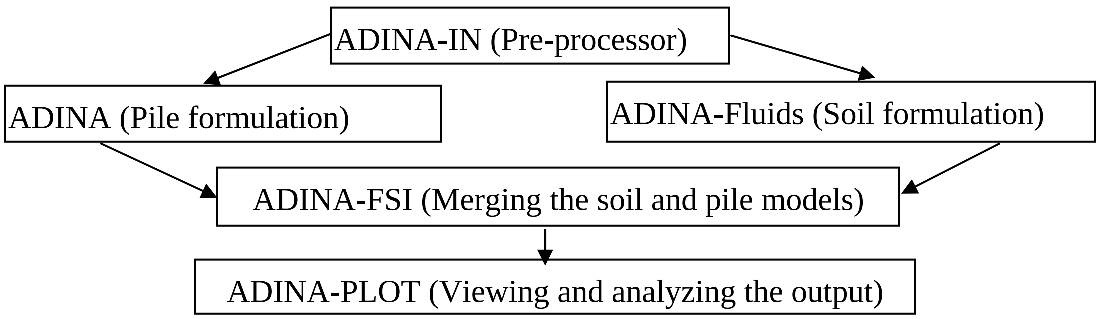

Figure 5-9 Flow chart indicating the various steps in the analysis of the plug.

Of interest is the onset of soil “plugging” within the pile cylinder as the pile moves downward. To demonstrate the latter, two plots showing both the “un-plugged” and the “plugged” condition, are presented, along with velocity profile of the soil around the pile. The plots were made using ADINA-Plot, and a 32-color scheme option. Figure 5-10 shows an axisymmetric pile section during the unplugged stage (pile has penetrated 16’ of 80’ length). The black rectangle within the plot area is pile wall (velocity not shown). The soil directly adjacent to the pile has the highest velocities (viscous shear). Evident, is that the pile and the small zone of soil directly adjacent is moving down with similar velocities, indicated by the blue color profile (top end of the color scheme). However, the soil within the pile is moving with a much smaller velocity (lower end of the spectrum), indicating a large relative velocity between the soil plug and the pile, signifying that the pile has not plugged.

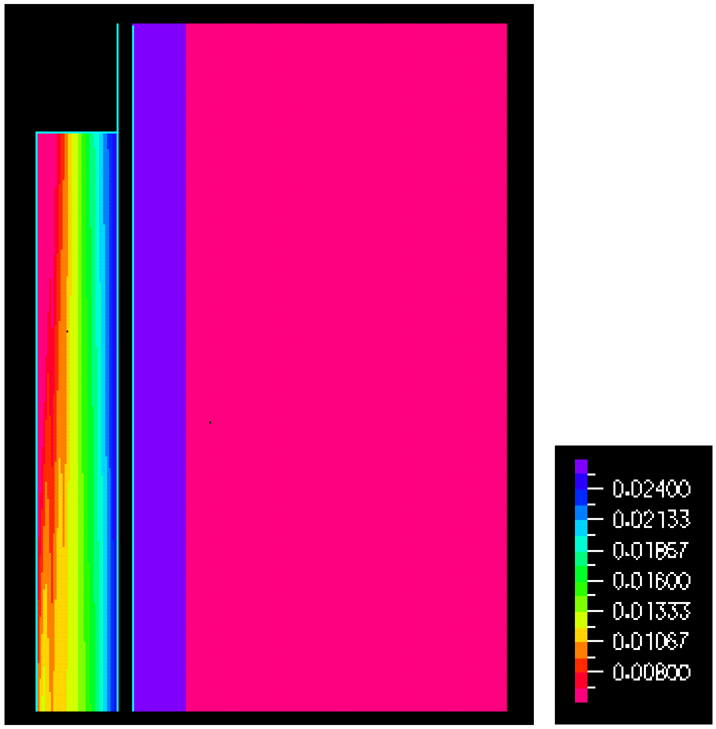

Figure 5-10 Velocity profile with in cylinder pile - unplugged condition.

Presented in Figure 5-11, is the same pile section, which has penetrated 70 ft of soil (pile is 80 ft long) and has 70 ft of soil within the pile cylinder. At this stage, a uniform velocity has been attained for the soil inside and outside the pile. At this stage, the pile, and the soil within, has almost zero relative velocity indicating formation of soil plug (pile and soil plug moving together). Note the difference in soil velocities between “unplugged” (Fig. 5-10) and “plugged” (Fig. 5-11). Also of interest in Figure 5-11 (plugged) are small non-uniform velocity zones within the soil plug, possibly suggesting the arching phenomenon (Fig. 5-1) put forth by Paikowsky (1990).

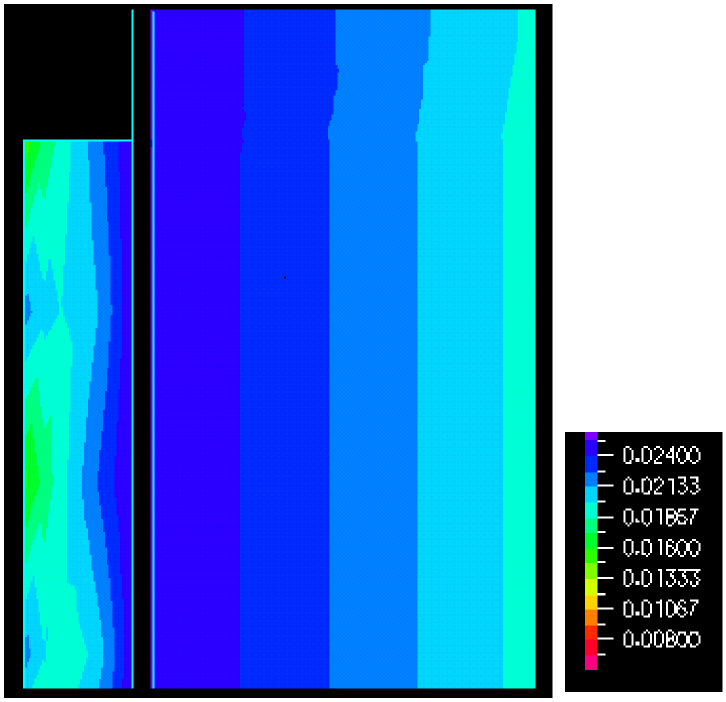

Figure 5-11 Velocity profile with in cylinder pile - plugged condition.

5.8 PARAMETRIC ADINA STUDY

In order to estimate the factors impacting the length of the soil plug, the following soil and pile parameters were each varied to identify their effect on soil “plugging” condition (i.e., height of plug):

1. Shell thickness.
2. Rate of pile penetration.
3. State of Soil (loose or dense).
4. Dynamic shear strength of soil.

5.8.1 Influence of Shell Thickness

Shown in Figure 5-12 are three different analysis of the St. Georges Pile (80’ total length) with three different pile wall thickness: 6”, 8”, and 10” and a constant outer diameter 54”. The soil was modeled as both compressible (loose) and incompressible (dense) states with an angle of internal friction of 30 degrees.

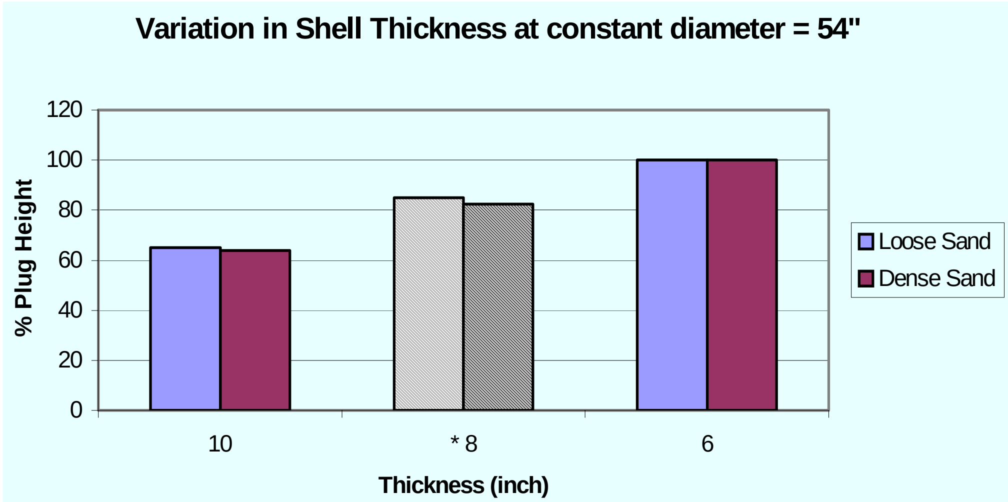

* Indicates standard pile used for comparison.
Outer Diameter = 54”, Shell Thickness = 8”, Unit Weight = 100 pcf,
Dynamic Shear Strength/Friction angle = 1000 pa-sec/30 deg,
Rate of Penetration = 0.5inch/sec.

Figure 5-12 Plot showing variation of shell thickness with height of soil plug.

The results observed in Figure 5-12 are in accordance with Kindel’s theory that, plug movements tend to stabilize faster with increased pile wall thickness (Paikowsky et al. 1990). One possible explanation of this phenomenon is that the larger the wall thickness, the larger the soil mass displaced by the pile, and the large the mass which will attempt to flow into the pile, leading to soil “plugging.” Note, the hatched region in Figure 5-12 indicates the pile used at the St. Georges Island Bridge Replacement Project. Also evident, both the loose and dense sands have similar response to wall thickness variations.

5.8.2 Rate of Pile Penetration

Of interest is the effect the rate of loading (pile load test) on soil “plugging.” Parametric study was carried out with rates varying from 0.3 inch/sec to 0.5 inch/sec. Again the study was carried out on the 54” St. Georges pile, but with three different pile velocities: 0.5, 0.4 and 0.3 in/sec.

Evident from Figure 5-13, the slower the pile penetration rate (i.e., 0.3 in/sec vs. 0.5 in/sec), the quicker the pile plugs. The latter may be attributed to either higher shear strength under slower penetration rates or possibly smaller shear stresses developed under slower the pile penetration rates.

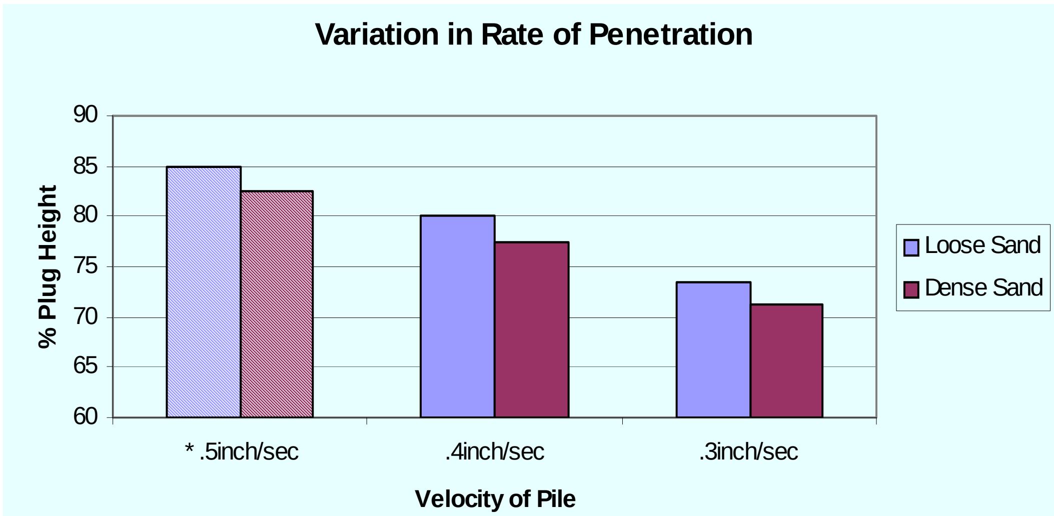

* Indicates standard pile used for comparison.
Outer Diameter = 54”, Shell Thickness = 8”, Unit Weight = 100 pcf,
Dynamic Shear Strength/Friction angle = 1000 pa-sec/30 deg,
Rate of Penetration = 0.5 inch/sec.

Figure 5-13 Variation in rate of penetration.

5.8.3 Variation in Soil Shear Strength

Also of interest is the influence of soil shear strength on soil “plugged” heights. Again the St Georges 80 ft pile with an 8” wall thickness was inserted at a 0.5 inch/sec penetration rate. The soil was modeled with an angle of internal friction of 27.5 to 35 degrees in 2.5-degree increments. Shown in Figure 5-14 are the “plugged” heights (i.e., zero relative velocity) in the pile. Evident from the figure, the friction angle has a strong influence on plug height. For instance, the plug heights went up 40% when the friction angle was reduced from 35 degrees to 27.5 degrees.

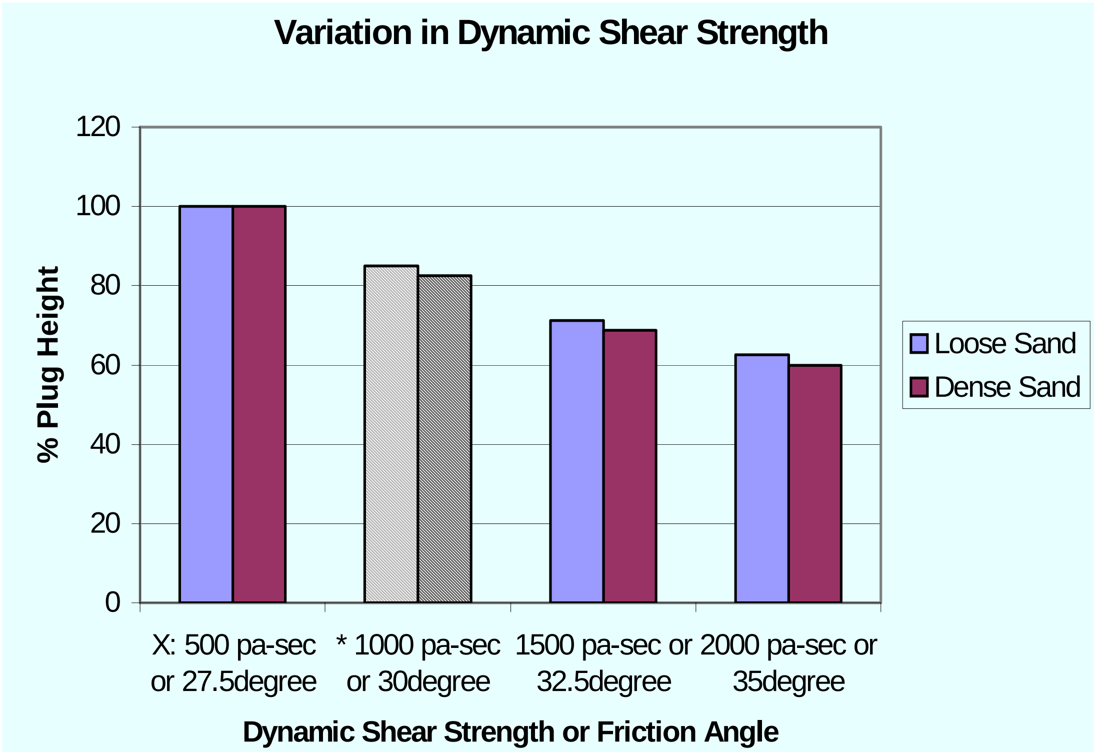

* Indicates standard pile used for comparison.
Outer Diameter = 54", Shell Thickness = 8", Unit Weight = 100 pcf,
Dynamic Shear Strength/Friction angle = 1000 pa-sec/30 deg,
Rate of Penetration = 0.5 inch/sec.

Figure 5-14 Variation in friction angle or dynamic shear strength.

5.9 SUMMARY

In assessing the axial capacity of driven open-ended cylinder piles from insitu data, the cross-sectional area for end bearing calculations, i.e., ring area of cylinder or total cross-sectional area is needed. Past approaches for assessing the latter was by measuring the height of soil columns within piles driven into representative soil formations (i.e., sand, clays, etc.). However, observations on the large diameter cylinder piles show that the piles "cookie cut" instead of plugging in all of the formations for which data were available.

Subsequently, an analysis of the forces on the soil column during driving and static loading was undertaken. Specifically in the case of driving, the analysis focused on the magnitude of skin friction force necessary for the soil column to be considered plugged or attached to the inside of the pile. To be considered attached (section 5.2), the soil's plug diameter had a significant impact on the magnitude of inertia forces acting on it. For instance, piles with diameters of 24" and smaller, required plug accelerations over 40 to 60 gs to overcome skin friction. Whereas for 54" outside diameter, and an 8" wall thickness, only 15 gs (Fig 5-2) of soil plug acceleration was needed to overcome skin friction on the inside of the pile. Typical prestressed concrete pile accelerations in the literature have been reported at 40 to 60 gs and in the case of steel piles they have accelerations well over 100gs (Stevens, 1988).

Since large diameter cylinder piles may not be plugged during driving, the question was if they would act plugged under static loading. Since the dynamic inertia forces would go to zero, only the skin resistance along the soil column and its own weight would resist the static resistance at the bottom of the soil pile tip, Qt. Finite element analysis of the quasi-static load-scenario, suggest, for typical pile wall thickness and soil strengths considered, as well as the rate of loading that the possibility of soil "plugging" was feasible. Moreover, even in the case of non-plugged scenarios (Figs. 5-10), the soil motion near the inside wall of the pile were zero and increasing outward. Suggesting significant shear stress at the pile-soil interface and decreasing inward. Consequently, it was believed that the end-bearing analysis needed to consider both the full cross-sectional area as well as the pile's ring area.

CHAPTER 6

SKIN FRICTION AND END BEARING CURVES

6.1 UNIT SKIN FRICTION AND UNIT END BEARING CURVES

For each load test which reached FDOT failure, the total resistance was separated into unit skin friction and end bearing (as discussed in Chapter 4), and plotted against the uncorrected blow counts (N), as a function of soil type and pile material. Subsequently, best-fit (regression) skin friction and end bearing curves vs. SPT N values for different pile material type were constructed. The five curves developed for skin friction acting on cylinder piles were separated into:

1. Concrete piles in sands.
2. Steel piles in sands.
3. Concrete piles in clays.
4. Steel piles in clays.
5. Concrete piles in silts and mixed type soils.

Three unit end-bearing curves vs. uncorrected SPT N values were developed for large diameter cylinder piles:

1. Piles in Sands.
2. Piles in Clays.
3. Piles in Silts and mixed soil types.

Also, in the case of end bearing, no distinction between pile types (i.e., steel and concrete) was found. The data (steel and concrete) is presented together for each soil type as a function of SPT N values. A discussion of unit skin friction and end bearing versus SPT N values follows.

6.1.1 Skin Friction in Sands

Presented in Figure 6-1 is the unit skin friction (tsf) versus the SPT N (uncorrected) for large diameter concrete cylinder piles driven in sands. Also shown is a linear regression (R^2 = 0.96) fit to the data. Since the line has a small negative offset (N = 0), zero unit skin friction is recommended for SPT N values smaller than 5. A similar approach is used in the FDOT's SPT 97 software for concrete piles in sand.

In the case of large diameter steel cylinder piles embedded in sand, Figure 6-2 shows the measured unit skin friction versus recorded SPT N values. A logarithmic curve is fit to the data with an R^2 = 0.85. Again due to the small negative offset (N = 0), zero unit skin friction is recommended for steel piles embedded in sands with SPT blow counts 5 and less.

A comparison of unit skin friction between concrete and steel cylinder piles (Figs. 6-1 and 6-2), reveal similar unit skin friction for low blow count sands (N < 20). For blow counts higher than 20, the concrete piles generate higher unit skin friction than steel piles.

6.1.2 Skin Friction in Clays

Presented in Figure 6-3 is the measured unit skin friction versus the SPT N (uncorrected) for large diameter concrete cylinder piles driven into clays. A logarithmic curve was fit to the data with an R^2 = 0.94. Figure 6-4 shows the measured unit skin friction versus SPT N (uncorrected) for large diameter steel pipe piles driven into clays. The logarithmic curve fit (R^2 = 0.9) is given in the figure. Note, the unit skin friction for steel piles is smaller than concrete piles for all ranges of SPT N values.

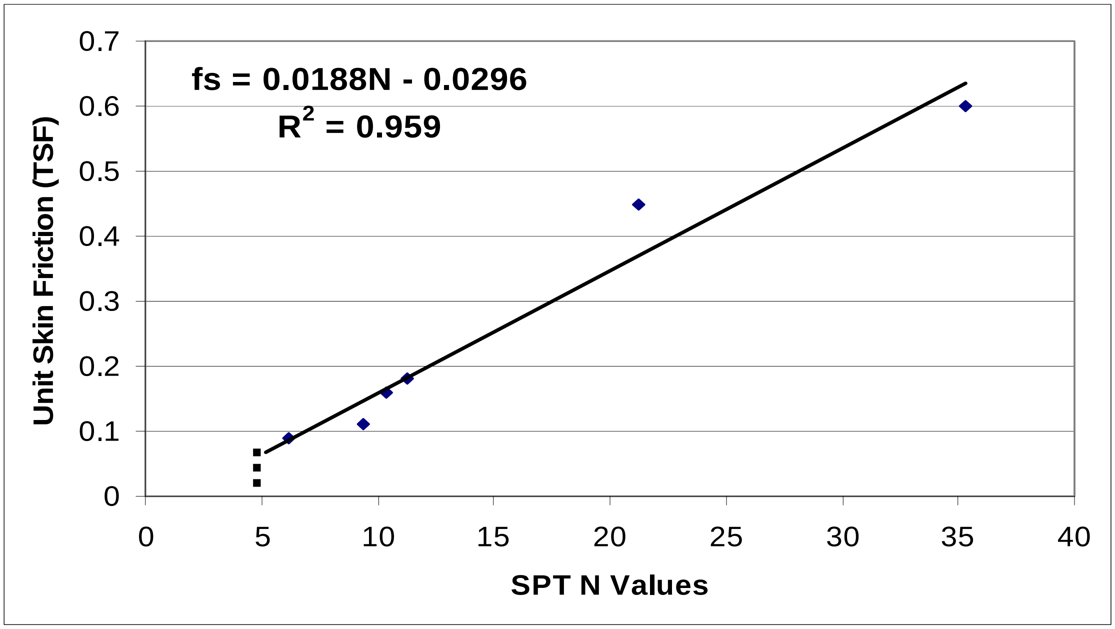

Figure 6-1 Skin friction (tsf) vs. N (uncorrected) for concrete piles in sand.

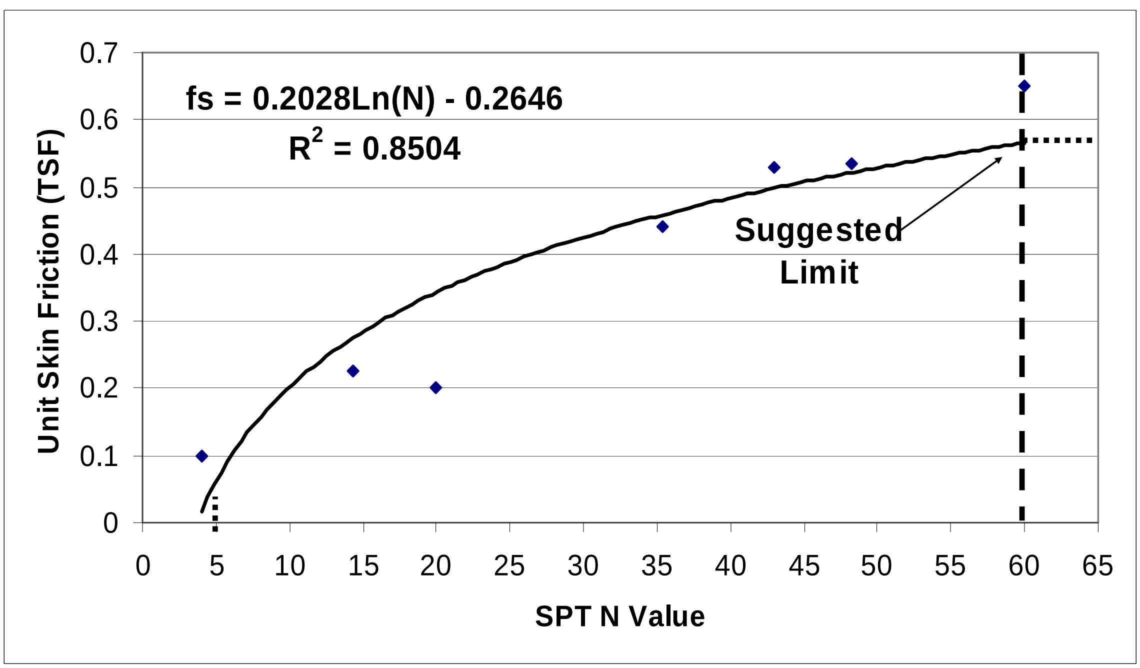

Modified trend line

Suggested limit

Figure 6-2 Skin friction (tsf) vs. N (uncorrected) for steel piles in sand.

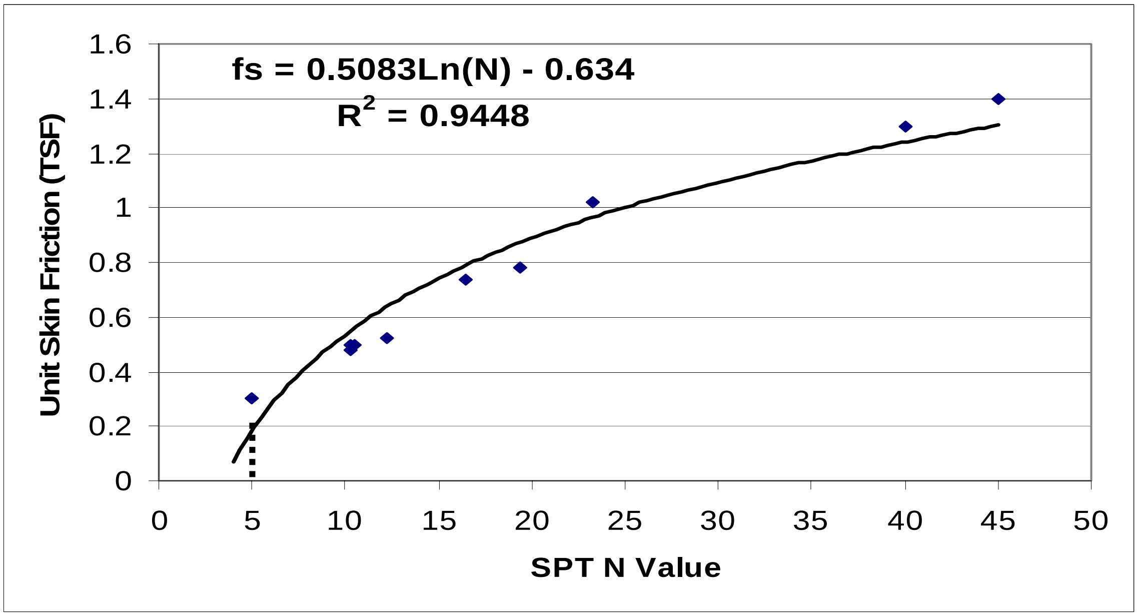

Figure 6-3 Skin friction (tsf) vs. N (uncorrected) for concrete piles in clay.

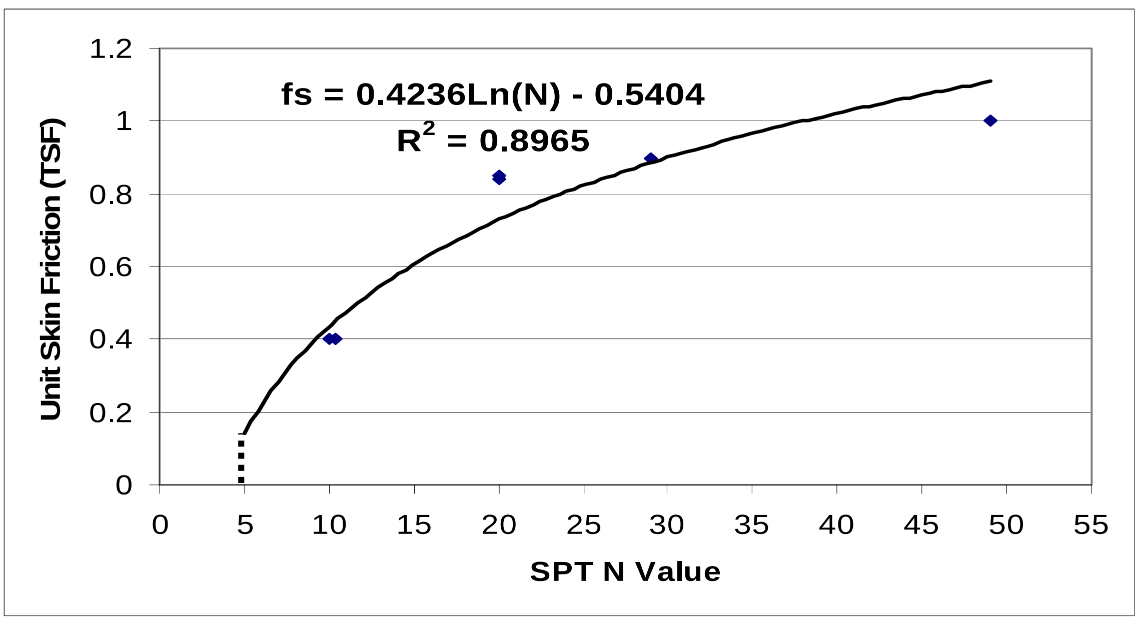

Modified trend line.

Suggested limit.

Figure 6-4 Skin friction (tsf) vs. N (uncorrected) for steel piles in clay.

6.1.3 Skin Friction in Silts

Presented in Figure 6-5 is the back computed unit skin friction for large (> 42") diameter concrete cylinder piles driven into silts. Unfortunately, the database had no unit skin friction values for SPT N values greater than 25. The later portion of the logarithmic curve (R^2 = 0.9) was fit to follow the clay (Fig. 6-3). A comparison of unit skin friction for smaller diameter piles is presented in section 6.2.

6.1.4 End Bearing in Sands

Shown in Figure 6-6 is the unit end bearing versus SPT N values for both steel and concrete large diameter piles driven into sand. Evident, the unit end bearing for both steel and concrete fall on the same trend line (R^2 = 0.88). Also, note a few of the piles (2) had unit end bearing above 50 tsf and SPT N values above 60, the standard cut off in SPT 97. Even though the piles are capable of developing the higher unit bearing for a short period of time (i.e., static load test), under sustained load, creep, associated deformation would ensue. Consequently, a maximum unit end bearing of 35 tsf or SPT N value of 60 is recommended for design (i.e., sustained load, service).

6.1.5 End Bearing in Clays

Presented in Figure 6-7 is the back computed end bearing versus SPT N values for large diameter steel and concrete piles driven into clays. Note, all the recovered data was for steel pipe piles. Also shown is the suggested linear trend line (R^2 = 0.96) for the data. Evident, there is a significant reduction in unit end bearing between the clays and sand (Fig. 6-6 vs. 6-8).

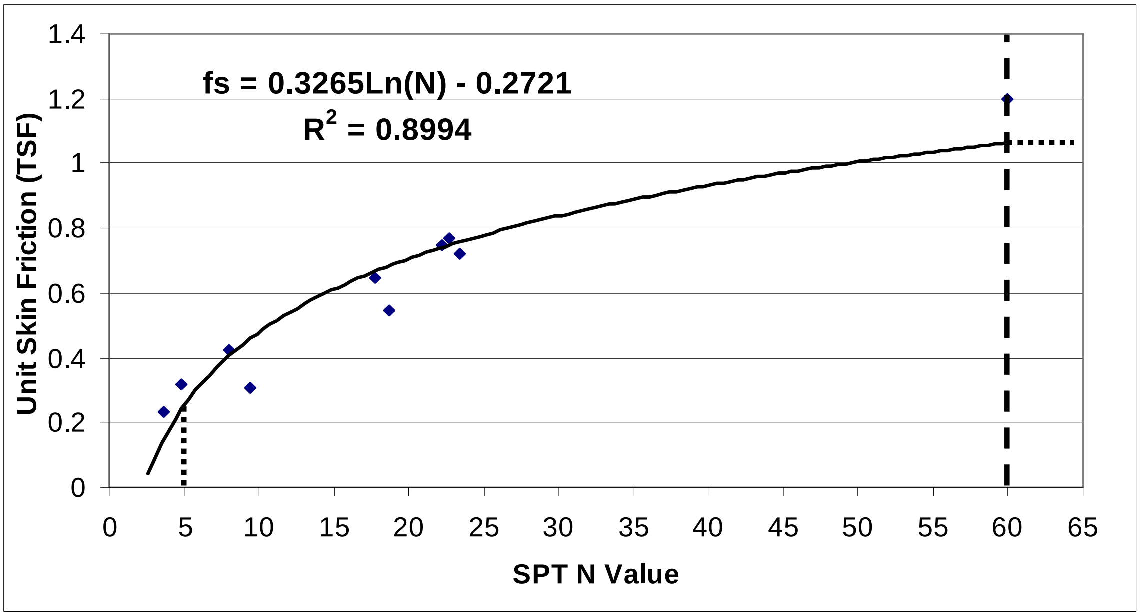

Figure 6-5 Skin friction (tsf) vs. N (uncorrected) for concrete piles in silts.

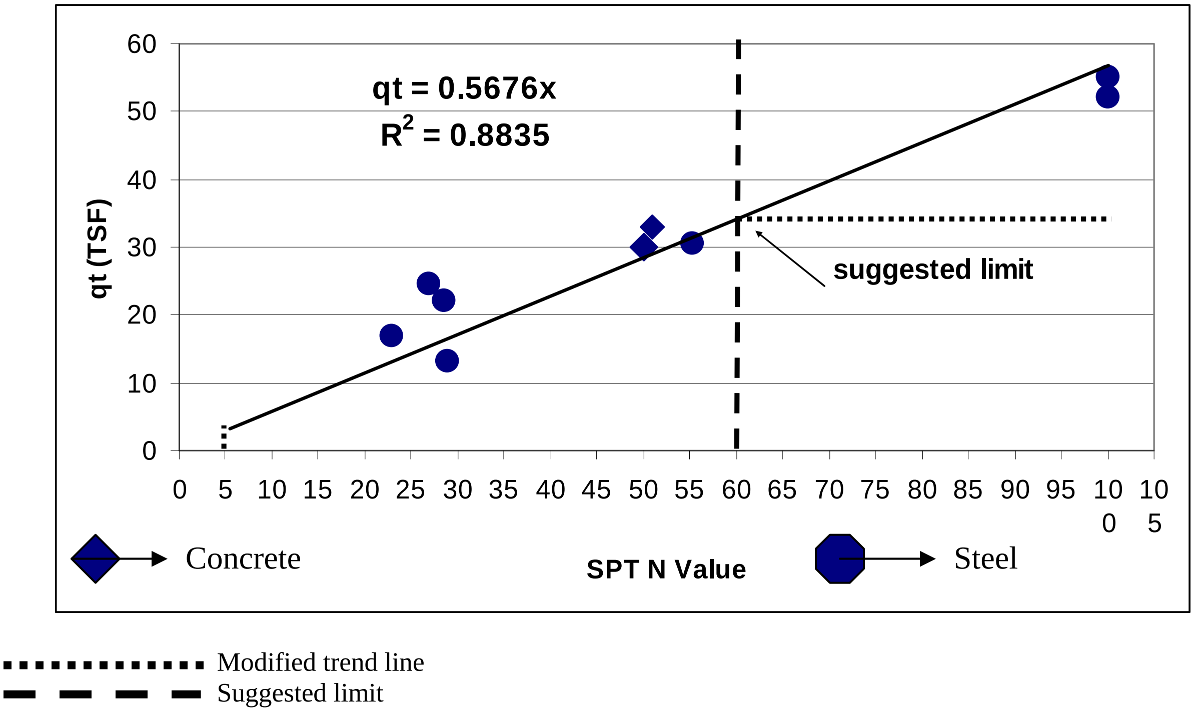

Figure 6-6 End bearing (tsf) vs. N (uncorrected) in sands.

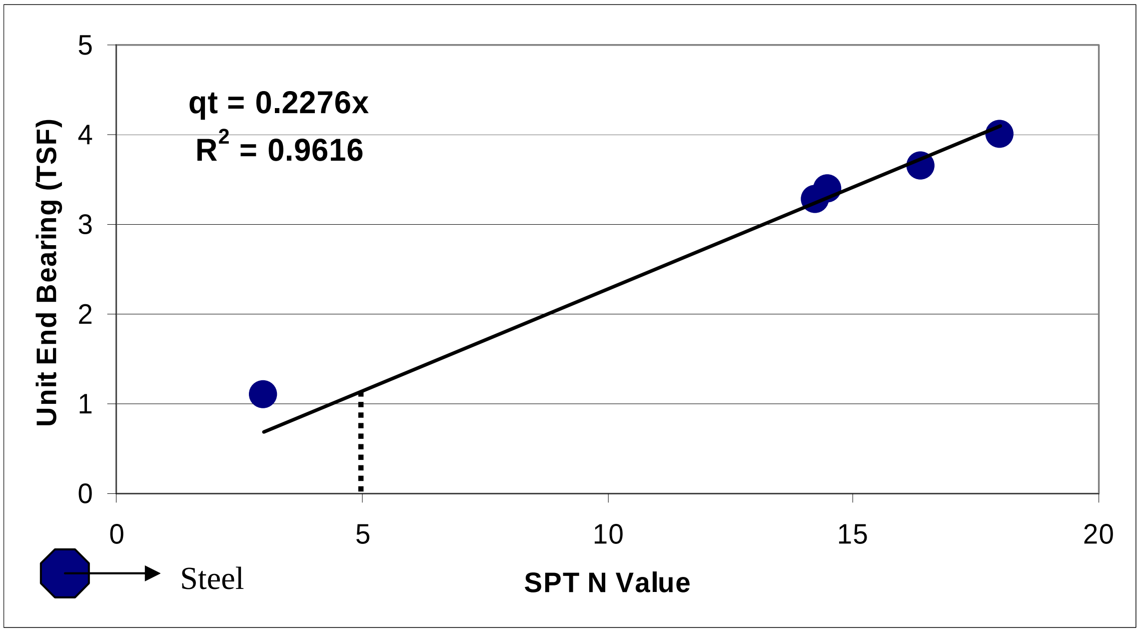

Figure 6-7 End bearing (tsf) vs. N (uncorrected) in clays.

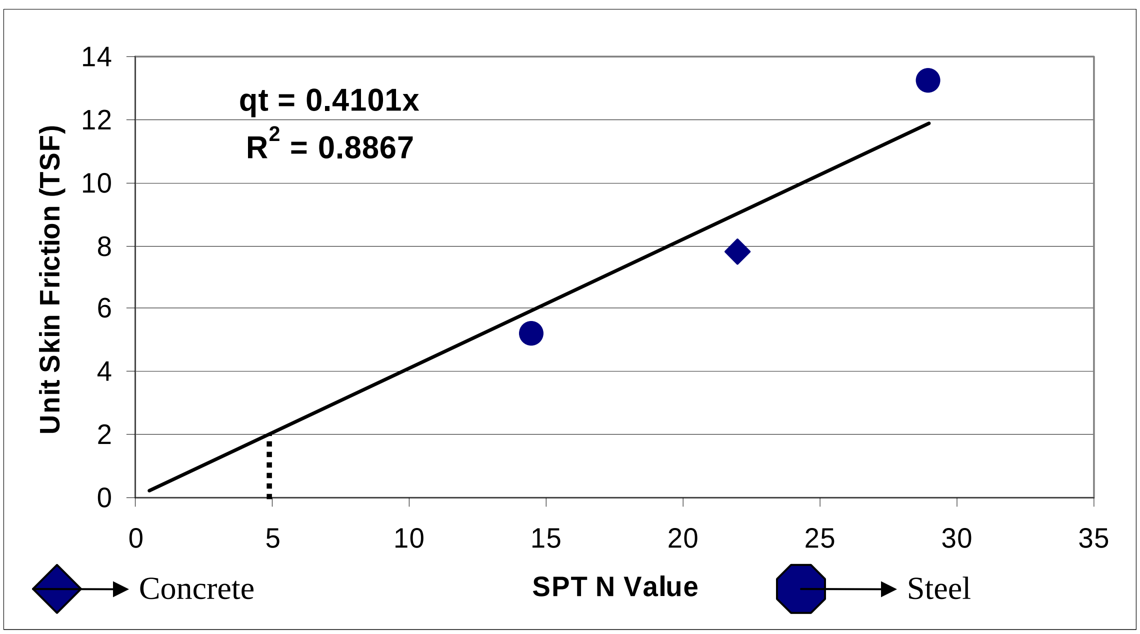

Modified trend line.

Figure 6-8 End bearing (tsf) vs. N (uncorrected) for silts.

6.1.6 End Bearing in Silts

Shown in Figure 6-8, is the back computed unit end bearing versus SPT N values for large diameter concrete and steel piles driven into silts. Both steel and concrete results are given along with a linear trend line (R^2 = 0.89) fitting the data. Comparison of the prediction with clays and sands, show it’s higher than clays, but lower than sands. The latter is in agreement with small diameter results (section 6.2).

6.2 COMPARISON OF SKIN FRICTION AND END BEARING WITH SPT97

Of significant interest, is a comparison of large diameter cylinder pile (steel and concrete) unit skin friction and end bearing with existing small diameter pipe and solid sections found in SPT97. Consequently, six graphs showing unit skin friction vs. SPT N values, and unit end bearing vs. SPT N values for, clays, silts, and sands were generated. Each plot shows four sets of curves representing:

1. SPT97 for small concrete piles.
2. SPT97 for steel pipe piles.
3. Large diameter cylinder pile, concrete.
4. Large diameter cylinder pile, steel.

Presented in Figure 6-9 is the comparison of unit skin friction versus SPT N values for both large diameter cylinder piles and small diameter concrete and steel pipe piles in SPT97 for clays. Evident from the plot, both small and large diameter concrete piles develop similar unit skin frictions in clay. Also, both small and large diameter steel pipe piles generate similar unit skin friction in clays, which are less than concrete piles. Note, for low SPT blow counts ($N < 10$), all pile types (steel & concrete, small and large) develop similar unit skin friction. A possible explanation is remolding or densification due to pile penetration.

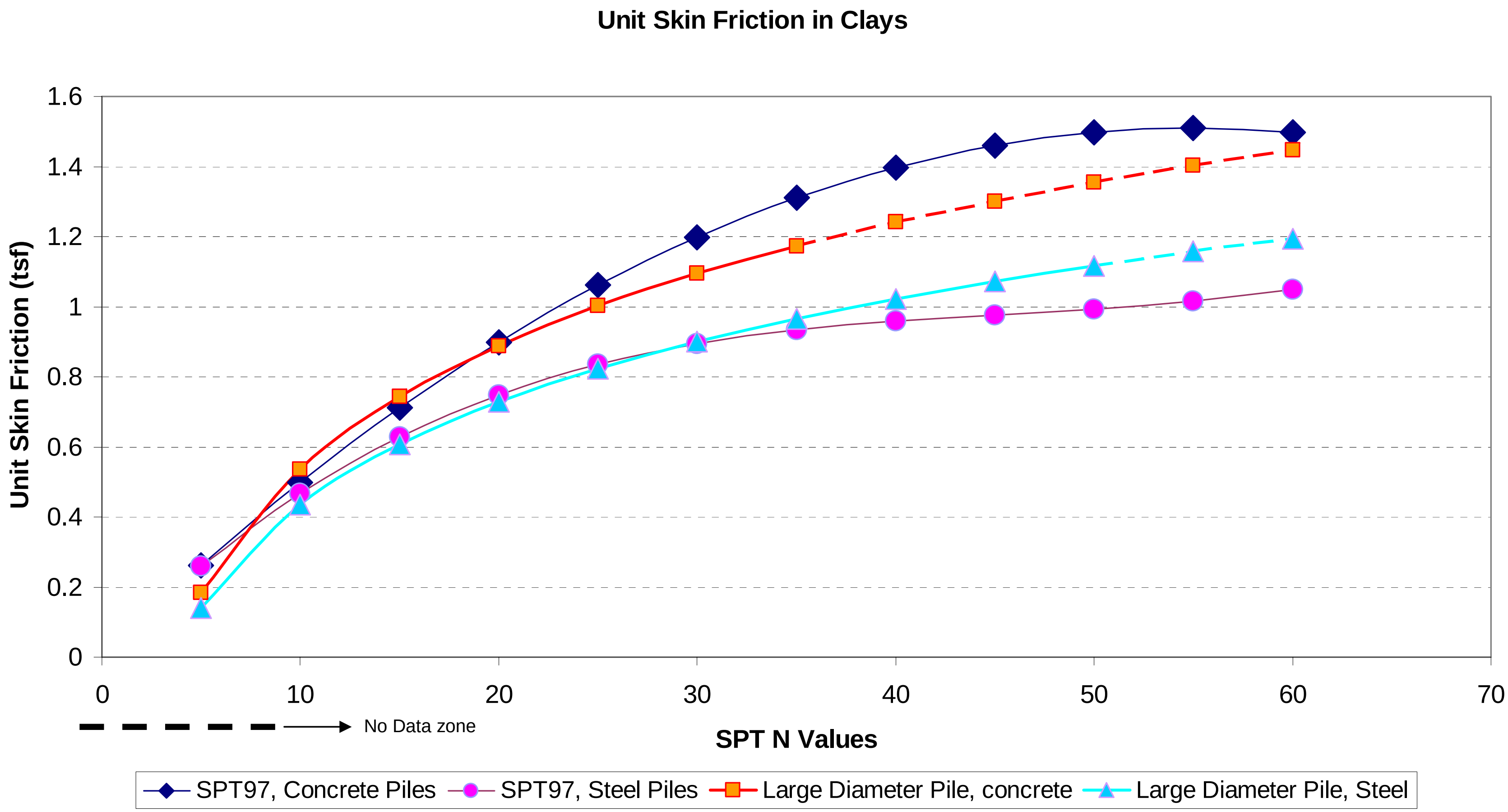

Figure 6-9 Comparison of various designs used for computing unit skin friction in clays.

Shown in Figure 6-10 is a comparison of unit skin friction for both small and large diameter piles driven into silts. The large diameter concrete cylinder piles (Fig. 6-5) agrees with the smaller solid concrete piles (SPT 97) up to a blow count of 25, above which there is no data (i.e., database). Consequently, it was decided to reduce the unit skin friction below the smaller diameter piles for the higher blow count soil. Also shown in the figure is the unit skin friction for small diameter steel piles in silts (SPT 97). Since there is no data available in the database for large diameter steel piles, it is expected they would be equal or slightly lower than the smaller diameter SPT 97 steel values (see Figs. 6-9 and 6-11).

Presented in Figure 6-11 is a comparison of unit skin friction versus SPT N values for all piles driven into sand. Evident both small and large diameter concrete piles have similar unit skin friction. However, in the case of small and large diameter steel pipe piles, the large diameter steel pipes have the lower unit skin friction. As with both silts and clays, the all piles have similar unit skin friction in sands at low blow counts less than 20.

In the case of unit end bearing in clays, both small and large diameter concrete, and steel piles have similar curves, Figure 6-12. However, in the case of silts, Figure 6-13, small solid concrete piles (SPT 97) have the highest unit end bearing, followed by small diameter steel pipe piles, followed by large diameter steel and concrete cylinder piles. The latter is also true for piles driven into sand, Figure 6-14. Small solid concrete piles have the highest unit end bearing, followed by small diameter steel pipe piles, and then large diameter steel and concrete cylinder piles.

Figures 6-15 and 6-16 present the final unit skin friction and end bearing curves vs. SPT N values for large diameter cylinder steel and concrete piles. Chapter 7 presents the computed capacities for the large diameter cylinder piles in the database using Figures 6-15 and 6-16. Based on the measured to predicted capacity values, the LRFD resistance factors, ϕ, are computed as a function of reliability.

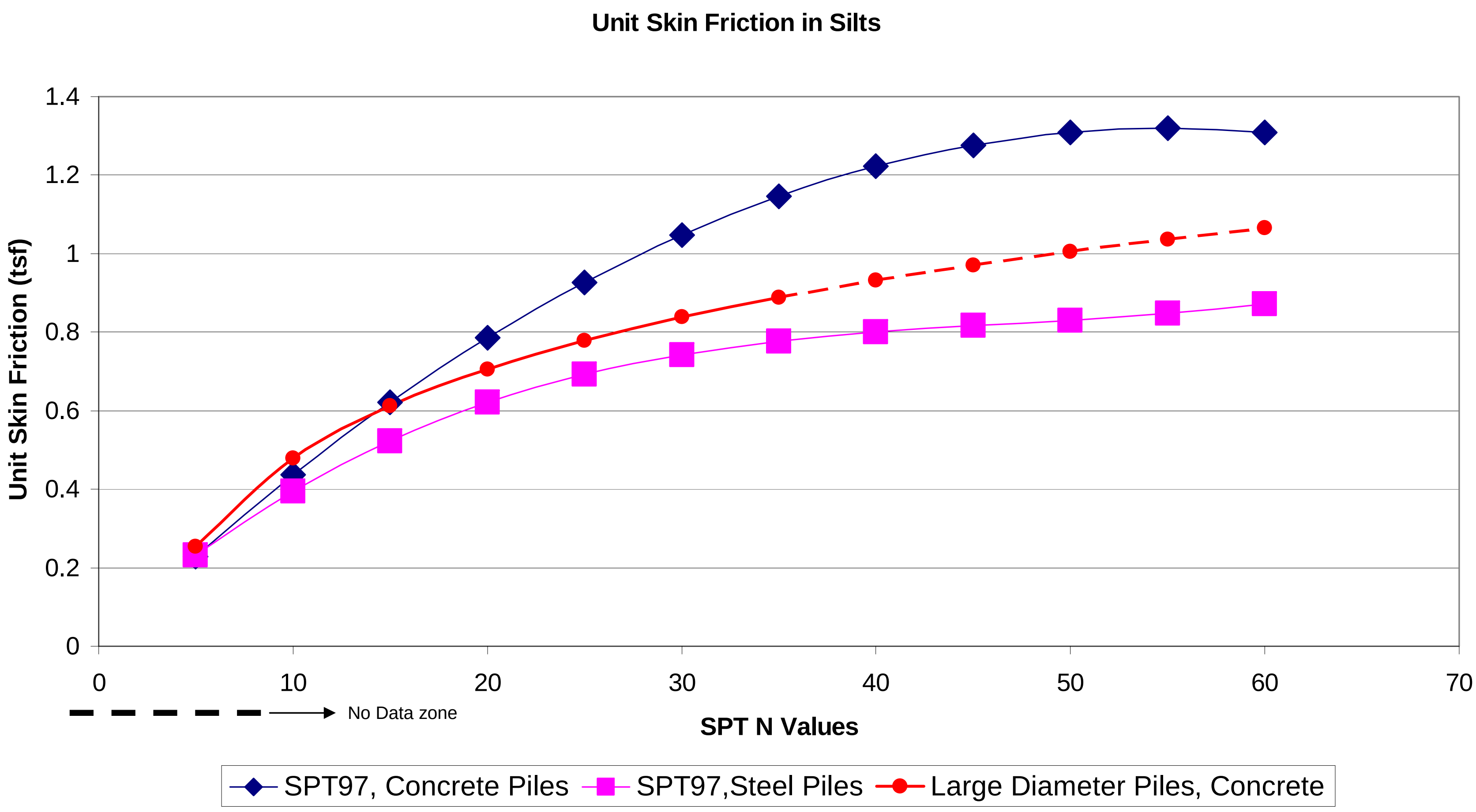

Figure 6-10 Comparison of various designs used for computing unit skin friction in silts.

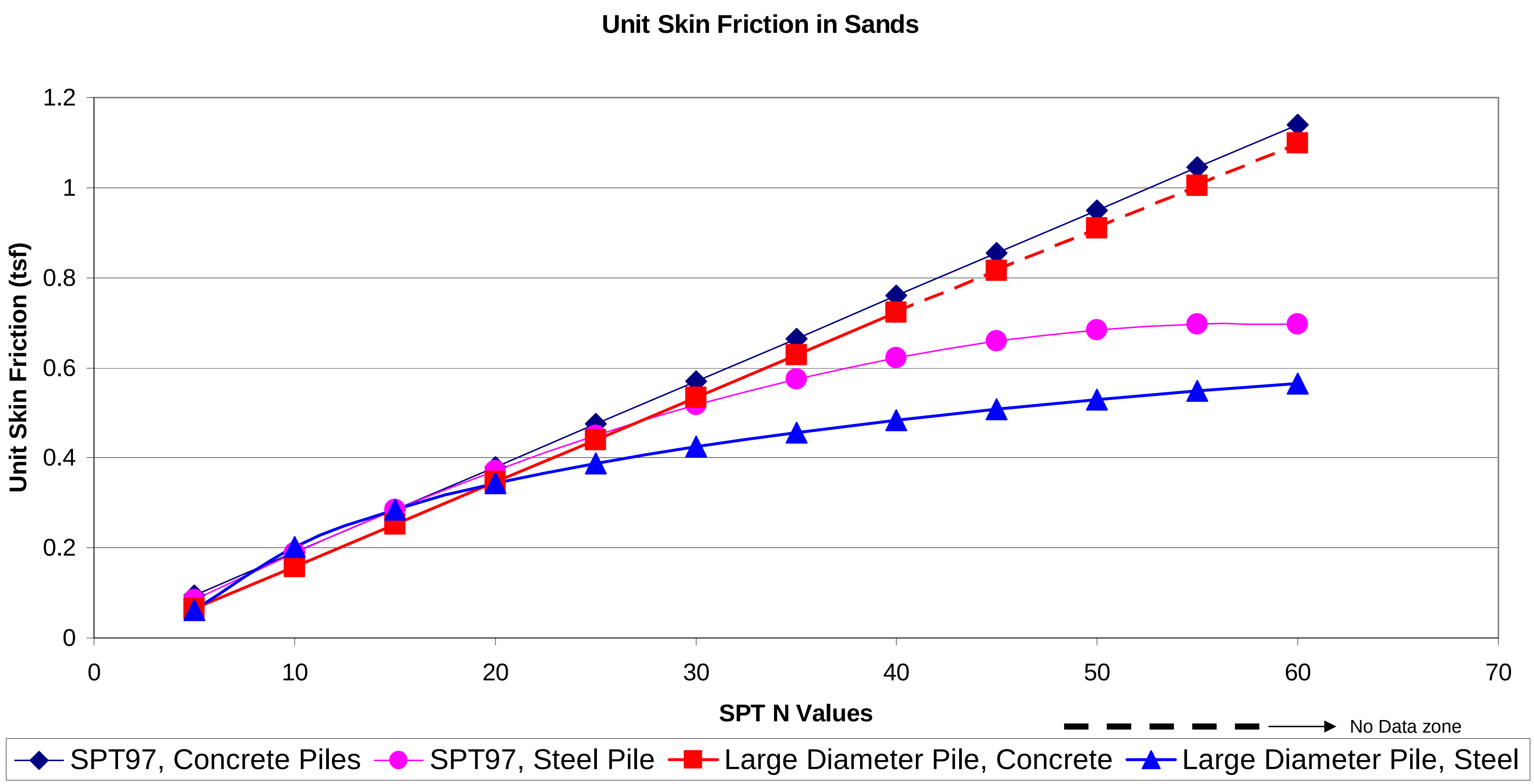

Figure 6-11 Comparison of various designs used for computing unit skin friction in sands.

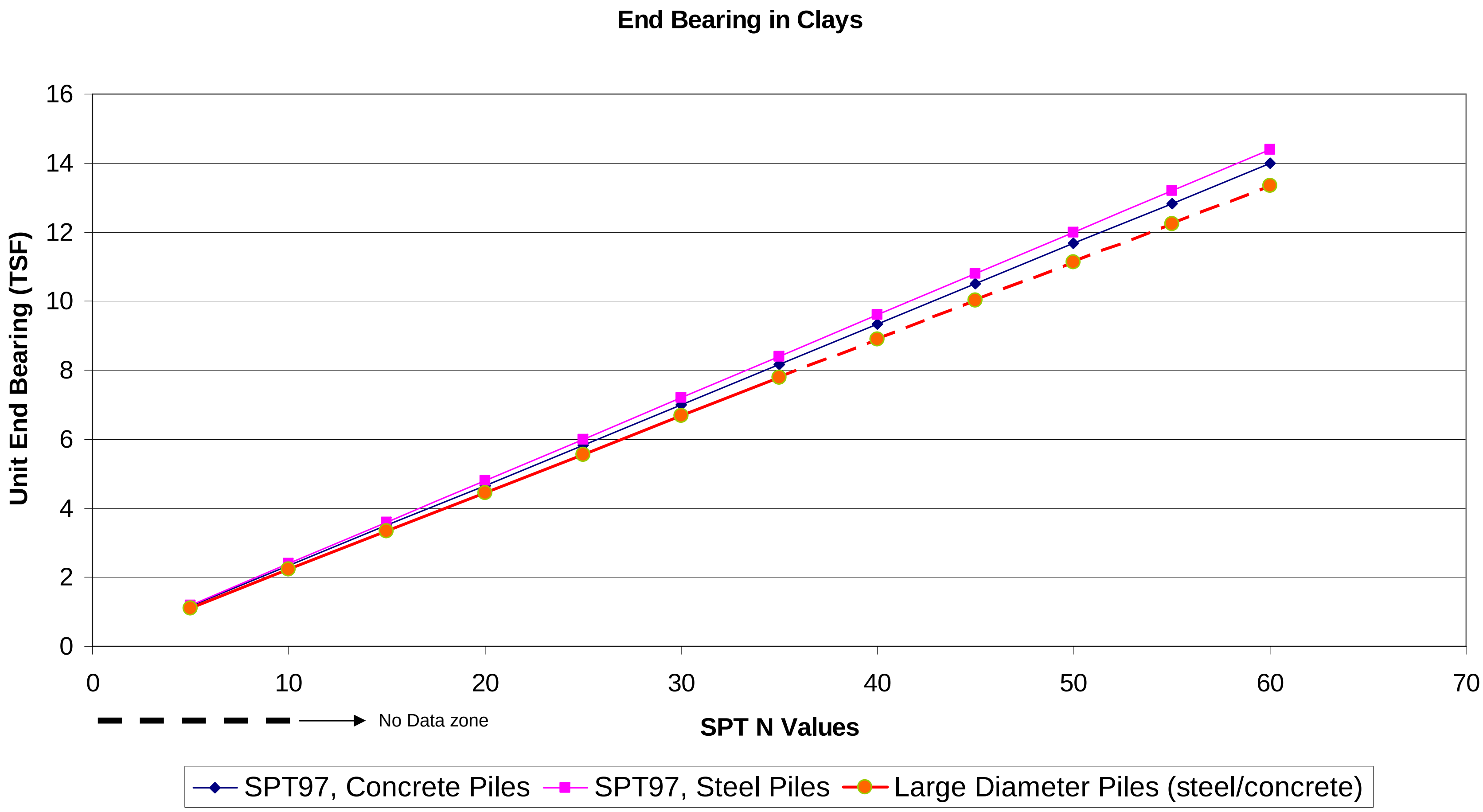

Figure 6-12 Comparison of various designs used for computing unit end bearing in clays.

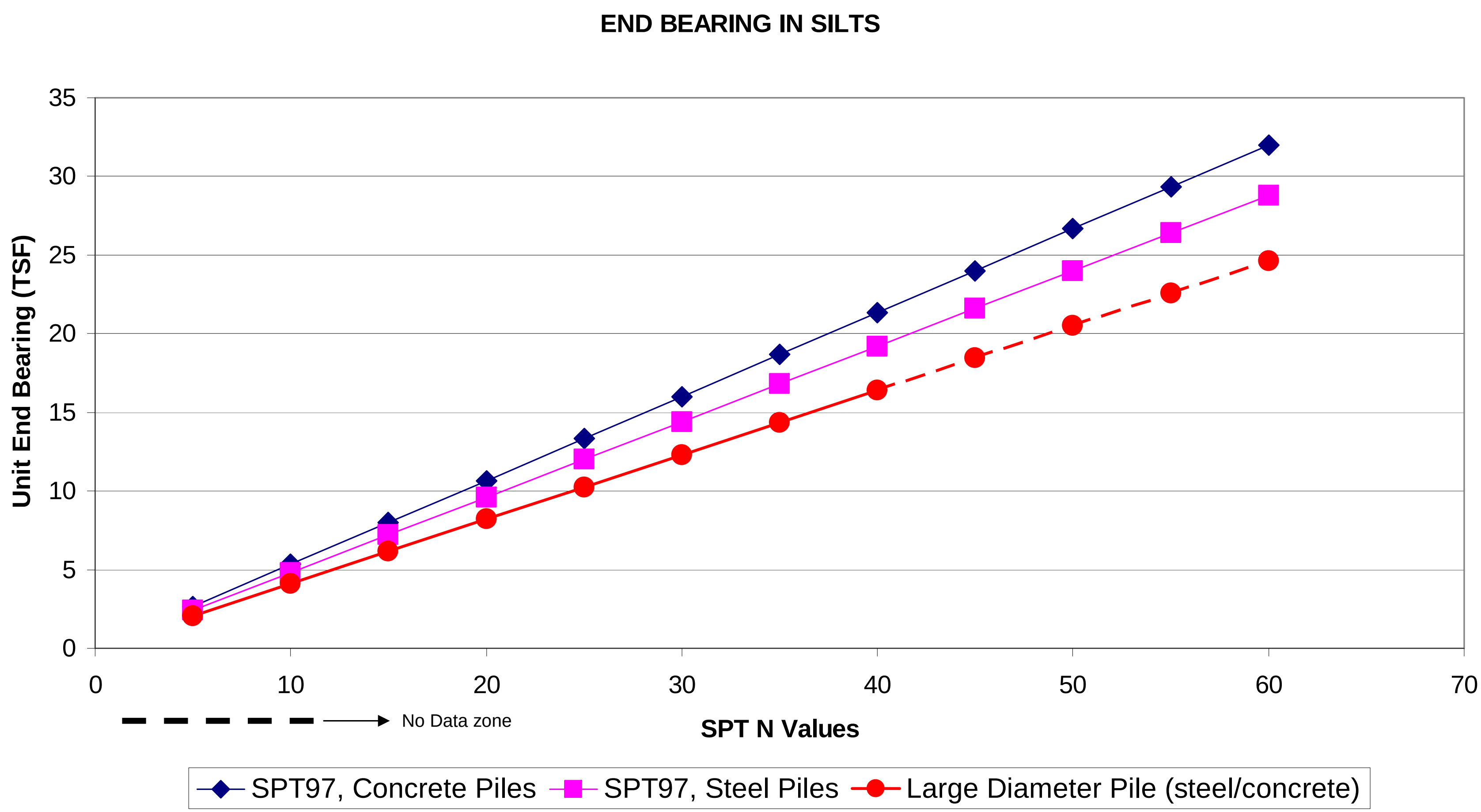

Figure 6-13 Comparison of various designs used for computing unit end bearing in silts.

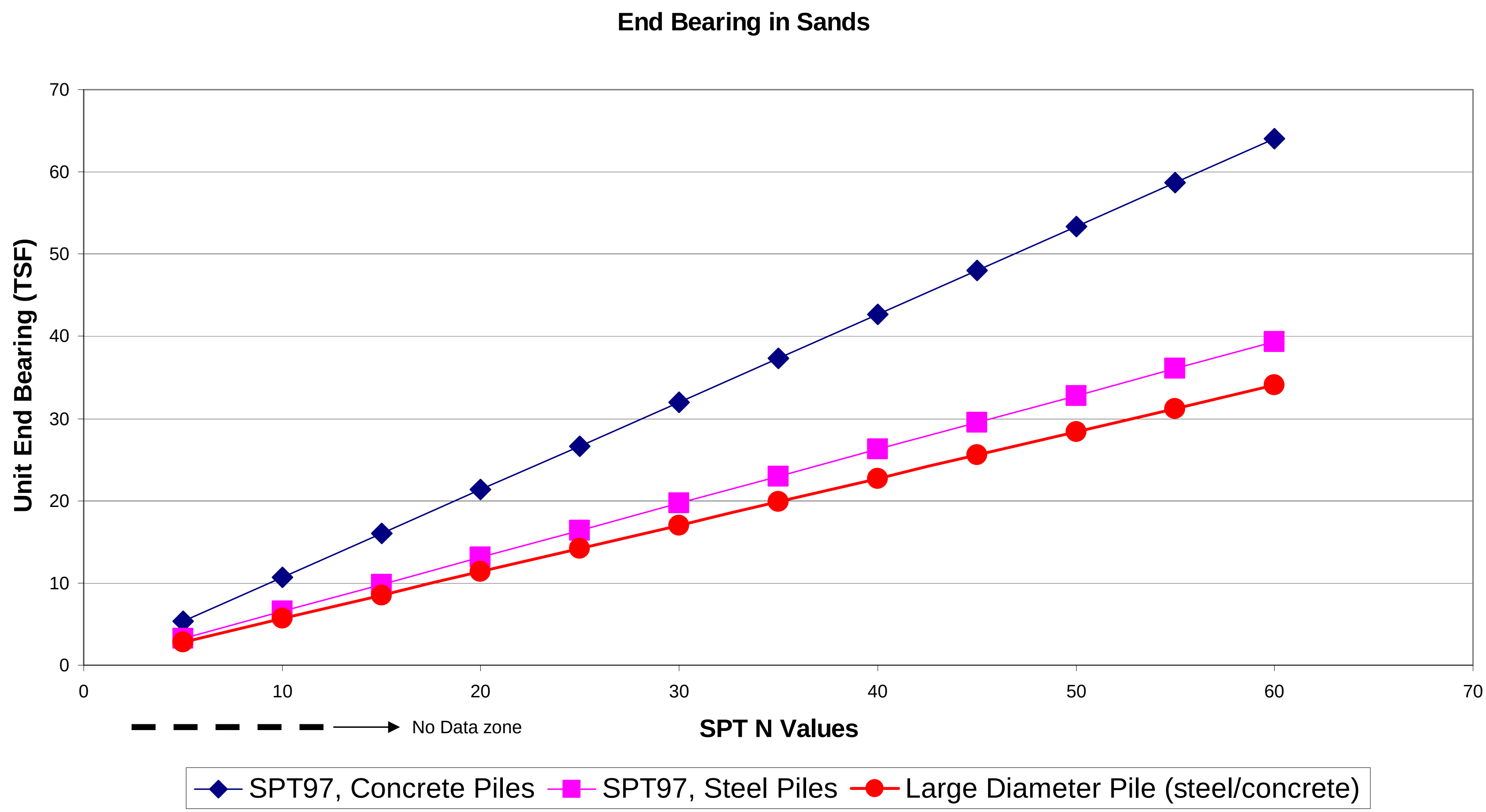

Figure 6-14 Comparison of various designs used for computing unit end bearing in sands.

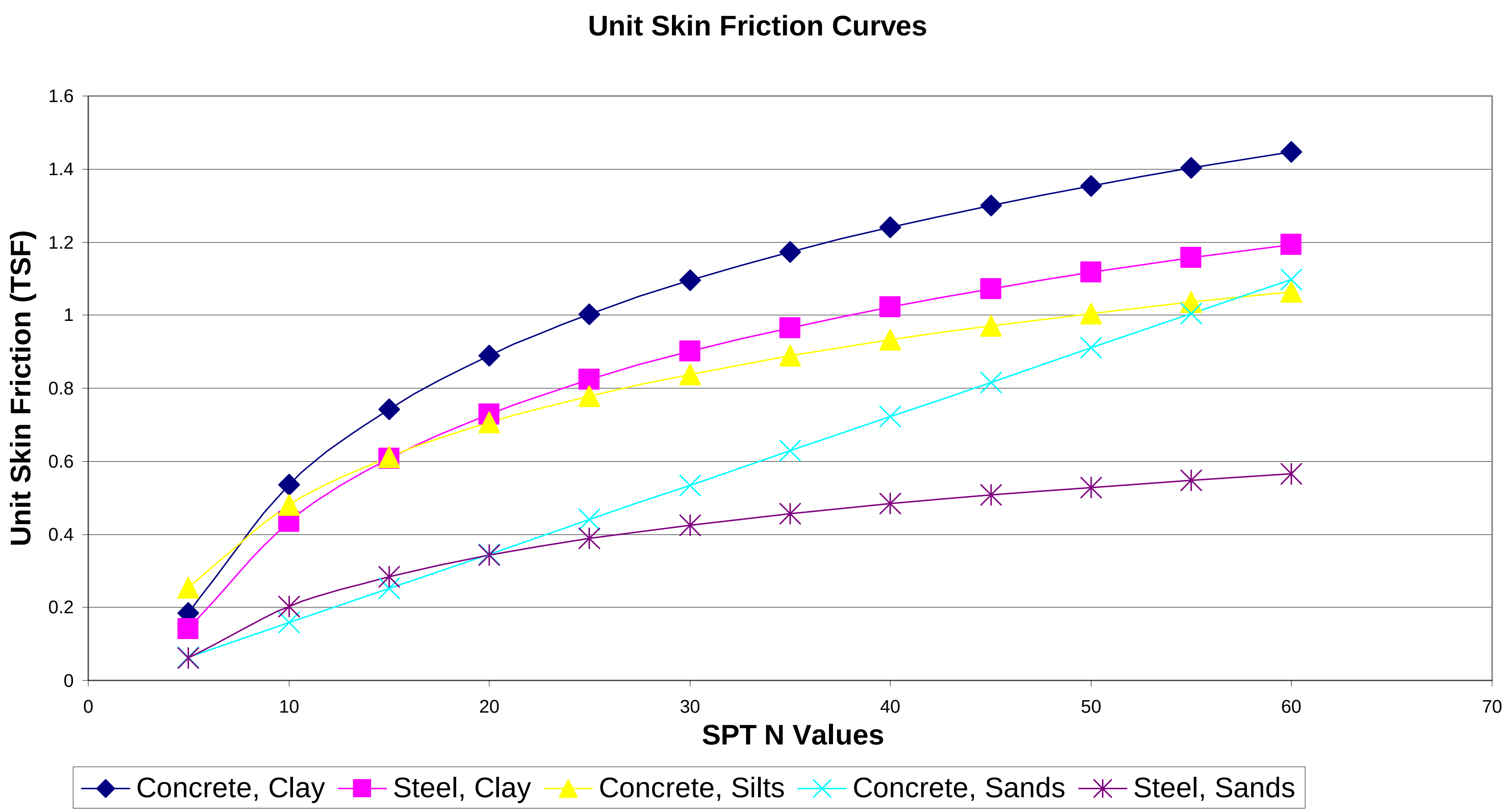

Figure 6-15 Comparison of unit skin friction vs. SPT N values, for various soil types, and pile materials, for large cylinder piles.

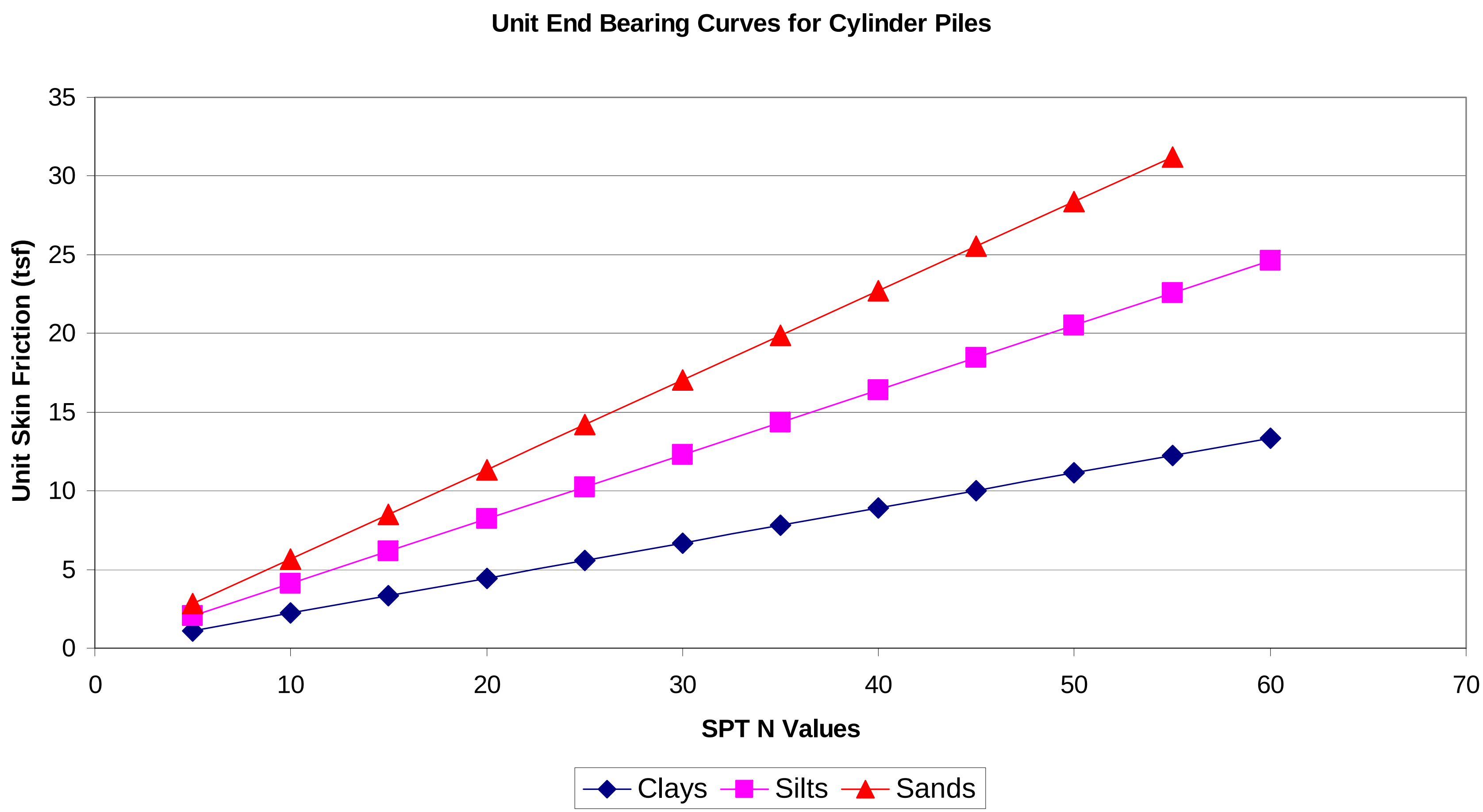

Figure 6-16 Comparison of unit end bearing vs. SPT N values, for various soils, for large diameter cylinder pile

CHAPTER 7

LOAD AND RESISTANCE FATOR DESIGN (LRFD)

7.1 INTRODUCTION

For many years, allowable stress design (ASD) was used for the design of bridges, building and other structures. In the 1970's, the American Association of State Highway and Transportation Officials (AASHTO) introduced a new design concept for bridge superstructures, called load factor design (LFD). It revolutionized the design of bridge superstructures through the use of different load factors depending on the type of load and its associated uncertainty. In the 1980s, the resistance factors were introduced, i.e., Load and Resistance Factored Design (LRFD), to account for uncertainty in prediction capacity. Unfortunately, only until recently (2000), the substructure design, in particular, soil structure interaction was designed with Allowable Stress Design, ASD. The latter requires the use of the un-factored loads and a safety factor. Recently, however, LRFD has been adopted by a number of DOTs (Florida, Pennsylvania, Washington, etc.) for the foundation design. A discussion of both follows.

7.2 ALLOWABLE STRESS DESIGN

Before the introduction of LRFD, ASD was used for all for foundation designs. ASD works by reducing the calculated or estimated resistance through a global factor of safety, resulting in a maximum design load. The estimated loads (or stresses) $\sum Q_i$ are restricted as shown bellow:

$$\frac{R_n}{Fs} \geq \sum Q_I \qquad \text{Eq. 7-1}$$

Where: R_n = Nominal resistance,
Fs = Factor of safety--usually from 2.0 to 4.0, and
ΣQ_i = Load effect (dead, live and environmental loads).

For pile foundations, the equation can be rewritten as:

$$R_n / Fs = (R_s + R_p) / Fs \geq Q_D + Q_L \qquad \text{Eq. 7-2}$$

Where: Q_D = Dead load,

Q_L = Live load,

R_s = Side resistance, and

R_p = Tip resistance.

7.3 LOAD RESISTANCE FACTOR DESIGN

The LRFD specifications as approved by AASHTO (AASHTO, 1996/2000) recommend the use of load factors to account for uncertainty in the loads, and resistance factors for the uncertainty in the material resistances. This safety criterion can be written as:

$$\phi R_n \geq \eta \sum \gamma_i Q_i \qquad \text{Eq. 7-3}$$

Where: R_n = Nominal resistance,

η = Load modifier to account for effects of ductility, redundancy and operational importance. The value of η usually ranges from 0.95 to 1.00. (η = 1.00 is used herein)

Q_i = Specific Load (dead, live, etc.)

γ_i = Load factor. Based on current AASHTO recommendation, the following factors are used:

γ_D = 1.25 for dead load,

γ_L = 1.75 for live load,

ϕ = Resistance factor--Usually ranges from 0.3 to 0.8.

The LRFD approach has the following advantages:

- It accounts for variability in both resistance and load. (In ASD, no consideration is given to the fact that different loads have different levels of uncertainty). For example, the dead load can be estimated with a high degree of accuracy; therefore, it has a lower factor (1.25) in LRFD.

- It achieves relatively uniform levels of safety based on the strength of soil and rock for different limit states and foundation types.
- It provides more consistent levels of safety in the superstructure and substructure as both are designed using the same loads for known probabilities of failure. In ASD, selection of a factor of safety is subjective, and does not provide a measure of reliability in terms of probability of failure.

The limitations of the LRFD approach include:

- Implementation requires a change in design procedures for engineers accustomed to ASD.
- Resistance factors vary with design methods and associated reliability, Beta (β).
- The most rigorous method for developing and adjusting resistance factors to meet individual situations requires the availability of statistical data and probabilistic design algorithms.

7.4 CALIBRATION OF RESISTANCE FACTOR FOR LRFD

Calibration of resistance factors is defined as the process of finding the ϕ values to achieve a required target probability of survival. There are three approaches that have traditionally been used in the LRFD calibration.

7.4.1 Engineering Judgment

The ϕ factor is assigned empirically by engineering judgment, and it is to be adjusted by the past and future performance of foundations designed using that factor.

7.4.2 Fitting ASD to LRFD

The resistance factor ϕ may be fitted to the factor of safety F_s in ASD by equating equation 7-1 to equation 7-3 through the resistance value, Rn:

$$\phi = \frac{\gamma_D \frac{Q_D}{Q_L} + \gamma_L}{F_s\left(\frac{Q_D}{Q_L} + 1\right)} \qquad \text{Eq. 7-4}$$

where the dead (Q_D) and live (Q_L) loads were used for Q_i and γ_D and γ_L are the associated load factors. For specific ASD Fs and Q_D /Q_L ratios (1 - 3), resistance Factors, ϕ, may be obtained.

7.4.3 Reliability Calibration

There are three levels of probabilistic design (Withiam et al., 1997). The fully probabilistic method (i.e., level III) requires knowledge of the probability distribution function of each random variable as well as correlations between variables.

The level II method, which is recommended by AASHTO and FHWA, is referred to as the advanced first order second moment method (FOSM). The latter method, adapted from the FHWA workbook (Withiam et al., 1997), are used herein.

7.4.3.1 Resistance Bias Factor - The resistance bias factor is defined as:

$$\lambda_{Ri} = \frac{R_m}{R_n} \qquad \text{Eq. 7-5}$$

Where: R_m = Measured Resistance,
R_n = Predicted (Nominal) Resistance

The mean, standard deviation and coefficient of variation of the set of bias data λ_{Ri} are

Mean: $$\lambda_R = \frac{\sum \lambda_{Ri}}{N} \qquad \text{Eq. 7-6}$$

Standard Deviation: $$\sigma_R = \sqrt{\frac{\sum\left(\lambda_{Ri} - \lambda_R\right)^2}{N-1}} \qquad \text{Eq. 7-7}$$

Coefficient of Variation: $COV_R = \frac{\sigma_R}{\lambda_R}$ Eq. 7-8

The value of Mean, λ_R, and the COV_R are used in the calculation of resistance factors, ϕ.

7.4.3.2 Probability of Failure and Reliability - Figure 7-1 shows the probability density functions for normally distributed load and resistance. The shaded area represents the region of failure where the resistance is smaller than the loads. For the load and resistance curves, the margin of safety can be defined in terms of the probability of survival as:

$$p_s = P(R > Q)$$ Eq. 7-9

And the probability of failure, p_f may be represented as

$$p_f = 1 - p_5 = P(R < Q)$$ Eq. 7-10

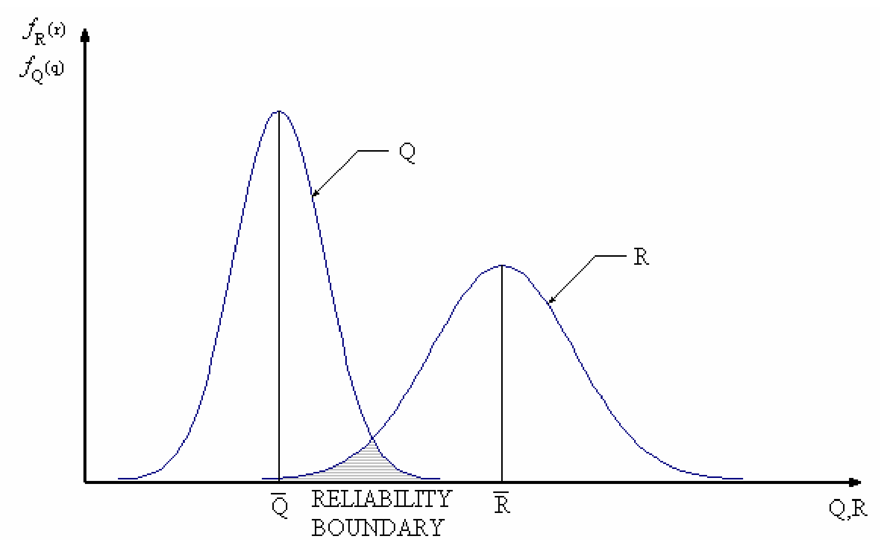

Figure 7-1 Probability density functions for normally distributed load and resistance.

Where the right hand of Equation 7-10 represents the probability, P, that R is less than Q.

It should be noted that the probability of failure may not be calculated directly from the shaded area in Figure 7-1. That area represents a mixture of areas from the load and resistance distribution curves that have different ratios of standard deviation to mean values. To evaluate the probability of failure, a single combined probability density curve function of the resistance and load may be developed based on a normal distribution, i.e.,

$$g(R, Q) = R - Q \qquad \text{Eq. 7-11}$$

If a lognormal distribution is used, the limit state function g (R, Q) can be written as:

$$g(R, Q) = \ln(R) - \ln(Q) = \ln(R / Q) \qquad \text{Eq. 7-12}$$

For both Equation 7-11 and 7-12, the limit state is reached when R = Q and failure will occurs when g (R, Q) < 0.

7.4.3.3 Reliability index - The reliability index is a simple method of expressing the probability of failure using function g (R, Q) (Eq. 7-12). The frequency distribution of g (R, Q) looks similar to the curve shown in Figure 7-2.

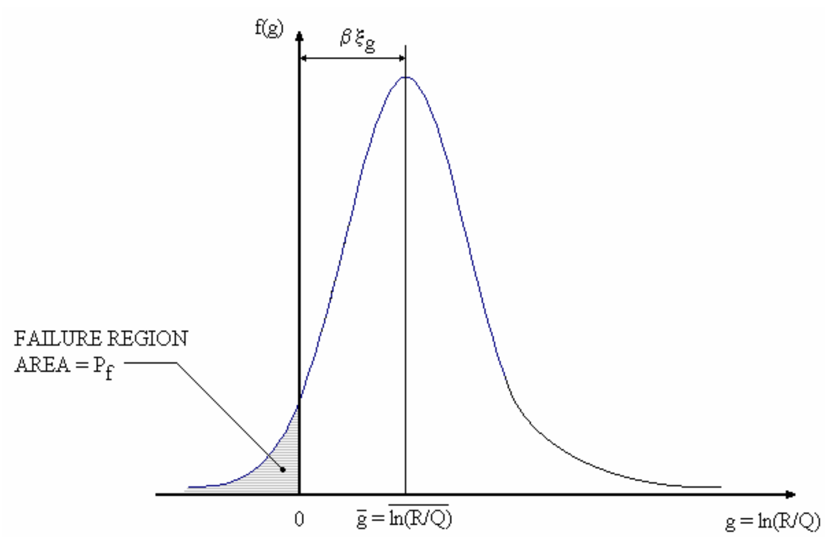

Figure 7-2 Definition of reliability index, β for lognormal distributions of R and Q.

Evident from the curve is that if the standard deviation is small or the mean value is located further to the right, the probability of failure will be smaller. The reliability index β, is defined as the number of standard deviations, ξ_g, between the mean value, g (average), and the origin, or:

$$\beta = \frac{\bar{g}}{\xi_g} \qquad \text{Eq. 7-13}$$

If the resistance, R, and load, Q, are both lognormally distributed random variables and are statistically independent, it can be shown that the mean values of g (R, Q) is:

$$g = \ln\left[\frac{\bar{R}}{\bar{Q}}\sqrt{\frac{1+COV_Q^2}{1+COV_R^2}}\right] \qquad \text{Eq. 7-14}$$

and its standard deviation is:

$$\xi_g = \sqrt{\ln\left[\left(1+COV_R^2\right)\left(1+COV_Q^2\right)\right]} \qquad \text{Eq. 7-15}$$

Substituting Equations 7-14 and 7-15 into Equation 7-13, the relationship for the reliability index, β, can be expressed as:

$$\beta = \frac{\ln\left[\left(\bar{R}/\bar{Q}\right)\sqrt{\left(1+COV_Q^2\right)/\left(1+COV_R^2\right)}\right]}{\sqrt{\ln\left[\left(1+COV_R^2\right)\left(1+COV_Q^2\right)\right]}} \qquad \text{Eq. 7-16}$$

Equation 7-16 is very convenient because it depends only on statistical data and not on the distribution of the combined function g (R, Q). A very precise definition of probability of failure, p_f, is in terms of reliability index, $F_u(\beta)$ (Withiam et al. 1997).

$$p_f = 1 - F_u\left(\beta\right) \qquad \text{Eq. 7-17}$$

A graphical representation of Equation 7-17 is presented in Figure 7-3. The shaded area in Figure 7-3 represents the probability of failure, p_f, to achieve a target reliability index, β_T.

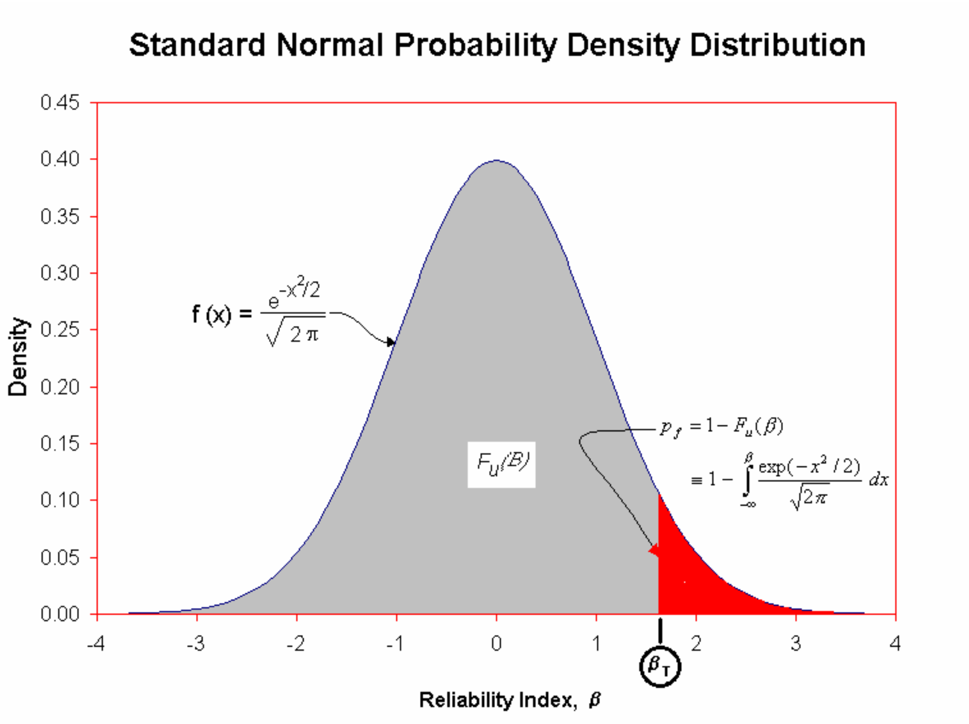

Figure 7-3 Reliability definition based on standard normal probability density function.

In the latter equation, $F_u(x)$ is the standard normal cumulative distribution function.

$$F_u(\beta) = 1 - \int_{\beta}^{\infty} \frac{1}{\sqrt{2\pi}} \exp\left(-\frac{1}{2}x^2\right) dx \qquad \text{Eq. 7-18}$$

Another commonly accepted relationship between the reliability index, β, and the probability of failure, p_f, has been developed by Rosenblueth and Esteva (1972) for values between 2 and 6 as:

$$p_f = 460 \exp(-4.3\,\beta) \qquad \text{Eq. 7-19}$$

Figure 7-4 presents a comparison of the results for both, the Rosenblueth and Esteva method and the Withiam method, to determine the reliability index, β. It can be observed that Rosenblueth and Esteva approximation method will yield good values of probability of failure for values of reliability index between 2.0 and 6.0 as recommended by the authors of the method.

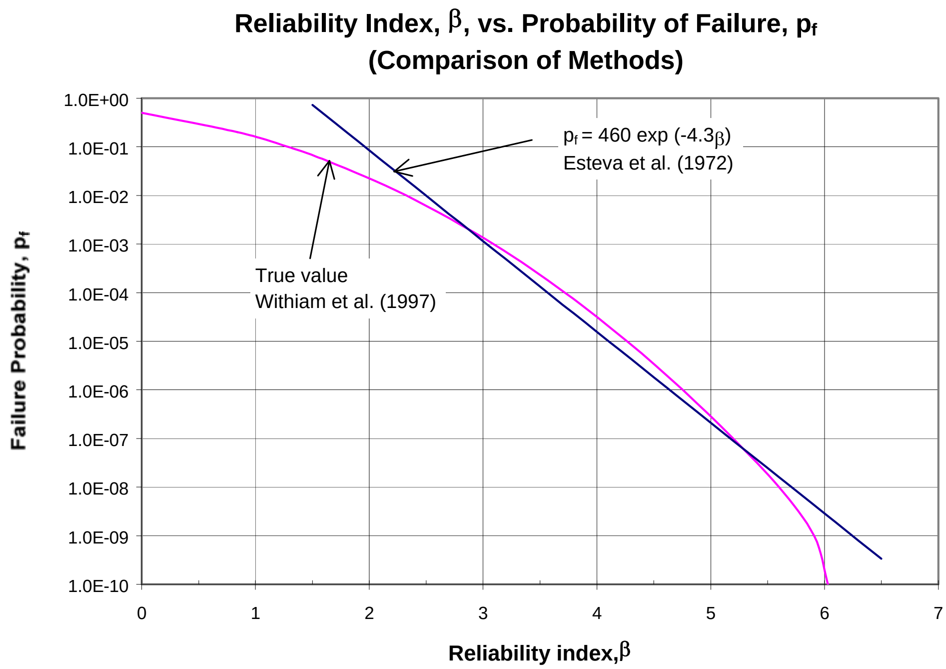

Figure 7-4 Comparison of Esteva and Withiam Methods to obtain reliability index, β.

7.4.3.4 Resistance factor, ϕ - Once the reliability index, β, is selected then a resistance factor, ϕ, may be calculated. Assuming lognormal distributions of load and resistance in Eq. 7-3 substituted into Eq. 7-16 gives the follow resistance, ϕ, equation:

$$\phi = \frac{\lambda_R \left(\gamma_D \dfrac{Q_D}{Q_L} + \gamma_L \right) \sqrt{\dfrac{1 + COV_{QD}^2 + COV_{QL}^2}{1 + COV_R^2}}}{\left(\lambda_{QD} \dfrac{Q_D}{Q_L} + \lambda_{QL} \right) \exp\left(\beta_T \sqrt{\ln\left[\left(1 + COV_R^2\right)\left(1 + COV_{QD}^2 + COV_{QL}^2\right) \right]} \right)} \qquad \text{Eq. 7-20}$$

where:
- ϕ Resistance Factor
- λ_R Resistance Bias Factor
- COV_R Resistance Coefficient of Variance
- β_T Target Reliability Index
- λQD, λ_{QL} Bias (Dead and Live Load)
- Q_D/Q_L Dead to Live Load Ratio

The dead to live load ratio (Q_D/Q_L) in Eq. 7-20 varies with the bridge span, values from 1 to 6 were investigated.

7.5 CAPACITY PREDICTION

In developing the LRFD resistance factors, ϕ, two different capacities, Rn, assessments were considered:

1. (Skin friction over the outside area) + (end bearing over the ring area)
2. (Skin friction over the outside area) + (end bearing over the entire cross-sectional area, C/S)

In approaches one and two, the unit skin friction was determined from Figure 6-15 based on average blow counts in the layers adjacent to the pile. Subsequently, the total pile side friction (Force) was determined by multiplying the unit skin friction (stress) for each layer by the outside surface area of the pile in each layer. For tip resistance calculation (Force), two approaches were used. The first used the blow counts in the vicinity of the pile tip to obtain unit end bearing (Fig. 6-16), which was then multiplied by the ring area of the pile bottom. In the second approach, the resistance (Force) was obtained by multiplying the unit end bearing (stress) by the total cross-sectional area of the pile. Note, the second approach assumes the soil within the pile is "plugged," whereas, the first approach assumes that the pile is "un-plugged" and the unit skin friction within the pile is negligible (i.e., very conservative). This is contrast to the results in Chapter 5, which revealed that even if the pile does not plug during driving, the particle velocities near the pile wall are negligible (Figs. 5-10 and 5-11) The latter suggests that the skin friction on the inside of the pile is not zero and it would contribute to pile capacity. However, the phenomenon cannot be detected through dynamic field-testing (i.e., PDA), and it would

Table 7-1 Measured vs. Predicted Pile Capacities

Sno	Project	Measured*	Ring Area **	λri **	Full C/s ***	λri ***
1	St. Georges Island Project	1050	803.92	1.31	1146.31	0.92
2	St. Georges Island Project	1400	1208.45	1.15	1604.15	0.87
3	St. Georges Island Project	1275	1081.69	1.17	1499.86	0.85
4	St. Georges Island Project	1425	834.08	1.71	1237.07	1.15
5	Chesapeake Bay Bridge LT-4	700	477.75	1.47	770.94	0.91
6	Chesapeake Bay Bridge LT-6	460	324.34	1.42	399.26	1.15
7	San Mateo Hayward Bridge	775	699.23	1.11	729.47	1.06
8	South Test-4	650	328.54	1.98	553.28	1.17
9	Woodrow Wilson Bridge	1475	1185.97	1.24	1600.36	0.92
10	Woodrow Wilson Bridge	1500	1230.65	1.22	1530.27	0.98
11	Woodrow Wilson Bridge	900	781.81	1.15	951.49	0.95
12	Salinas River Bridge	750	517.45	1.45	862.22	0.87
13	Port Of Oakland 27NC	625	462.39	1.35	544.57	1.15
14	Port Of Oakland 17NC1	512.5	439.08	1.17	592.09	0.87
15	Port Of Oakland 10NC1	450	400.47	1.12	598.50	0.75
16	Port Of Oakland 31NC	600	532.43	1.13	592.55	1.01
17	I-880 Oakland Site 3C	450	382.82	1.18	467.41	0.96
18	I-880 Oakland Site 3H	600	506.92	1.18	600.44	1.00
19	Santa Clara River Bridge 13	925	947.67	0.98	1205.60	0.77
20	Santa Clara River Bridge 7	1070	996.90	1.07	1436.45	0.74
21	Berenda Slough Br 4	800	702.77	1.14	798.97	1.00

* Measured capacity in Tons.

** Capacity prediction using end bearing over the ring area in Tons.

*** Capacity prediction using end bearing over the entire cross sectional area in Tons.

significantly complicate the WEAP modeling. Consequently interior pile friction was neglected and the pile ring area as identified in approach 1 was investigated.

Shown in Table 7-1 are both the measured and predicted (Approaches 1 & 2) capacities for all large diameter cylinder piles that reached FDOT failure in the database. Figures 7-5 and 7-6 are a comparison of measured and predicted response for both approaches.

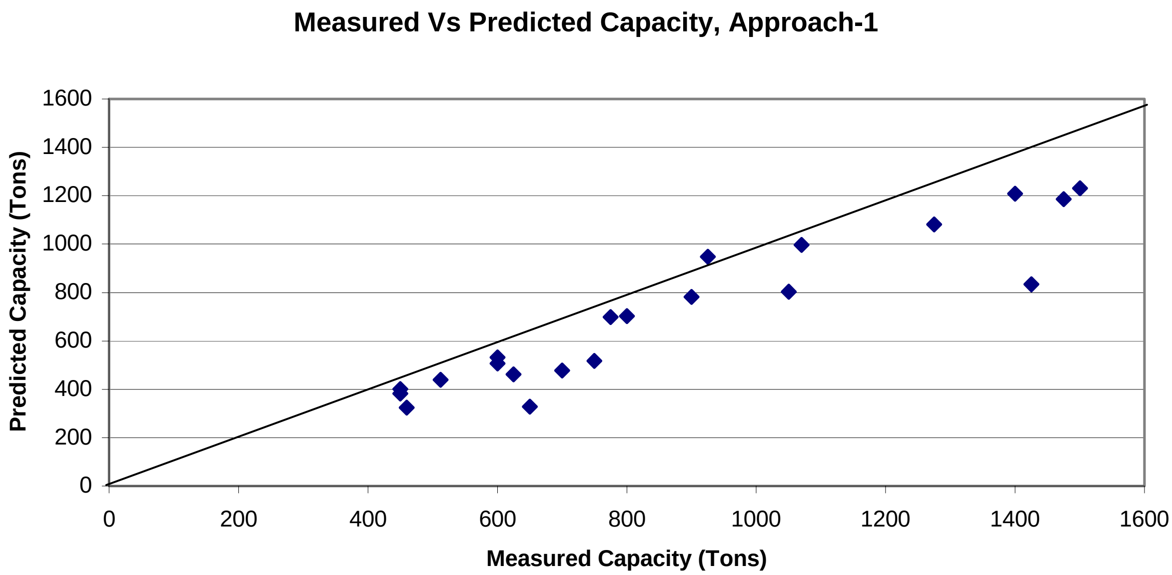

Figure 7-5 Comparison of measured vs. predicted capacities, approach-1.

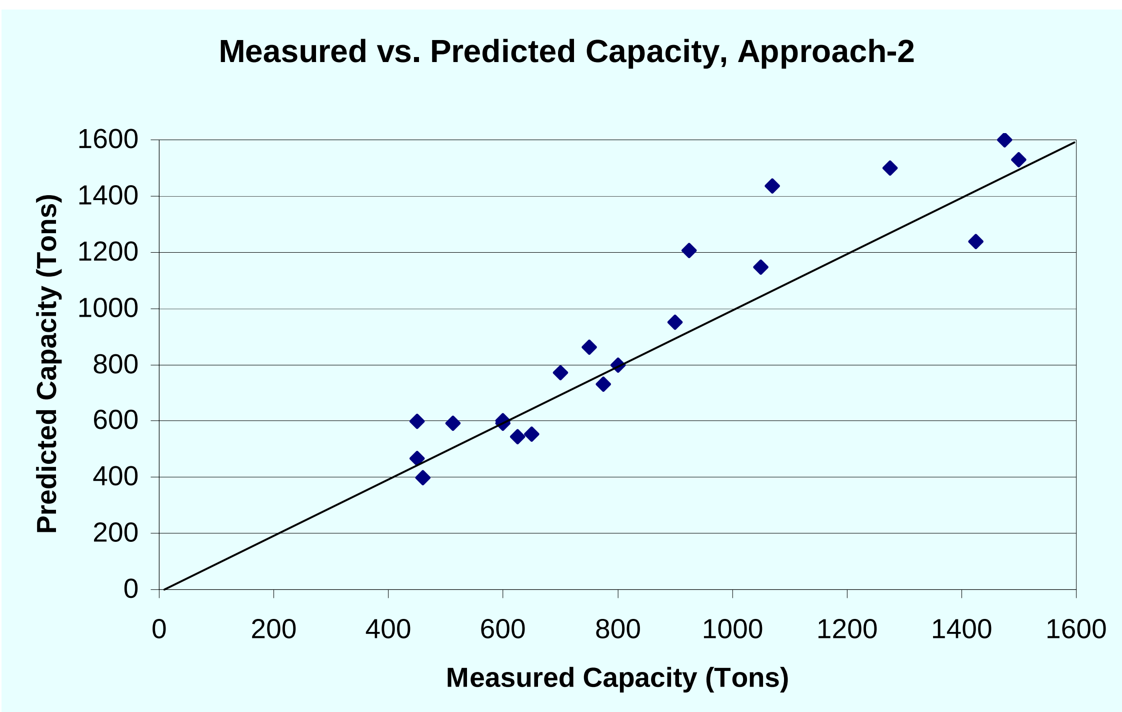

Figure 7-6 Comparison of measured vs. predicted capacities, approach-2.

Presented in Table 7-2 are the mean (Eq. 7-6), standard deviation (Eq. 7-7), and coefficient of variation (Eq. 7-8) of the measured to predicted pile capacities. Evident from the means (λr), approach-1 is conservative (λr = measured/predicted > 1), whereas, approach-2 with a mean of approximately one fits quite well, suggesting that a plugged pile is more the norm. Also of interest, is the lower standard deviation, λr, for approach-2, which will ensure a greater percentage of FDOT failure capacity available for design.

Table 7-2 Statistics on Predicted Capacities

	Approach – 1 (Ring Area)	Approach – 2 (Full C/S)
λ_r	1.27	0.955
σ_r	.23	.13
C.O.V.	.18	.13
ϕ	.76	.61

Using the measured to predicted pile statistics (Table 7-2), load factors, variable dead to live ratios, Q_D/Q_L, and variable reliability values, the LRFD resistance factors, ϕ, for approach 1 and 2 were determined. Figures 7-7 and 7-8 plot the resistance factors, ϕ, as a function of Q_D/Q_L, and reliability, β.

Evident from a comparison of Figures 7-7 and 7-8, the LRFD resistance factors, ϕ, for approach –1 (use of pile tip ring area) are higher than approach-2 (total pile cross-sectional area). This is explained by the higher bias (mean, λr >1: conservative) of approach-1 compared to approach-2. However, one should note that the FDOT failure capacity available for design:

$$\phi / \lambda r \qquad \text{Eq. 7-21}$$

is higher for approach-2 than approach-1.

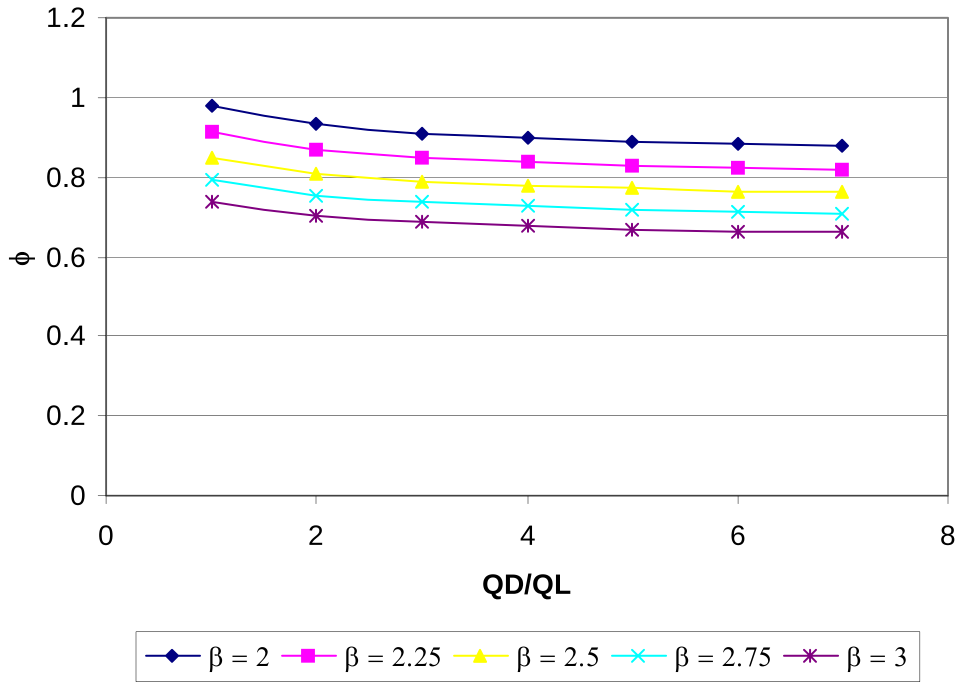

Figure 7-7 Resistance factor vs. dead to live load ratio, large diameter cylinder pile with ring area.

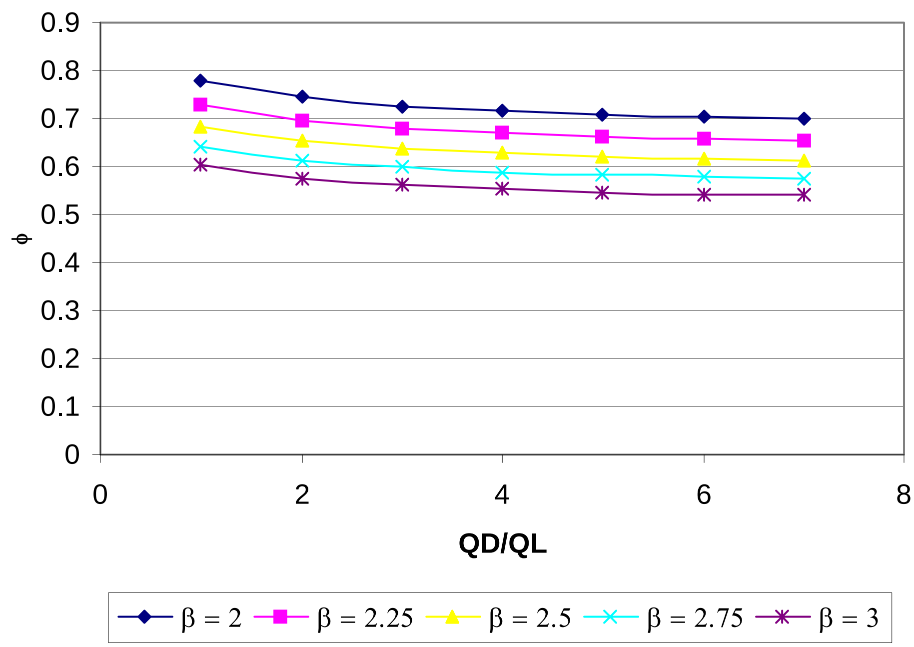

Figure 7-8 Resistance factor vs. dead to live load ratio, large diameter cylinder pile with total cross-sectional area.

Using a target reliability index, β_T =2.75 from previous FDOT LRFD calibration work (McVay et al., 1998), a ϕ-factor of 0.76 was obtained for approach-1, and a value of 0.61 was determined for approach-2 and they are presented in Table 7-2.

CHAPTER 8

RESULTS AND CONCLUSION

8.1 CYLINDER PILE DATABASE

In order to develop a design procedure for large diameter cylinder piles, a database of insitu and field load test information was collected. Over eighty Geotechnical consulting companies, federal and state department transportation (DOTs) agencies were contacted throughout the US and around the world. Of those contacted, FDOT (Florida Department of Transportation), CALTRANS (California Department of Transportation), VDOT (Virginia Department of Transportation), NCDOT (North Carolina Department of Transportation) and MSHA (Maryland State Highway Administration) had sites with either single or multiple static load tests on large diameter cylinder piles. All of the recorded axial load tests were performed in accordance ASTM D 1143-81 (1994).

A total of 35 load tests were collected (22 concrete & 13 steel) from both DOTs and their consultants. Shown in Table 8-1 is a description of the piles. Table 8-2 gives a description of soil types adjacent to the piles. Note a few of the piles were driven through multiple soil layers. Of the 35 load tests with associated load vs. settlement data, 21 of the piles reached FDOT

Table 8-1 Cylinder Pile Sizes and Wall Thickness

Outer Diameter	Number	Shell Thickness	Number
84-inch	1	8-inch	4
72-inch	2	6.9-inch	2
66-inch	3	6-inch	7
54-inch	18	5-inch	9
42-inch	10	1-inch to 2-inch	5
36-inch	1	<1-inch	8

failure (Davisson with offset of 0.15 + D/30), which were used to assess unit skin and tip resistance vs. SPT N values. A further discussion of the database is found in Chapter 2.

Table 8-2 Soil Type and Description

Soil Type	Predominate Soil Type Around the Pile	Number of piles
1	Plastic Clay	13
2	Clay-silt-sand mixtures, very silty sand, silts and marls	11
3	Clean Sands	18
4	Soft Limestone, very shelly sands	2

Impacting a cylinder pile's capacity is the selection of unit cross-section area at the pile tip, i.e., ring area or total cross-sectional area. An analysis of the behavior of the soil column both during driving and following, i.e., static loading was subsequently undertaken.

8.2 MODELING OF SOIL COLUMN WITHIN THE PILE

The study initiated with a comparison of the forces acting on the soil column during driving assuming that the soil was attached to the pile, i.e., plugged. The investigation revealed the inertia forces acting on the soil column increased quadratically with the pile diameter as shown in Figure 8-1. For instance, a 24" diameter by 60ft soil column would remain plugged if the average pile acceleration remained below 40 gs whereas a 54" diameter by 60 ft soil column would behave un-plugged for any pile acceleration above 15 gs. Since prestressed concrete piles, on average have pile accelerations in the range of 40 to 60 gs (using FDOT 455 specifications), piles with diameter exceeding 24" should "cookie cut" into the ground (i.e., behave unplugged). In the case of steel piles, which have much higher g levels, i.e., values over 100 gs are typical (Stevens, 1988), the likelihood of plugging is less.

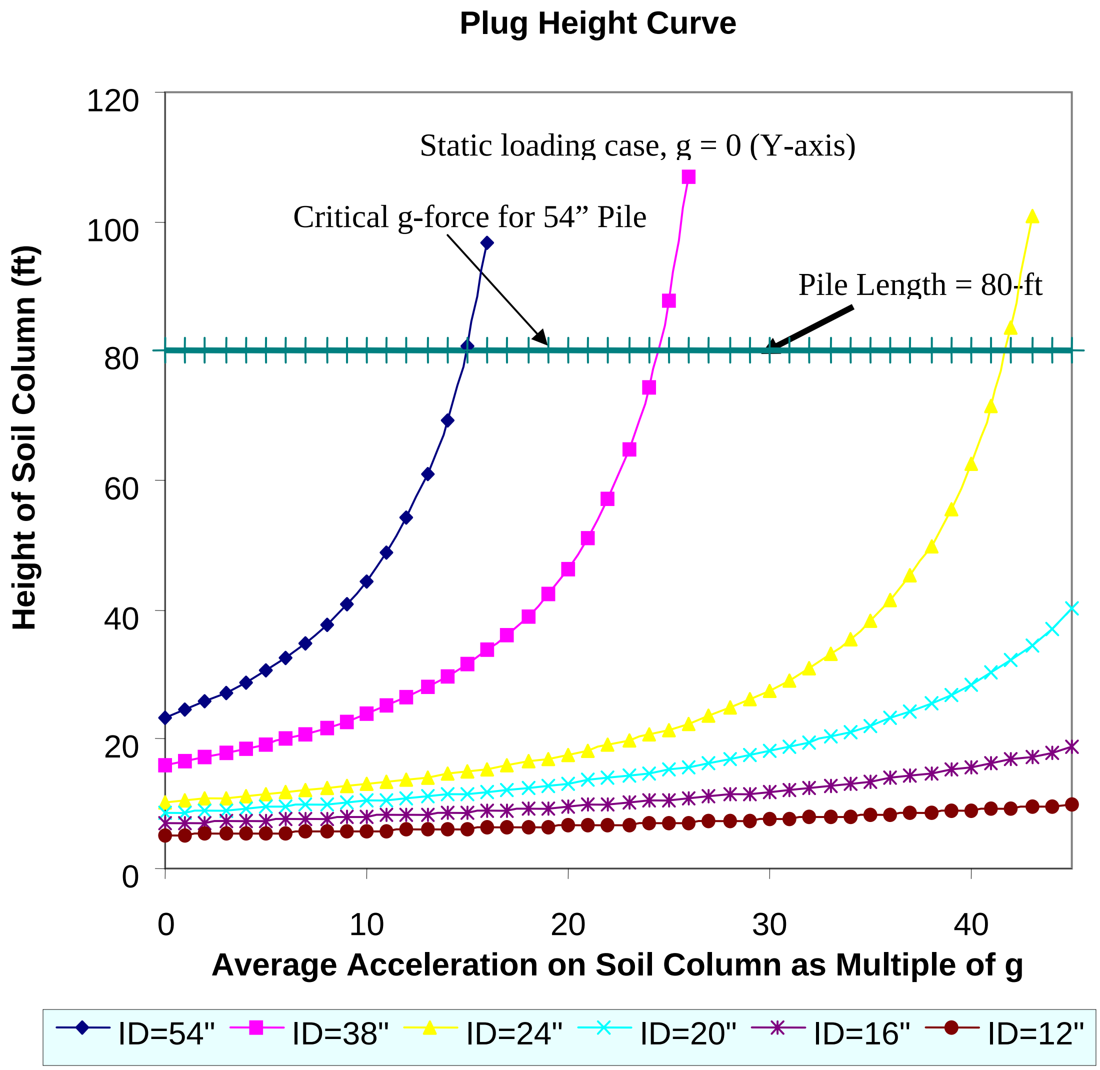

Figure 8-1 Pile Diameter vs. maximum soil column acceleration to maintain plug state

After pile driving, the inertia forces on the soil column are no longer present, and the soil within the cylinder may behave plugged (i.e., soil column attached to pile) during quasi-static loading. To study the latter, a finite element analysis of the open cylinder pile quasi-penetrating a soil (modeled as fluid) was undertaken.

The FEM study was unable to predict the actual plug height (i.e., soil moving together with the pile, Fig 5-10 vs. Fig. 5-11) in the pile due to uncertainties in soil properties, pile surface roughness, etc., however it was able to identify the parameters which had a strong influence on plug height:

1. Shell Thickness: There was a 40% increase in the required soil column height (from 60% to 100%) for "plugging," if the shell thickness was reduced from 10" to 6". The latter may be explained as follows: 1) as the diameter of the soil column increases (i.e., pipe wall decrease), the skin friction force goes up linearly (fs · Asurf), the tip resistance that it balances increases quadratically (Qt = qt Across); and 2) the thicker the pipe wall, the larger the volume of soil mass being displaced and the more likely the soil, i.e., sand, silt, etc. will dilate within the pipe and plug, which would develop high shear strengths at the pipe-soil interface.
2. Rate of Penetration: There was a 15% increase in the soil column height before plug formed when the rate of penetration was increased from 0.3 inch/sec to 0.5 inch/sec. The latter may be explained in terms of the particle soils velocity, and the higher shearing resistance or force (stress · area, i.e., length of column) to slow and or stop the relative movement between the pile and soil.
3. Friction Angle: There was a 40% increase in the soil column's height before it plugged, if the friction angle of the soil was reduced from 35 degrees to 27.5 degrees. The reduction in the soil's angle of internal friction reduces the mobilized shear stress on the inside wall of the pipe and requires a longer soil column height to balance the mobilized tip resistance.
4. Outer Diameter: There was a 10% increase in the soil column height before plugging, when the diameter was increased from 48" to 54" (same shell thickness of 8"). This is in accordance with explanation (1), the large the diameter, the unit skin friction increases linearly, and the end bearing quadratically, requiring longer lengths to plug

Based on both the driving analysis, as well as the quasi-static finite element study, it was decided to consider both total cross-sectional and ring area in estimating a pile's end bearing from insitu tests for pile design.

8.3 EVALUATING UNIT SKIN AND TIP RESISTANCE

Using the database of piles, which reached FDOT failure, equations of unit skin friction end bearing vs. SPT N values were developed. Approximately 9 piles had instrumentation along their length to separate unit skin friction from end bearing. For the other piles, DeBeer method of plotting load vs. displacement on a log-log plot was employed. Specifically, the break in the slope was the mobilization of skin friction, and the difference between Davisson and ultimate skin was the mobilized end bearing. Presented in Table 8-3 is the equations of the best-fit lines (see chapter 6) for unit skin friction and end bearing vs. SPT N values.

8.4 LRFD STUDY

Based on the equations developed unit skin friction, and end bearing curves, (Table 8-3) the capacities of the piles were predicted based on soil type, and uncorrected SPT blow counts. These were compared to capacities of the piles measured in the field.

Table 8-3 Skin Friction and Tip Resistance Equations
(in terms of uncorrected SPT blow counts),
Developed Using the Piles in the UF/FDOT Cylinder Pile Database

No	Soil Type	Skin Friction (tsf)		End Bearing (tsf)
1	Plastic clays	Concrete	$fs = .5083 * Ln(N) - .634$ 5 < N < 60	$qt = .2226 * N$
		Steel	$fs = .4236 * \ln(N) - .5404$ 5 < N < 60	
2	Clay-silt-sand mixtures	Concrete	$fs = .3265 * Ln(N) - .2721$ 5 < N < 60	$qt = .4101 * N$
3	Clean sands	Concrete	$fs = .0188 * N - .0296$ 5 < N < 60	$qt = .5676 * N$
		Steel	$fs = .2028 * Ln(N) - .2646$ 5 < N < 60	

Next, the FHWA's Load and Resistance Factor Design method, FOSM, for determining resistance factors (Withiam, 1998) was employed with both ring area and total cross-sectional area for pile capacity assessment (Table 8-4) using a reliability, β_T, of 2.75 (McVay, 1998).

Table 8-4 Statistics on Predicted Capacities

	Approach-1 (Ring Area)	Approach-2 (Full C/S)
λr	1.27	0.955
σr	.23	.13
C.O.V	.18	.13
ϕ	.76	.61

It should be noted that the even though the resistance factor, ϕ, of the Approach-1, 0.76, is higher than the Approach-2, 0.61, the percentage of Davisson capacity available for design, $\phi/\lambda r$, is higher for Approach-2, 0.64, vs. Approach-1, 0.60. The latter suggests that Approach-2, is a slightly better method and that more of the piles may be plugged during static loading.

8.5 RECOMMENDATIONS

To improve the findings of this research, it is suggested that

- More load tests be collected in stiffer, denser or higher blow count soils;
- More data on large diameter steel piles should be collected;
- Influence of pile freeze on large diameter piles should be investigated.

In addition, it is suggested that a number of full-scale load tests on instrumented large diameter cylinder piles be undertaken. The study should include pressure cells at the bottom of the piles, and strain gauges cast along the piles' length to differentiate end bearing from skin friction. The study should consider a range of different diameter piles and monitor the piles both during driving and under static load loading conditions. Of strong interest is the behavior of the soil column within the pile during driving and later under static loading. Chapter 5 analysis suggests that large diameter piles may "cookie cut" into the soil during driving (i.e., unplugged) but develop a "plugged" state under static loading. The latter scenario is currently unaccounted for in static assessment of pile capacities during driving (i.e., PDA & CAPWAP).

REFERENCES

ASSHTO, 1996/2000. LRFD Bridge Design Specification, 2nd Edition-2000 Interim Revisions. Washington, DC.

Azzouz, A.S., Baligh, M.M., and Whittle, A.J., (1990). "Shaft resistance of piles in clay." J. Geotech. Engrg., ASCE, 116(2), 205-221.

Brucy, F., Meunier, J., Nauroy, J. F., (1991). "Behavior of Pile Plug in Sandy Soils During and After Driving," Paper Presented at the 23rd Annual Offshore Technology Conference, Texas, May 6-9.

Chow, Y.K., (1981). "Dynamic Behavior of Piles." Ph.D. Thesis, University of Manchester.

Davisson, M.T., (1976), "High Capacity Piles." Proceedings, Soil Mechanics Lecture Series on Innovations in Foundation Construction. American Society of Civil Engineers, Illinois Section, Chicago, 81-112.

DeBeer, E., (1970). Proefondervindellijke bijdrage tot de studie van het grandsdraagvermogen van zand onder funderinger op staal. English version, Geotechnique, Vol. 20, No. 4, 387-411.

Kishida, H., and Isemoto, N., (1977). Behavior of sand plugs in open-end steel pipe piles. Proc. 9th Int. Conf. on Soil Mechanics and Foundation Engineering, 1:601-604.

Kyuho, P., Salgado, R., (2003). "Determination of Bearing Capacity of Open-Ended Piles in Sand," Journal of Geotechnical and Geoenvironmental Engineering, Jan 2003.

Madabhushi, S.P.G., and Haig, S.K., "Finite Element Analysis of Pile Foundation Subjected to Pull out."

McVay, M.C., Kuo, C.L., and Singletary, W.A., 1998. "Calibrating Resistance Factors in the Load and Resistance Factor Design for Florida Foundations," Final Report to the Florida Department of Transportation, State Job Jo. 997700-339-010, contract # Ba512, December, 92 pages

Paik, K.H., and Lee, S.R., (1993). "Behavior of Soil Plugs in Open Ended Model Piles Driven into Sands," Marine Georesources and Geotechnology, vol. 11, pp. 353-373.

Paikowsky, S.G., (1990). "The Mechanism of Pile Plugging in Sand." Paper Presented at the 22nd Annual Offshore Technology Conference in Houston, Texas, May 7-10.

Paikowsky, S.G., and Whitman, R.V., (1990). "The Effects of Plugging on Pile Performance and Design," Canadian Geotechnical Journal, vol. 27, pg. 429-440.

Paikowsky, S.G., Whitman, R.V., and Baligh, M.M., "A New Look at the Phenomenon of Offshore Pile Plugging," Marine Geotechnology, Vol. 8, pp. 213-230.

Smith, I.M., Wilson, S.M., "Plugging of Pipe Piles." Proceedings of the 3rd International Conference on Numerical Methods in Offshore Piling, May 21-22, 1886.

Stevens, R.F., (1988), “The Effect of Soil Plug on Pile Drivability in Clay.” Application of Stress-Wave theory to Piles, Third International Conference, May 25-27.

Szechy, C.H., (1958), “Test With Tubular Piles,” Published in Hungarian in the periodical Magyar Tudományos Akadémia Mûszaki Tudományok Osztálya Közleményei, vol. 22.

Vipulanandan, C., Wong, D., Ochoa, M., and O’Niell, M.W., 1989. Modeling displacement piles in sand using a pressure chamber. *Foundation Eng. Current Principles Pract. ASCE* 1:526-541.

Withiam, J., Voytko, E., Barker, R., Duncan, M., Kelly, B., Musser, S., and Elias, V., 1998. Load and Resistance Factor Design (LRFD) of Highway Bridge Substructures. FHWA Publication no. HI-98-032, July, Washington, D.C.

APPENDIX A
DATA REDUCTION AND DATABASE

Table A-1: Current database entry and description.

S.No	Project Name	# *	O.D*	T*	L*	Le*	Material
1	St. Georges Island Project	59	54-inch	8-inch	80-ft	51-ft	Concrete
2	St. Georges Island Project	60	54-inch	8-inch	80-ft	46-ft	Concrete
3	St. Georges Island Project	61	54-inch	8-inch	80-ft	59.5-ft	Concrete
4	St. Georges Island Project	62	54-inch	8-inch	80-ft	46.7-ft	Concrete
5	Chesapeake Bay Bridge	52	54-inch	6-inch	184-ft	139.7-ft	Concrete
6	Chesapeake Bay Bridge	53	54-inch	6-inch	146.9-ft	104.88-ft	Concrete
7	Chesapeake Bay Bridge	55	54-inch	6-inch	172-ft	77.17-ft	Concrete
8	Chesapeake Bay Bridge	56	66-inch	6-inch	200-ft	94-ft	Concrete
9	Chesapeake Bay Bridge	57	66-inch	6-inch	204-ft	105-ft	Concrete
10	Chesapeake Bay Bridge	58	54-inch	6-inch	128-ft	44-ft	Concrete
11	San Mateo Hayward Bridge	92	42-inch	6.9-inch	42.25-m	35.31-mtr	Concrete
12	San Mateo Hayward Bridge	93	42-inch	6.9-inch	40.8-m	26.5-mtr	Concrete
13	Oregon Inlet	50	66-inch	6-inch	130.5-ft	71.5-ft	Concrete
14	I-664 Bridge North	51	54-inch	5-inch	104-ft	68.4-ft	Concrete
15	South Test-4	66	54-inch	5-inch	47.9-ft	27-ft	Concrete
16	South Test-5	67	54-inch	5-inch	93.3-ft	68.4-ft	Concrete
17	South Test-6	68	54-inch	5-inch	96.3-ft	73.67-ft	Concrete
18	South Test-10	69	54-inch	5-inch	172-ft	145.1-ft	Concrete
19	South Test-11	70	54-inch	5-inch	143-ft	115.3-ft	Concrete
20	South Test-12	71	54-inch	5-inch	133.17-ft	95.9-ft	Concrete
21	South Test-13	72	54-inch	5-inch	125.33-ft	88.9-ft	Concrete
22	South Test-14	73	54-inch	5-inch			Concrete
23	Woodrow Wilson Bridge	63	54-inch	1-inch	164-ft	132.2-ft	Steel
24	Woodrow Wilson Bridge	64	42-inch	1-inch	125-ft	107-ft	Steel
25	Woodrow Wilson Bridge	65	36-inch	1-inch	96-ft	90.6-ft	Steel
26	Salinas River Bridge	81	72-inch	.75-inch		114-ft	Steel
27	Port Of Oakland 27NC	82	42-inch	.625-inch		91.5-ft	Steel
28	Port Of Oakland 17NC1	83	42-inch	.75-inch		98.8-ft	Steel
29	Port Of Oakland 10NC1	84	42-inch	.75-inch		94-ft	Steel
30	Port Of Oakland 31NC	85	42-inch	.625-inch		91.5-ft	Steel
31	I-880 Oakland Site 3C	86	42-inch	.75-inch	100.5-ft	83.5-ft	Steel
32	I-880 Oakland Site 3H	87	42-inch	.75-inch	100.5-ft	83.5-ft	Steel
33	Santa Clara River Bridge 13	88	72-inch	1.5-inch	135.136-ft	114.472-ft	Steel
34	Santa Clara River Bridge	89	84-inch	1.74-inch	66.256-ft	52.48-ft	Steel
35	Berenda Slough Br 4	90	42-inch	.625-inch		101.68-ft	Steel

*

- #: UF/FDOT Database entry number.
- O.D: Outer diameter.
- t: Shell thickness.
- L: Total length.
- Le: Embedded length.

Table A-2: Soil type, insitu test, and plug status.

Sno	Project Name	Soil Type Skin	Soil Type End	Insitu Test	Plug Status
1	St. Georges Island Project	Sand	Limestone	SPT/CPT	Unplugged
2	St. Georges Island Project	Sand	Limestone	SPT/CPT	Unplugged
3	St. Georges Island Project	Sand	Limestone	SPT/CPT	Unplugged
4	St. Georges Island Project	Sand	Limestone	SPT/CPT	Unplugged
5	Chesapeake Bay Bridge	Silt	Silt	CPT/SPT	Plugged
6	Chesapeake Bay Bridge	Silt	Silt	CPT/SPT	Unplugged
7	Chesapeake Bay Bridge	Silt	Silt	CPT/SPT	Unplugged
8	Chesapeake Bay Bridge	Sand	Sand	CPT/SPT	Plugged
9	Chesapeake Bay Bridge	Sand	Sand	CPT/SPT	Plugged
10	Chesapeake Bay Bridge	Sand	Sand	SPT	Plugged
11	San Mateo Hayward Bridge	Silt	Silt	SPT	Unplugged
12	San Mateo Hayward Bridge	Silt	Silt	SPT	Unplugged
13	Oregon Inlet	Silt	Silt	CPT/SPT	Unplugged
14	I-664 Bridge North	Clay	Clay	SPT	Unplugged
15	South Test-4	Sands	Sands	SPT	Unplugged
16	South Test-5	Sands	Sands	SPT	Unplugged
17	South Test-6	Sands	Sands	SPT	Unplugged
18	South Test-10	Sands	Sands	SPT	Unplugged
19	South Test-11	Sands	Sands	SPT	Unplugged
20	South Test-12	Sands	Sands	SPT	Unplugged
21	South Test-13	Sands	Sands	SPT	Unplugged
22	South Test-14	Sands	Sands	SPT	Unplugged
23	Woodrow Wilson Bridge	Sands	Clays	SPT	Unplugged
24	Woodrow Wilson Bridge	Sands	Clays	SPT	Unplugged
25	Woodrow Wilson Bridge	Sands	Clays	SPT	Unplugged
26	Salinas River Bridge	Clays	Clays	SPT	Unplugged
27	Port Of Oakland 27NC	Clay	Clays	SPT	Unplugged
28	Port Of Oakland 17NC1	Clay	Clays	SPT	Unplugged
29	Port Of Oakland 10NC1	Clay	Clays	SPT	Unplugged
30	Port Of Oakland 31NC	Clay	Clays	SPT	Unplugged
31	I-880 Oakland Site 3C	Clay	Clays	SPT	Plugged
32	I-880 Oakland Site 3H	Clay	Clay	SPT	Plugged
33	Santa Clara River Bridge 13	Sand	Sands	SPT	Plugged
34	Santa Clara River Bridge 7	Sand	Sands	SPT	Plugged
35	Berenda Slough Br 4	Silts	Silts	SPT	Unplugged

Table A-3: Data used for concrete piles in sand.

N *	fs *	D*	Project Name	#*
6.15625	0.088189752	66	Chesapeake Bay LT-5	57
9.4230769	0.109994345	54	Chesapeake Bay LT-3	55
10.342105	0.160078473	66	Chesapeake Bay LT-4	56
11.25	0.18	54	I-664 Test-4 DeBeer's	66
21.25	0.45	54	Chesapeake Bay LT-6	58
35.307692	0.6	54	I-664 Test-14 DeBeer's	73

Table A-4: Data used for steel piles in sand.

N *	fs *	D*	Project Name	# *
14.33	0.224934149	54	Woodrow Wilson-C	63
35.375	0.633	36	Woodrow Wilson-I	65
43	0.529292342	54	Woodrow Wilson-C	63
48.2	0.535064525	54	Woodrow Wilson-C DeBeer's	63
50.172	0.934955607	42	Woodrow Wilson-F DeBeer's	64
80	1	36	Woodrow Wilson-I	65
85	1.15	42	Woodrow Wilson-F	64
91.33	1.65	42	Woodrow Wilson-F	64

*

- N: Uncorrected SPT blow count.
- fs: Skin friction in tsf.
- D: Outer diameter of the pile.
- #: UF/FDOT database entry number.

Table A-5: Data used for concrete piles in clay.

N *	fs *	D	Project Name	# *
10.27	0.20253552	54	Chesapeake Bay LT-1	52
10.3	0.245123125	54	I-664 Test-7 DeBeer's	66
10.5	0.387002901	42	Oakland 10 NC1	84
12.20588	0.3	54	Chesapeake Bay LT-2	53
16.4	0.521819486	42	Oakland 31NC	85
19.33	0.596365126	42	Oakland 27NC	82
23.25	1.02	42	Oakland 17NC-1	83

Table A-6: Data used for steel piles in clay.

N *	fs *	D	Project Name	# *
55.25	1.2	54	Woodrow Wilson-C	63
49	1.15	42	Woodrow Wilson-F	64
29	0.85	42	Woodrow Wilson-F	64
10.4	0.381209445	42	I-880 3C	86
10.4	0.353980198	42	I-880 3H	87
10	0.397093171	72	Salinas River Bridge	81

Table A-7: Data used for concrete piles in silt.

N *	fs *	D *	Project Name	# *
3.6	0.033382	54	St. Georges LT-1	59
4.875	0.120239	54	St. Georges LT-3	61
8	0.22441	54	St. Georges LT-2	60
9.423077	0.109994	54	Chesapeake Bay LT-3	55
17.75	0.445944	54	St. Georges LT-4	62
18.67	0.344521	54	St. Georges LT-2	60
22.22	0.549678		San Mateo Hayward A	
22.7	0.57	54	St. Georges LT-4	62
23.4	0.52	54	St. Georges LT-3	61

*

- N: Uncorrected SPT blow count.
- fs: Skin friction in tsf.
- D: Outer diameter of the pile.
- #: UF/FDOT database entry number.

Table A-8: Data used for the end bearing in sand.

N *	Qt *	D *	Project Name	# *	Material *
50	30	66	Chesapeake Bay LT-4	56	Concrete
51	33.0199	54	I-664 Test-4 DeBeer's	66	Concrete
23	16.79968844	72	Santa Clara 13-1	88	Steel
27	24.667	42	Berenda Slough	90	Steel
28.5	22.10485321	72	Santa Clara 13-2	88	Steel
29	13.2001161	84	Santa Clara 7-1	89	Steel
55.33	30.5764579	84	Santa Clara 7-2	89	Steel
100	51.96	42	Woodrow Wilson-F DeBeer’s	64	Steel
100	55	42	Woodrow Wilson-F	64	Steel

Table A-9: Data used for end bearing in silt.

N *	Qt *	D *	Project Name	# *	Material *
14.5	5.196896	42	Oakland 10NC-1	84	Steel
22	7.795344	92	San Mateo Hayward Bridge	92	Concrete
29	13.20012	84	Santa Clara 7-1	89	Steel
50	30	66	Chesapeake Bay LT-4	56	Concrete
55.33	30.57646	84	Santa Clara 7-2	89	Steel

Table A-10: Data used for end bearing in clay.

N *	Qt *	D *	Project Name	# *	Material *
3	1.1	42	Oakland 17NC-1	84	Steel
14.25	3.27	72	Salinas River Bridge	81	Steel
16.4	3.65	42	Oakland 31NC	85	Steel
18	4	42	I-880 3C	86	Steel

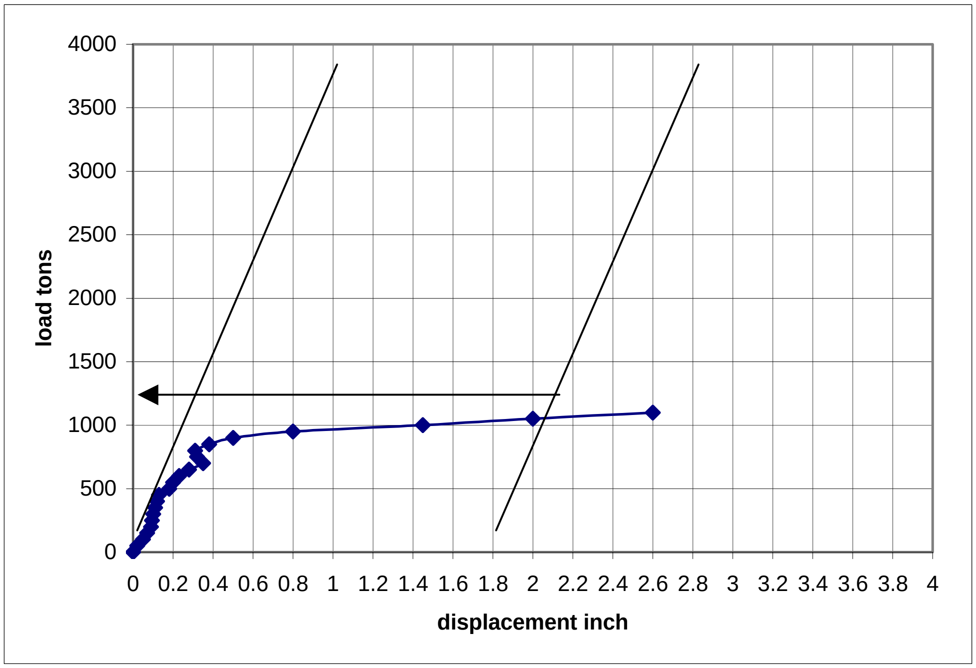

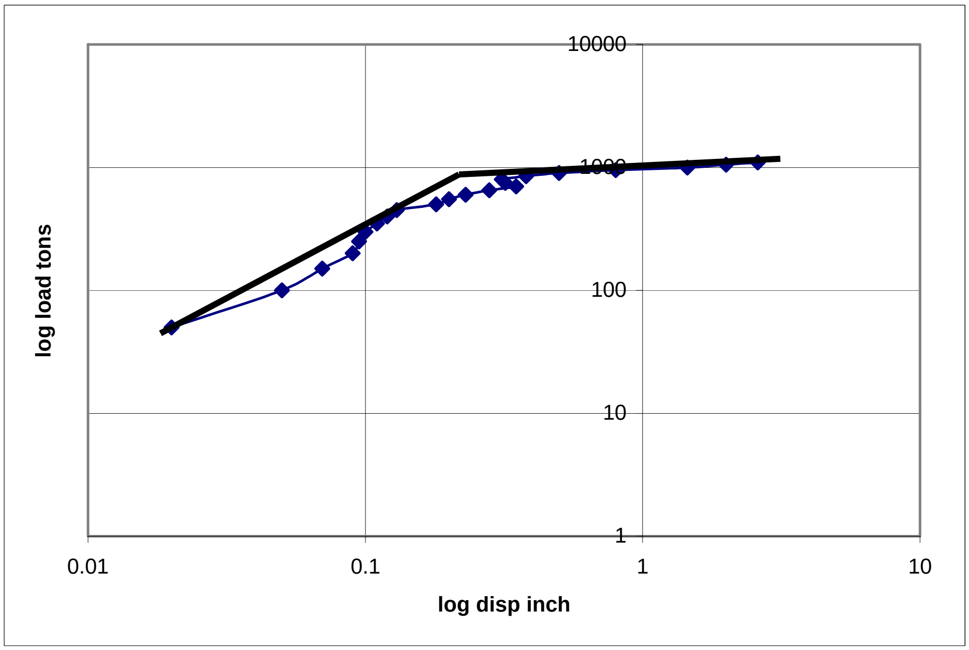

St. Georges Island Bridge Replacement Project LT-1	
Skin Friction Capacity	850 Tons
End Bearing Capacity	200 Tons
FDOT Capacity	1050 Tons

Figure A-1: St. Georges Island Bridge Replacement Project LT-1.

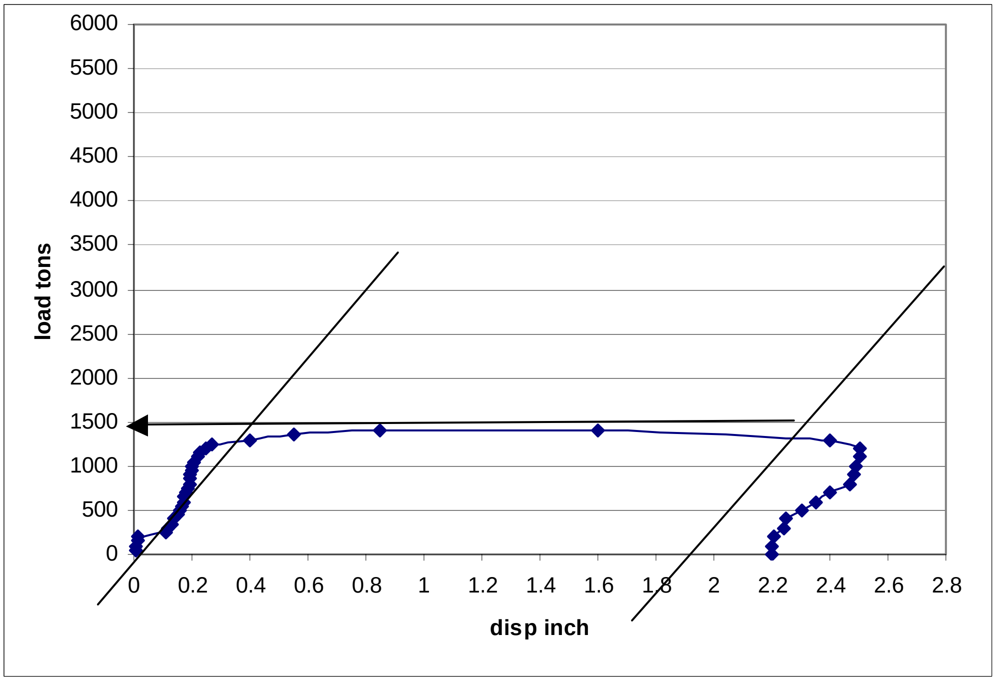

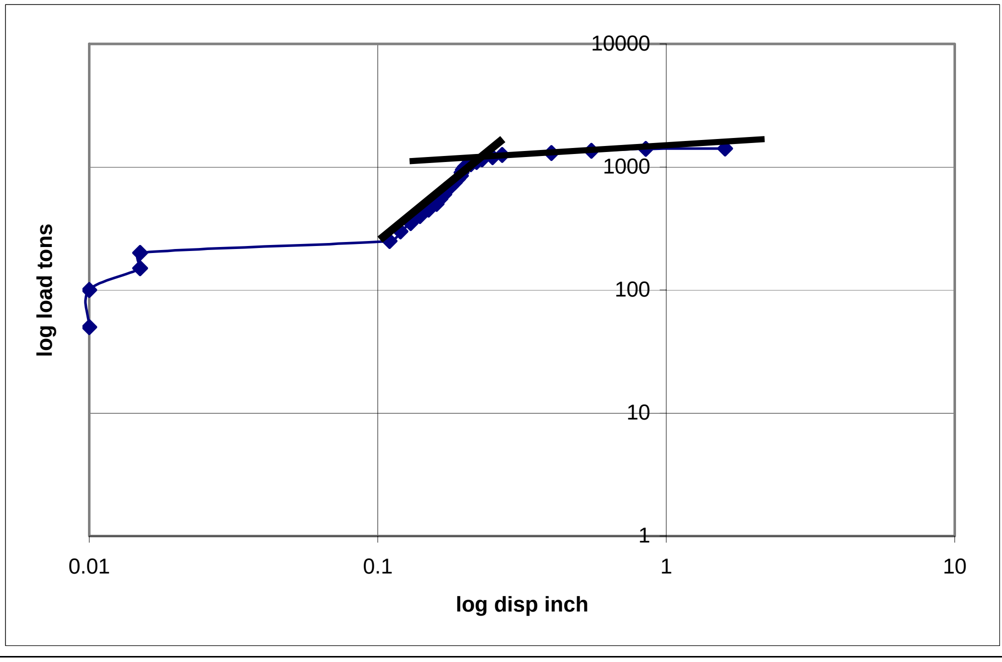

St. Georges Island Bridge Replacement Project LT-4.	
Skin Friction Capacity	1300 Tons
End Bearing Capacity	200 Tons
FDOT Capacity	1500 Tons

Figure A-2: St. Georges Island Bridge Replacement Project, LT-4.

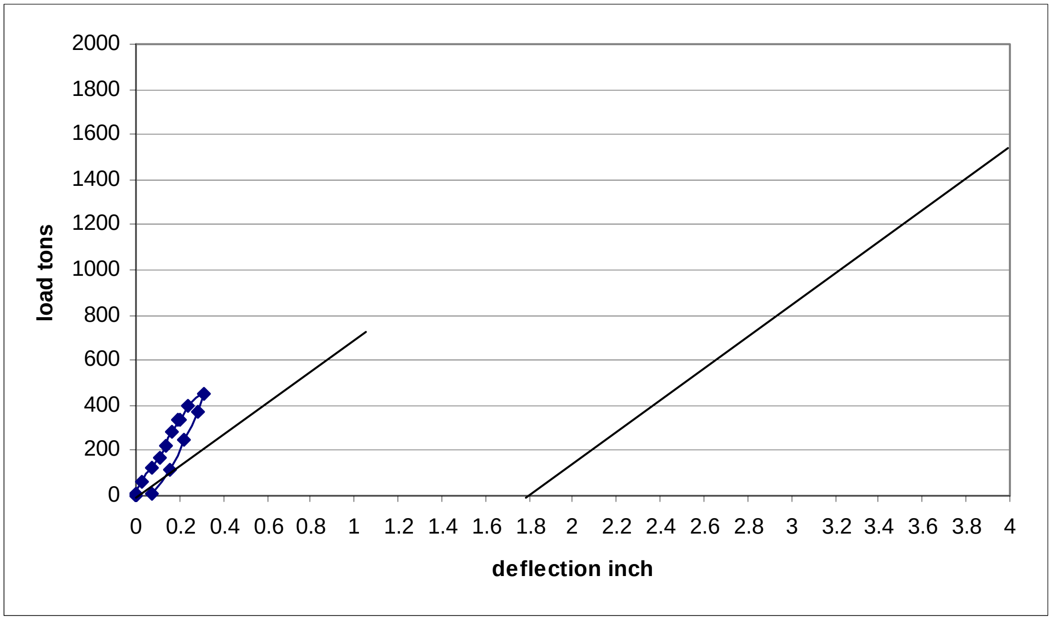

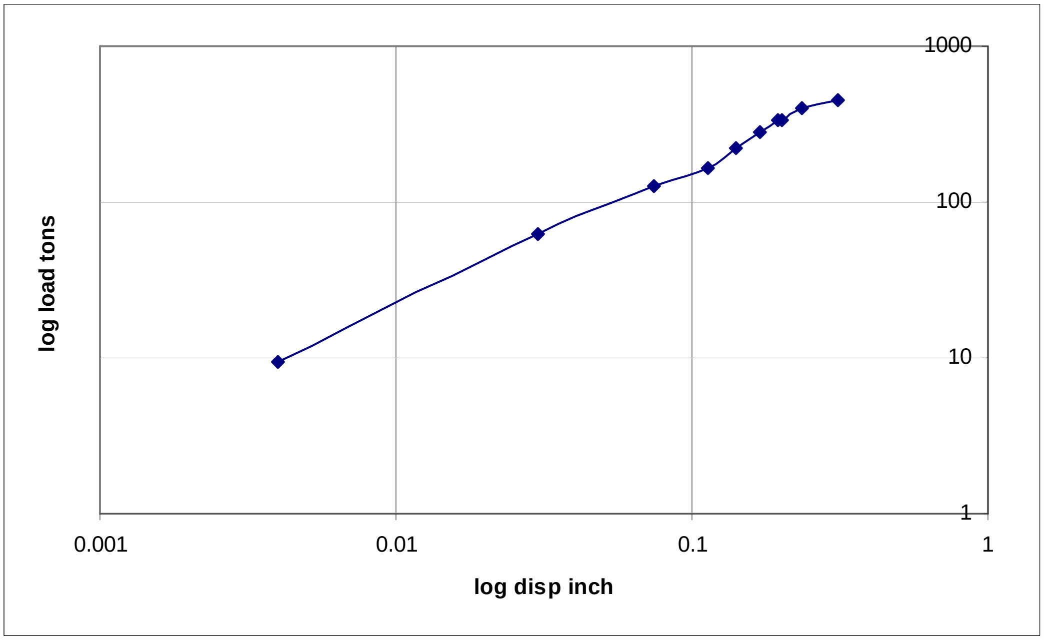

Chesapeake Bay LT-1.	
Skin Friction Capacity	N.A (not taken to failure)
End Bearing Capacity	N.A (not taken to failure)

Figure A-3: Chesapeake Bay LT-1.

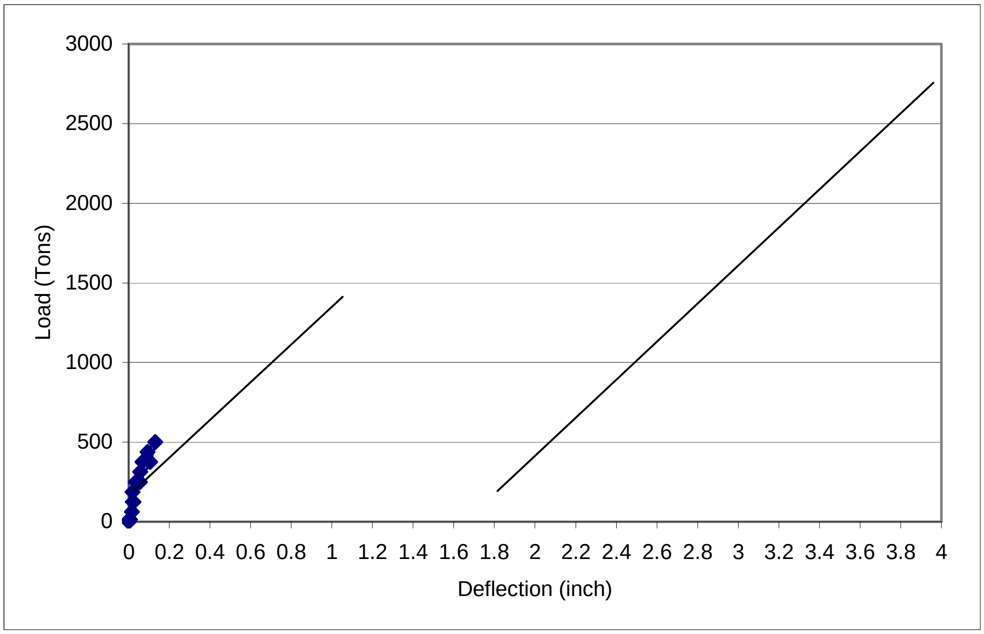

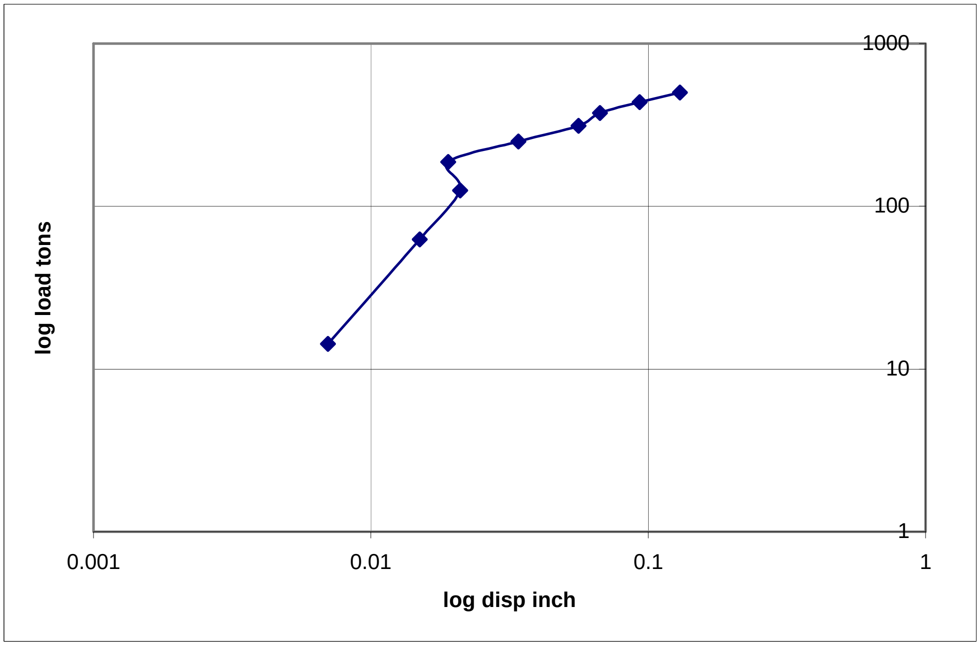

Chesapeake Bay LT-2.	
Skin Friction Capacity	N.A (not taken to failure)
End Bearing Capacity	N.A (not taken to failure)

Figure A-4: Chesapeake Bay LT-2.

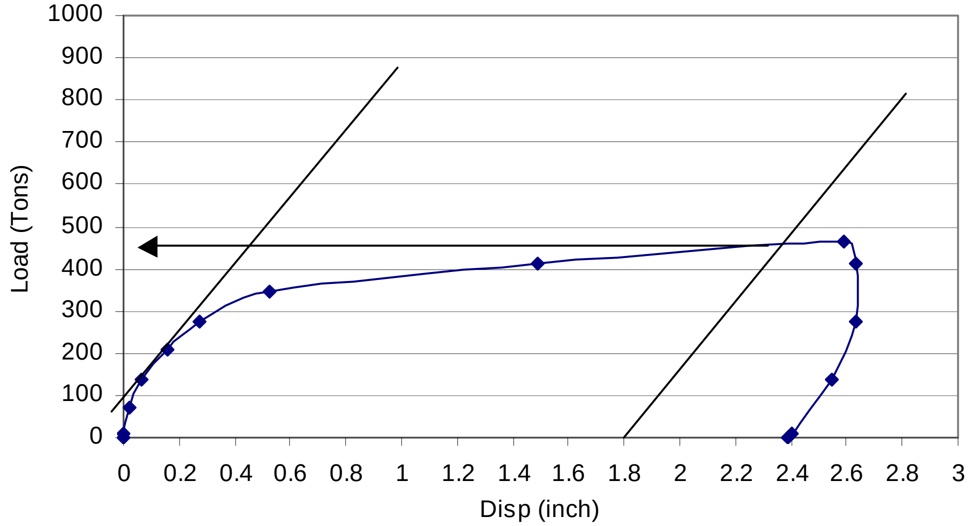

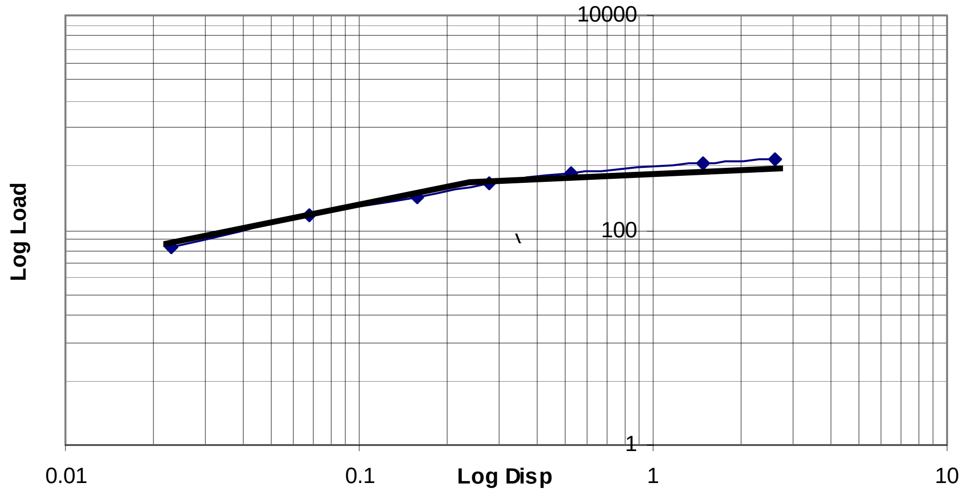

Chesapeake Bay LT-6.	
Skin Friction Capacity	300 Tons
End Bearing Capacity	150 Tons
FDOT Capacity	450 Tons

Figure A-5: Chesapeake Bay LT-6.

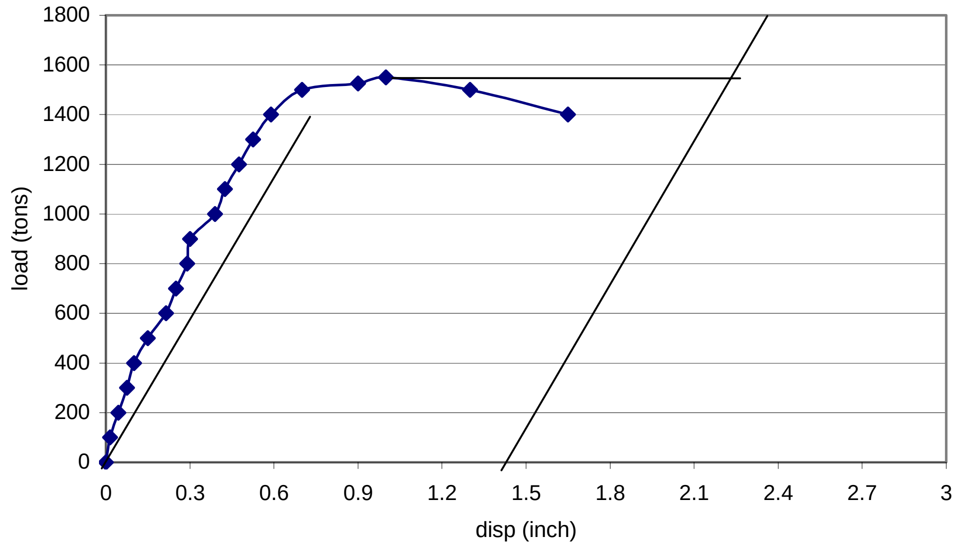

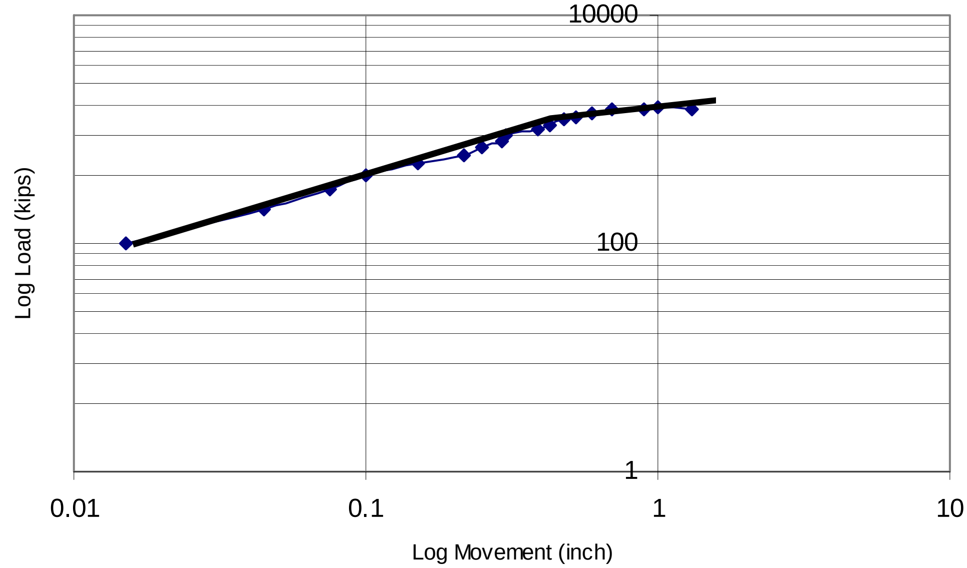

San Mateo Hayward Bridge- A.	
Skin Friction Capacity	700 Tons
End Bearing Capacity	75 Tons
FDOT Capacity	775 Tons

Figure A-6: San Mateo Hayward Bridge-A.

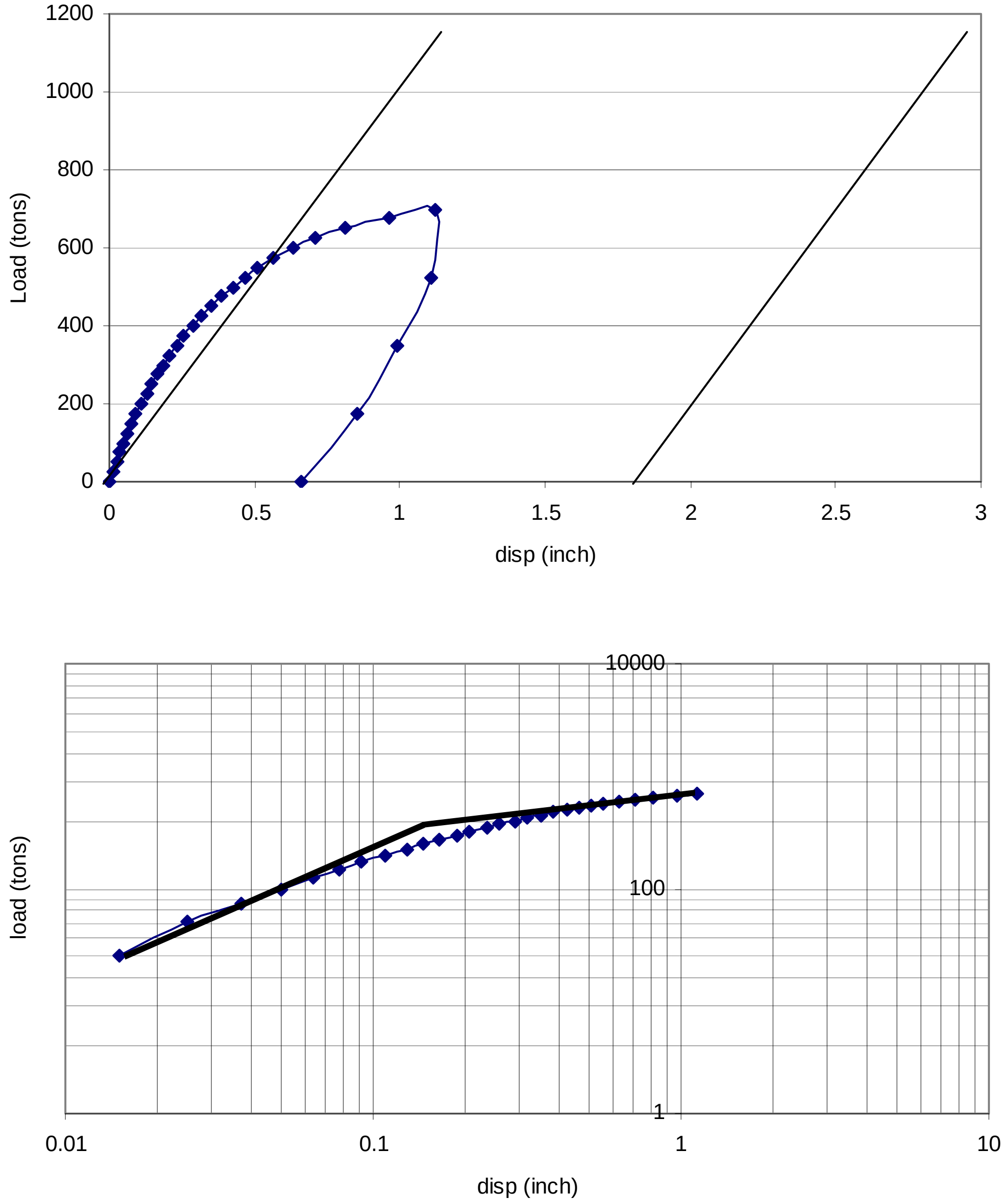

I-664 Bridge Test-4.	
Skin Friction Capacity	400 Tons
End Bearing Capacity	250 Tons
FDOT Capacity	650 Tons

Figure A-7: I-664 Bridge Test-4.

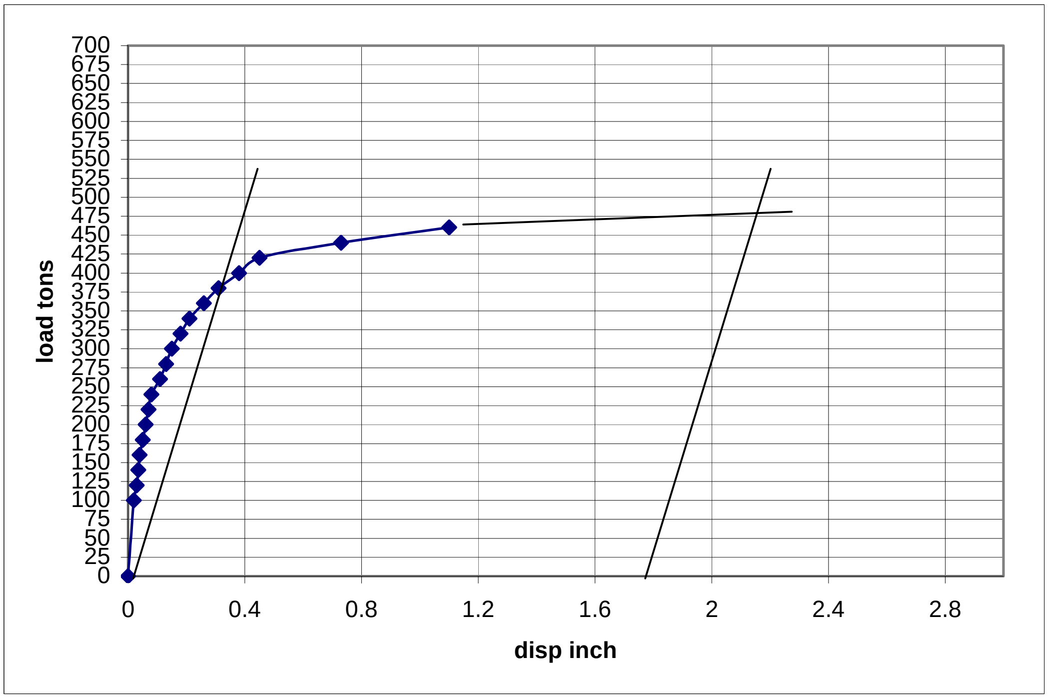

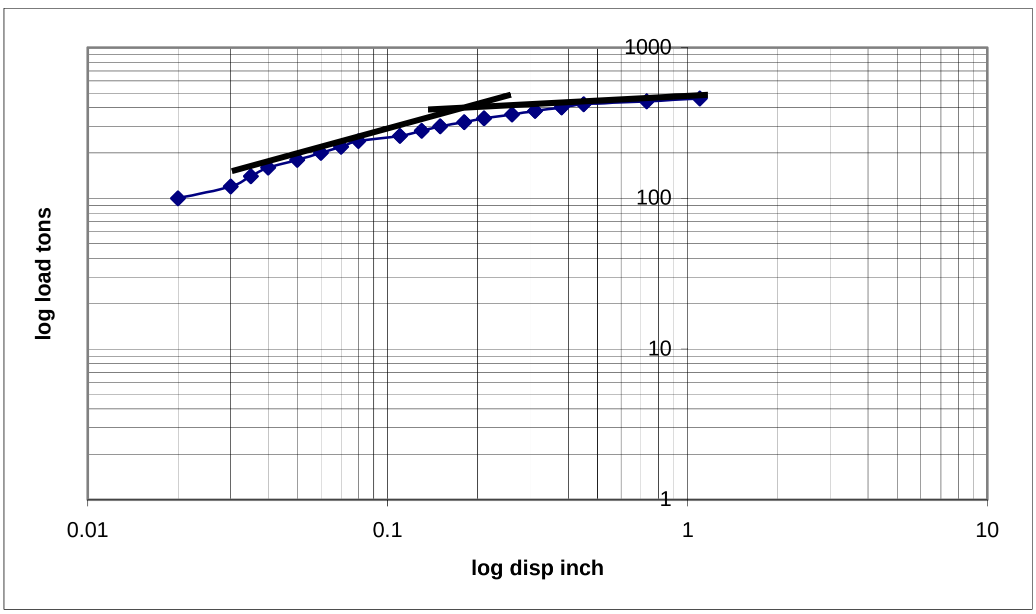

I-664 Bridge Test-7.	
Skin Friction Capacity	350 Tons
End Bearing Capacity	125 Tons
FDOT Capacity	475 Tons

Figure A-8: I-664 Bridge Test-7.

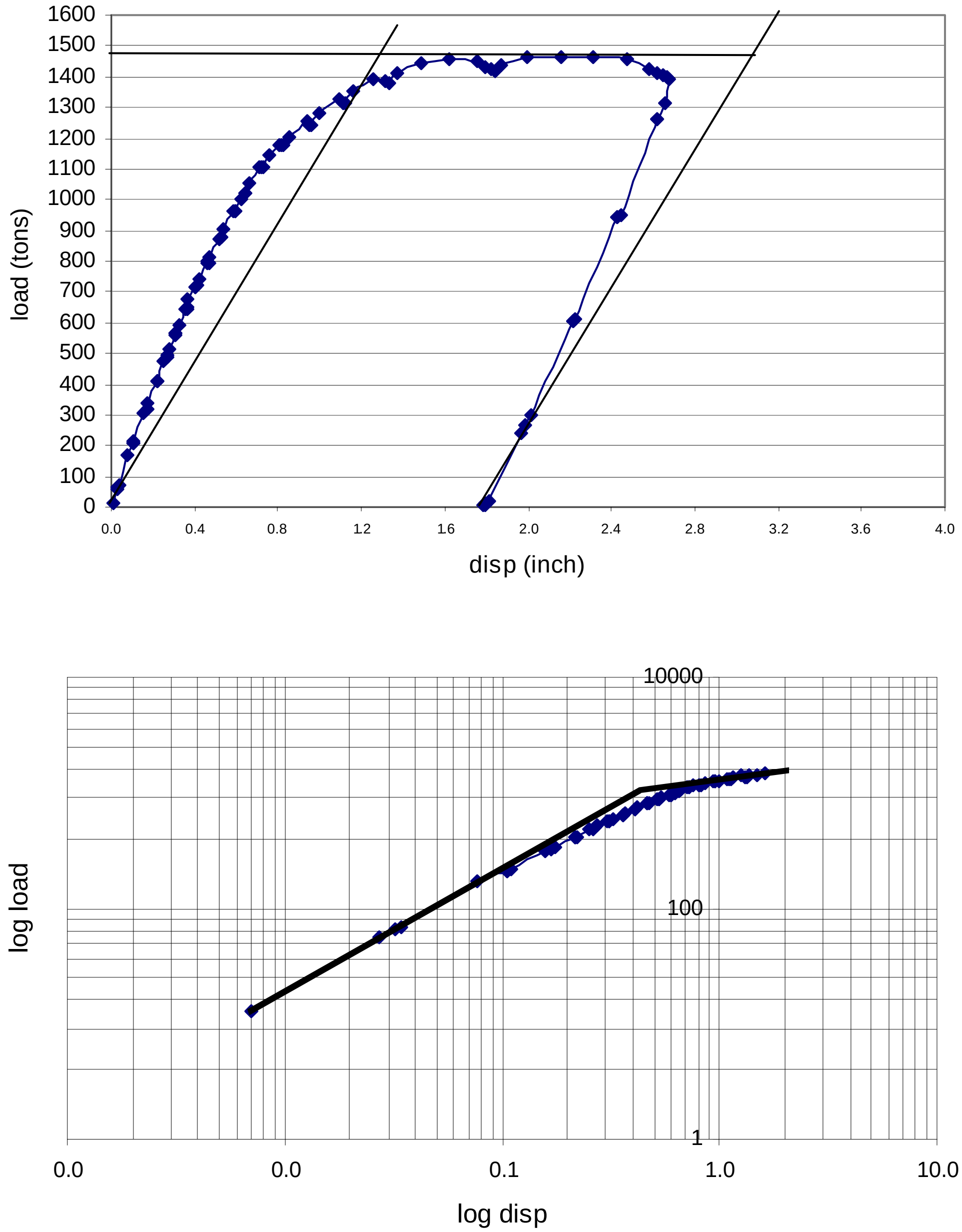

Woodrow Wilson Bridge-C.	
Skin Friction Capacity	1000 Tons
End Bearing Capacity	475 Tons
FDOT Capacity	1475 Tons

Figure A-9: Woodrow Wilson Bridge-C.

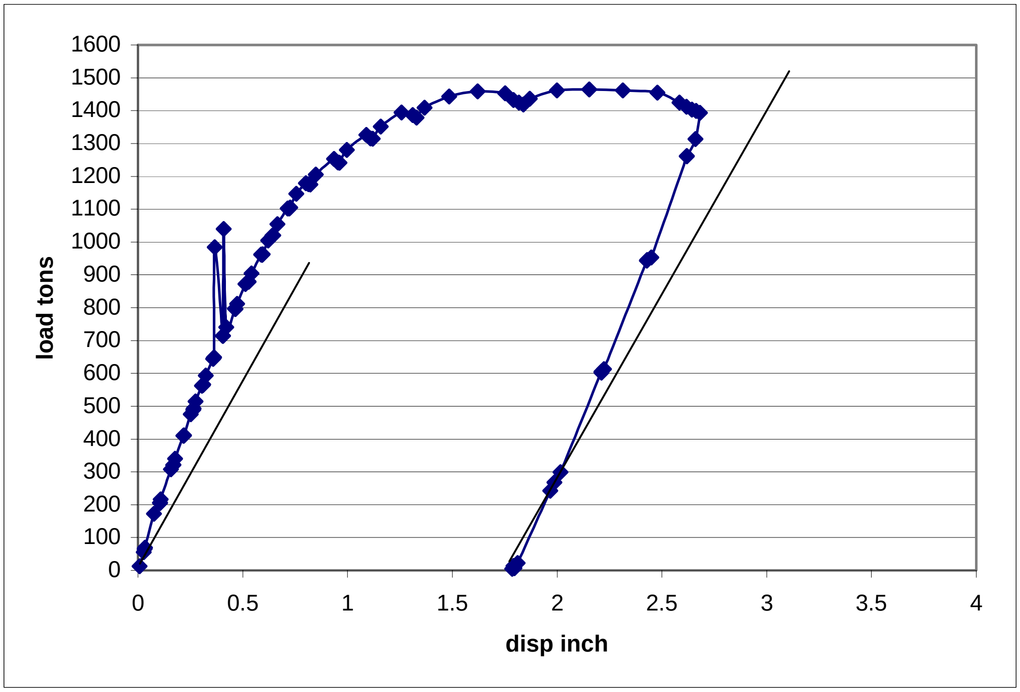

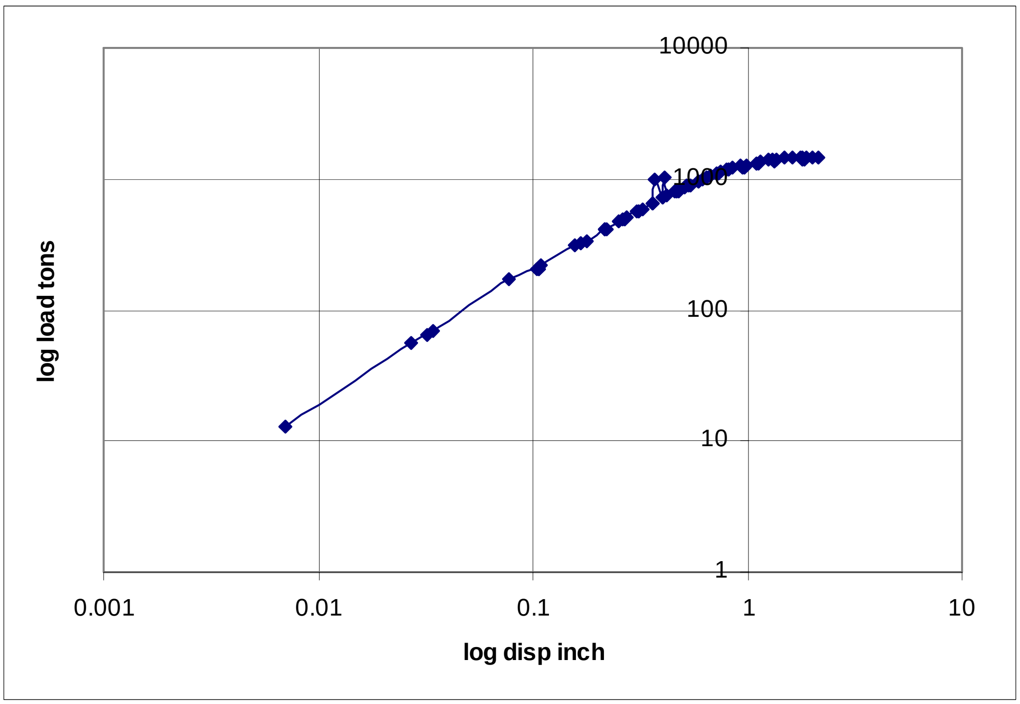

Woodrow Wilson Bridge-F.	
Skin Friction Capacity	1000 Tons
End Bearing Capacity	500 Tons
FDOT Capacity	1500 Tons

Figure A-10: Woodrow Wilson Bridge-F.

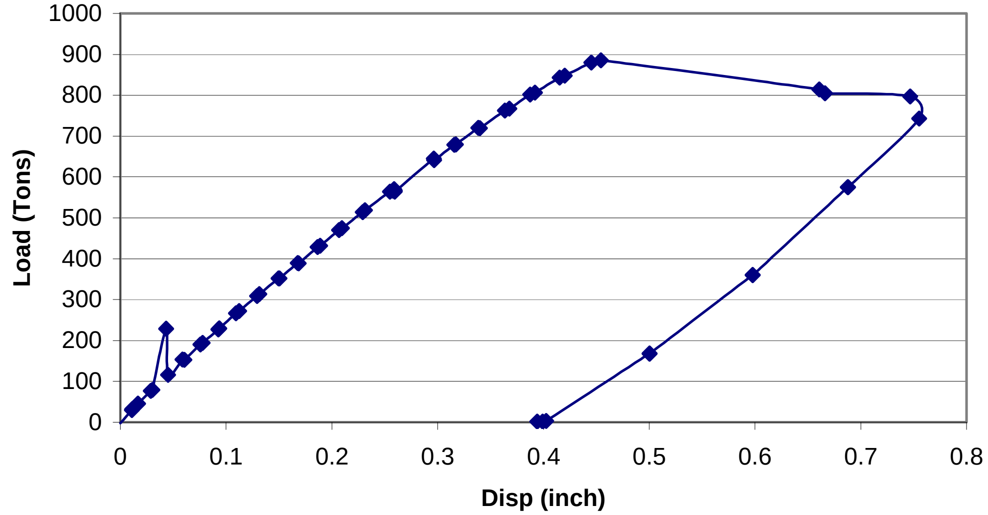

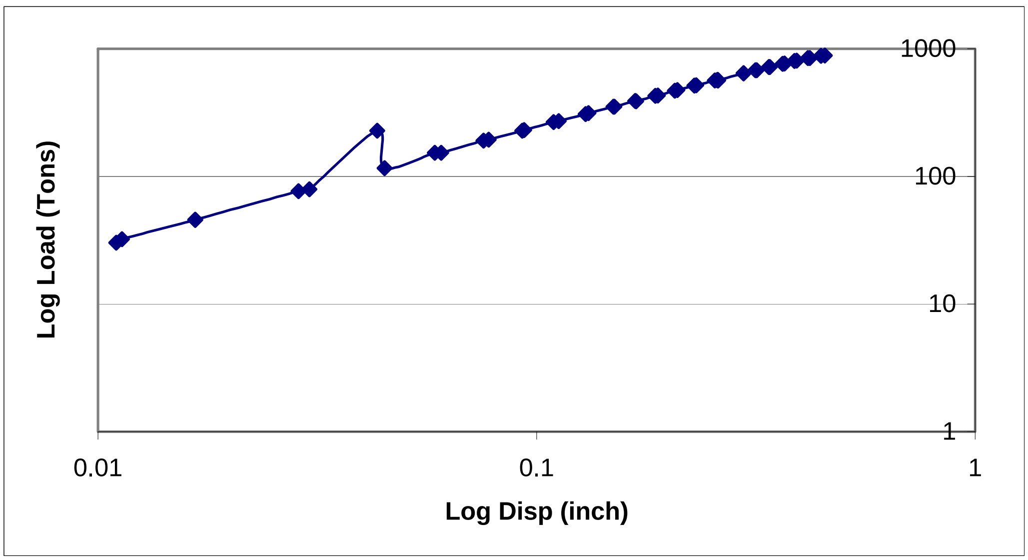

Woodrow Wilson Bridge-I.	
FDOT Capacity	900Tons

Figure A-11: Woodrow Wilson Bridge-I.

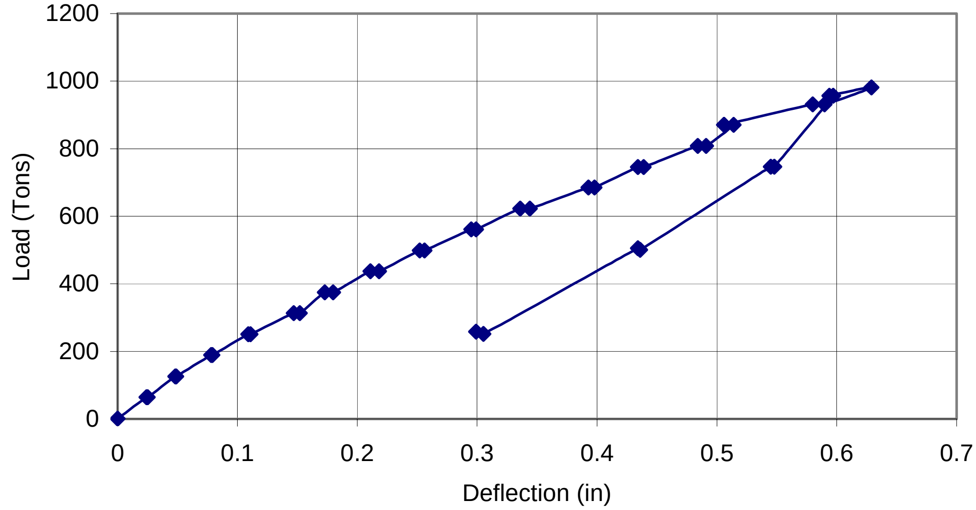

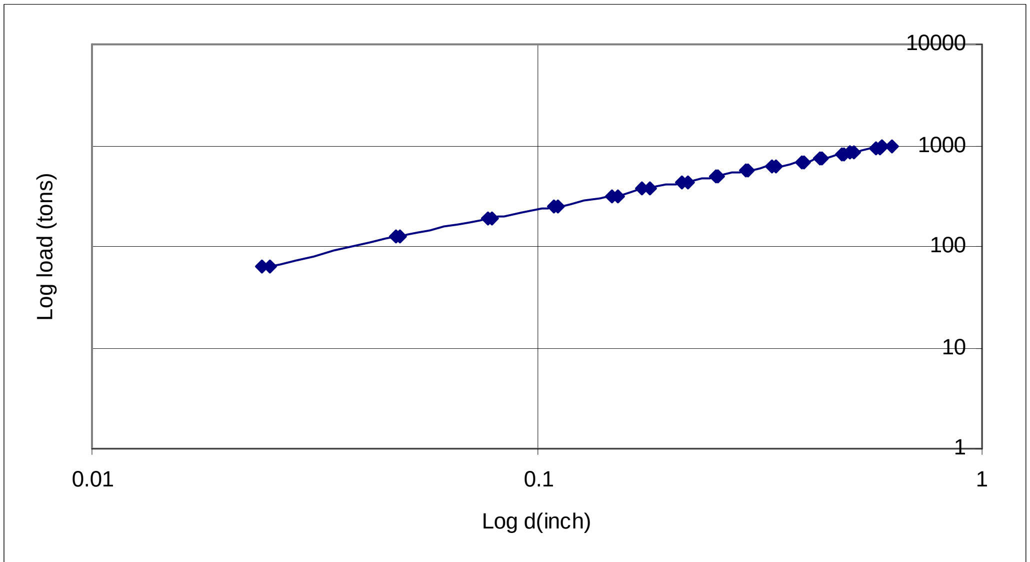

Oregon Inlet.	
Skin Friction Capacity	N.A (not taken to failure)
End Bearing Capacity	N.A (not taken to failure)

Figure A-12: Oregon Inlet.

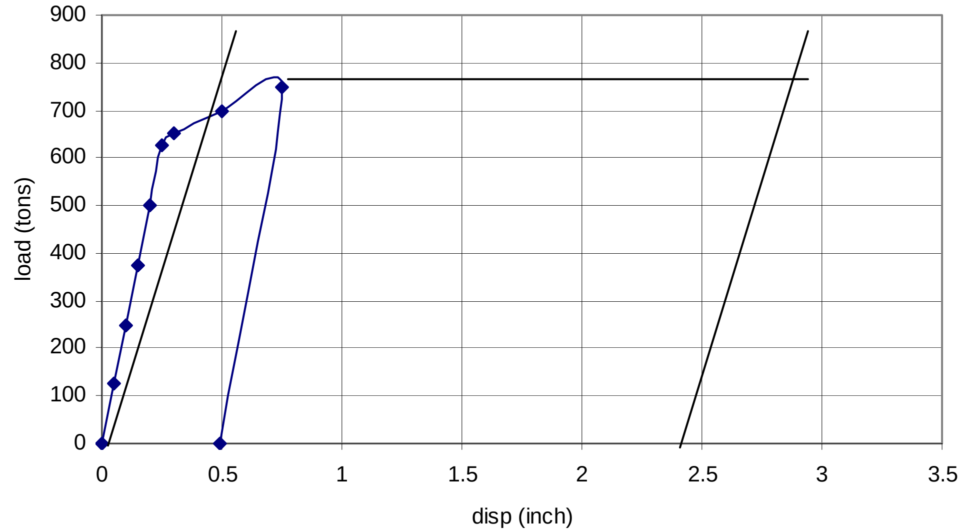

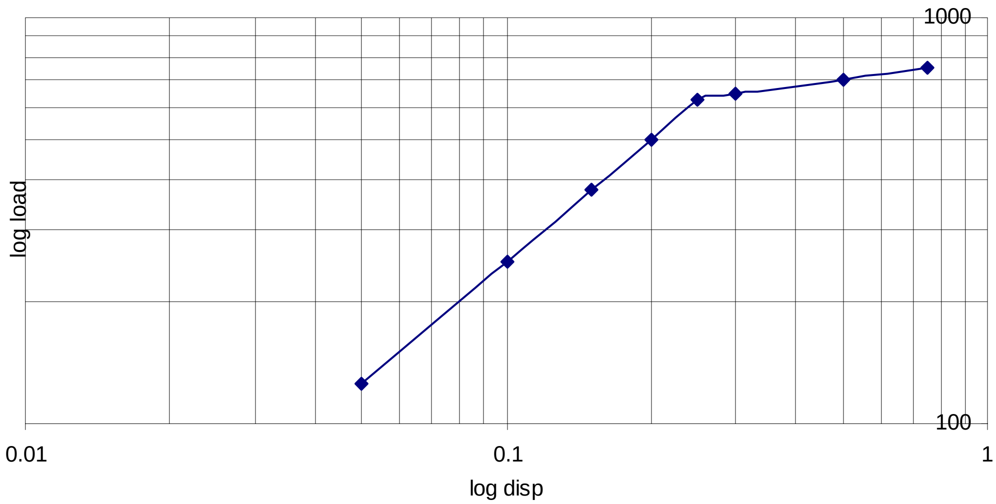

Salinas River Bridge	
Skin Friction Capacity	600 Tons
End Bearing Capacity	150 Tons
FDOT Capacity	750 Tons

Figure A-13: Salinas River Bridge.

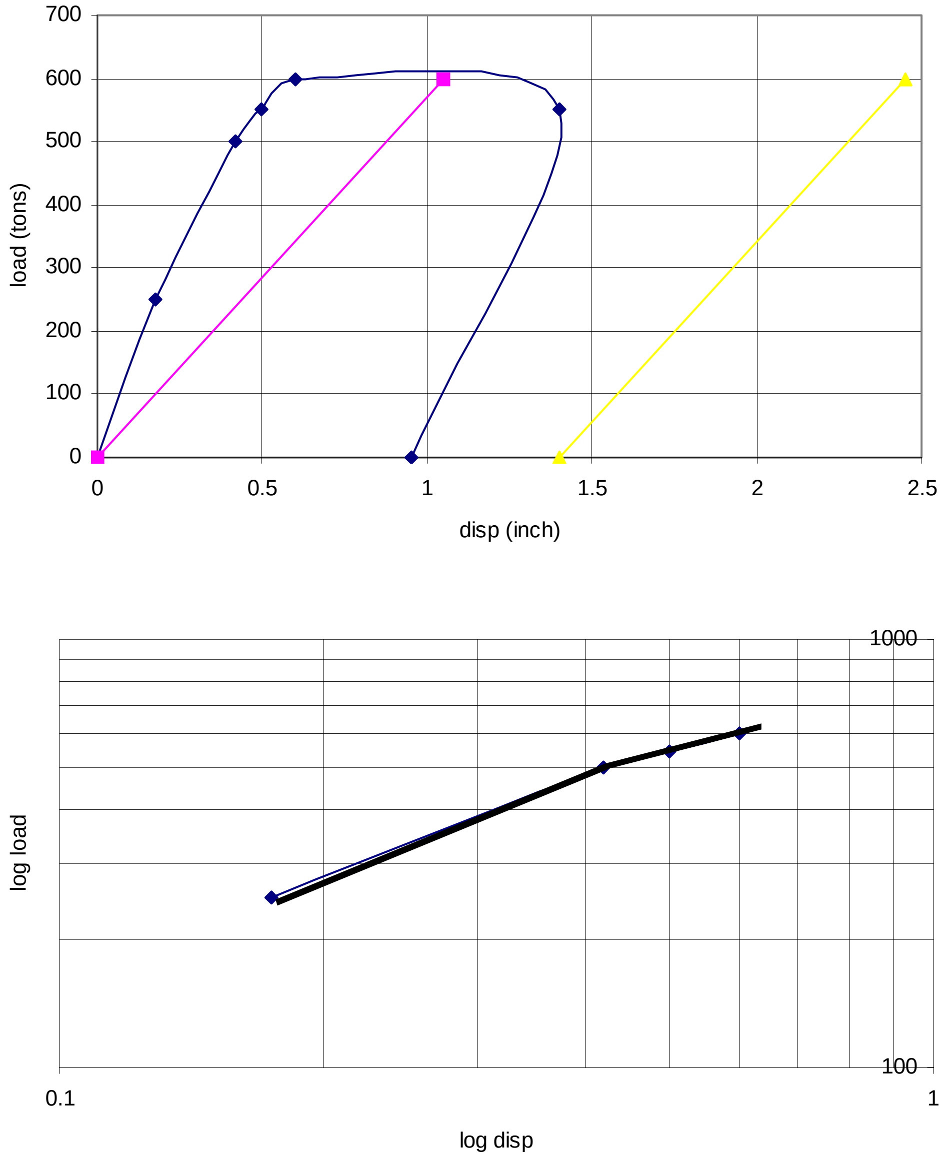

Port of Oakland Bridge 27NC.	
Skin Friction Capacity	550Tons
End Bearing Capacity	75 Tons
FDOT Capacity	625 Tons

Figure A-14: Port of Oakland Bridge 27NC.

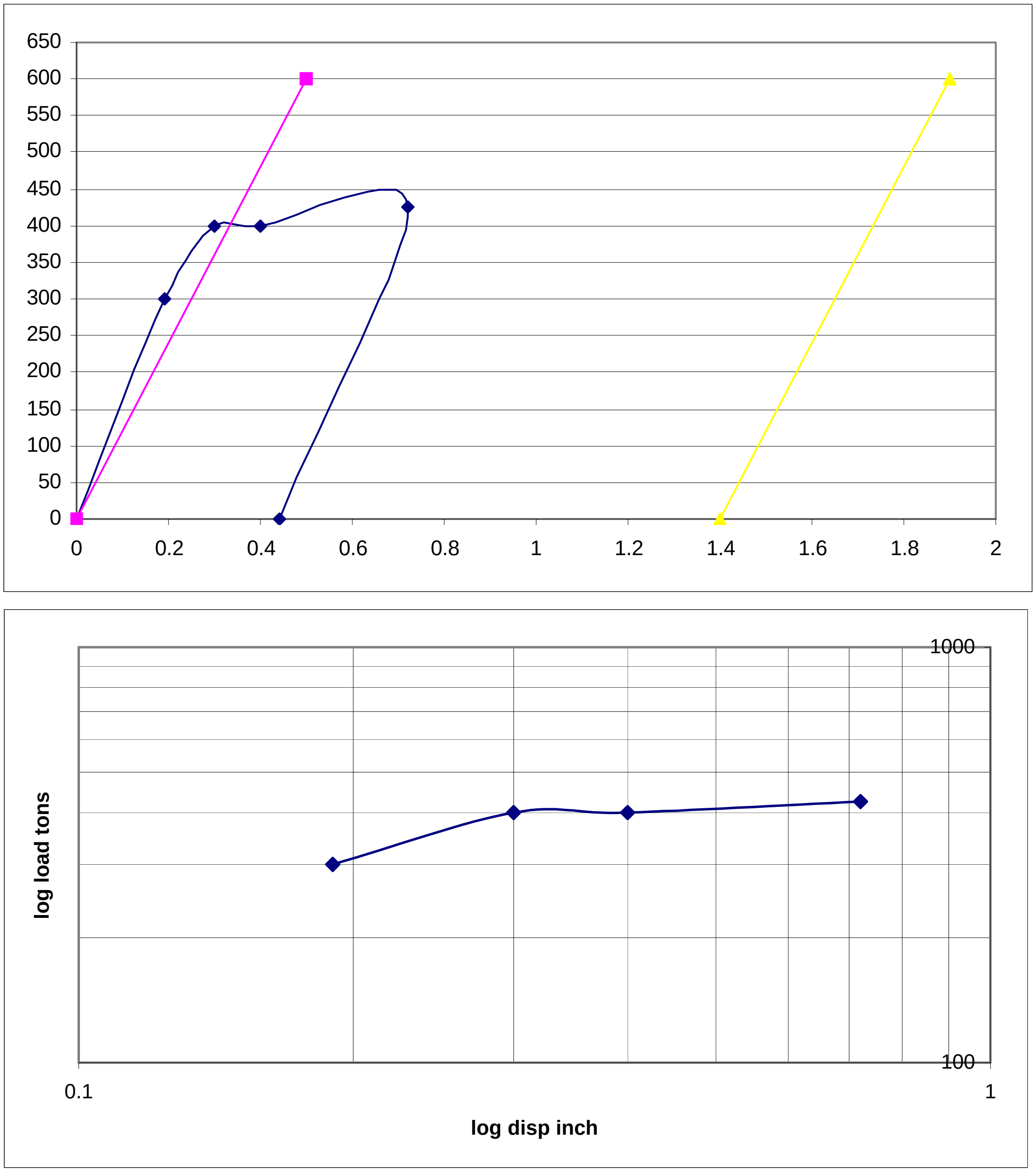

Port of Oakland Bridge 10NC.	
Skin Friction Capacity	400Tons
End Bearing Capacity	50 Tons
FDOT Capacity	450 Tons

Figure A-15: Port of Oakland Bridge 10NC.

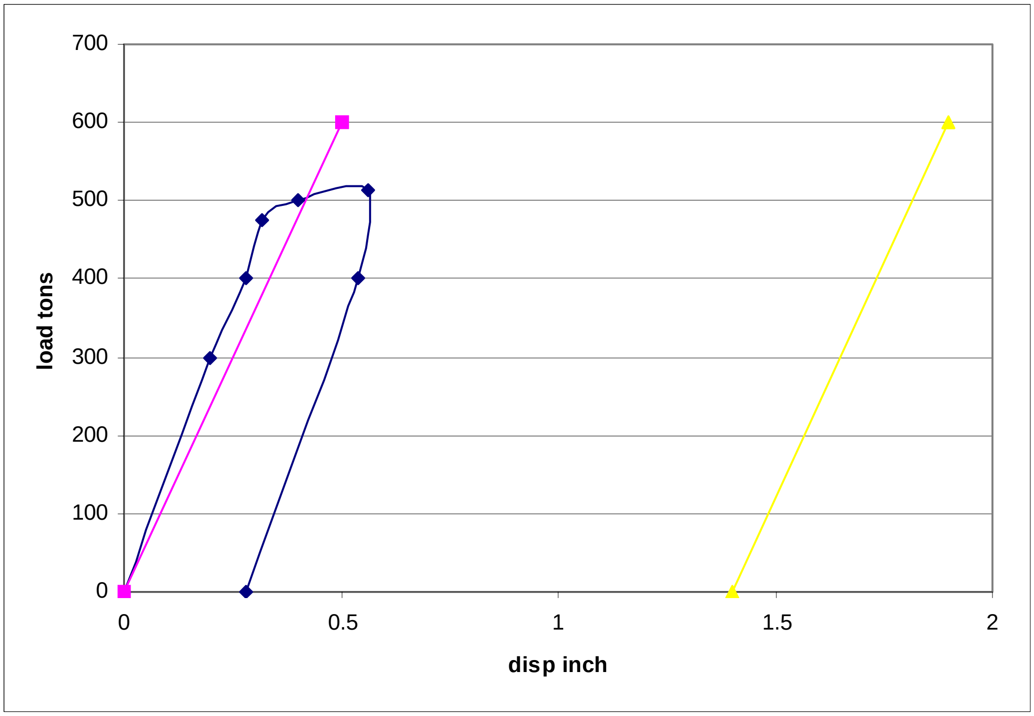

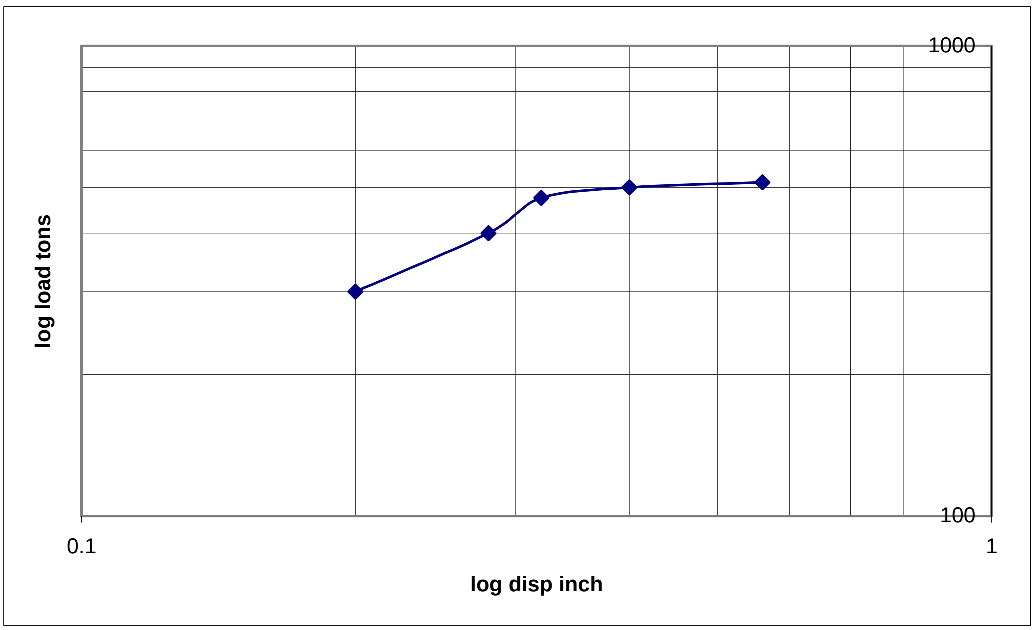

Port of Oakland Bridge 17NC.	
Skin Friction Capacity	475 Tons
End Bearing Capacity	37.5 Tons
FDOT Capacity	512.5 Tons

Figure A-16: Port of Oakland Bridge 17NC.

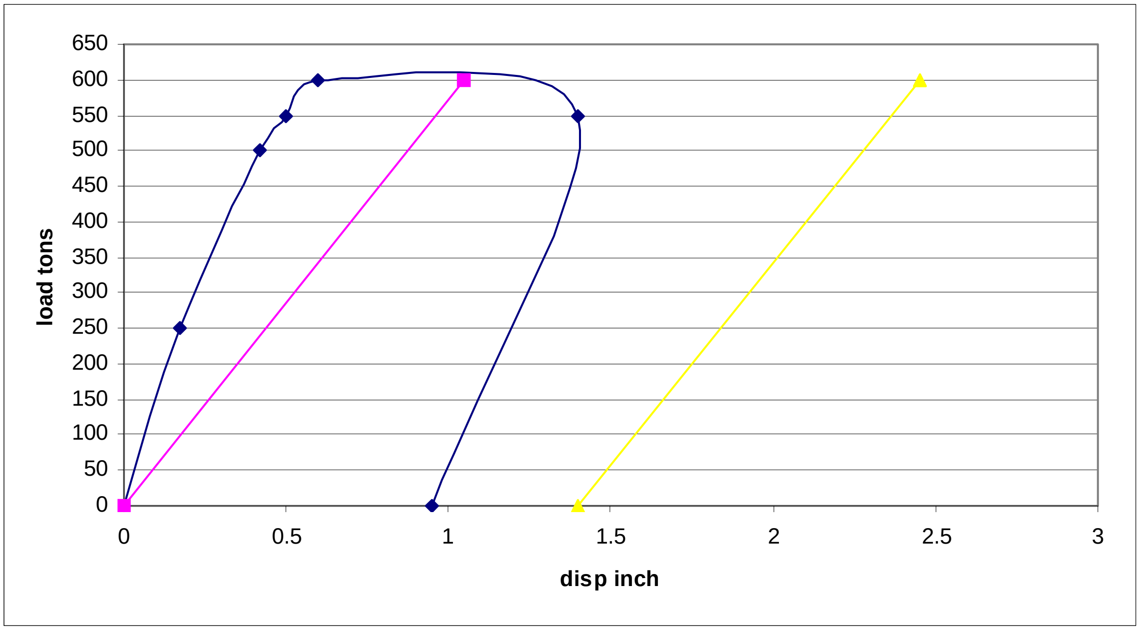

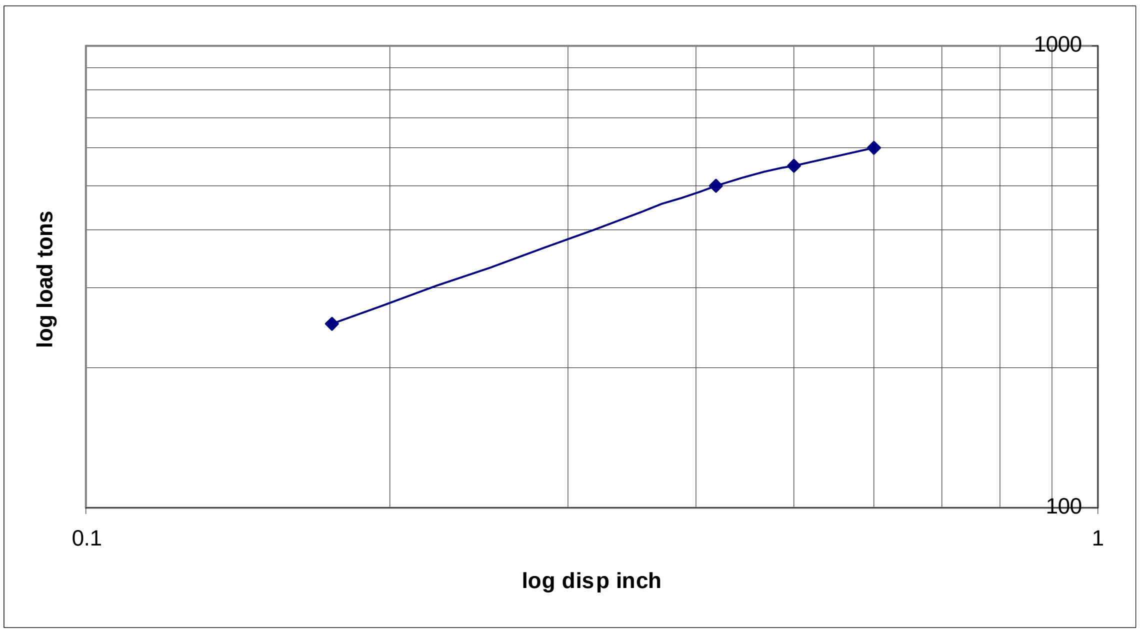

Port of Oakland Bridge 31NC.	
Skin Friction Capacity	525 Tons
End Bearing Capacity	75 Tons
FDOT Capacity	600 Tons

Figure A-17: Port of Oakland Bridge 31NC.

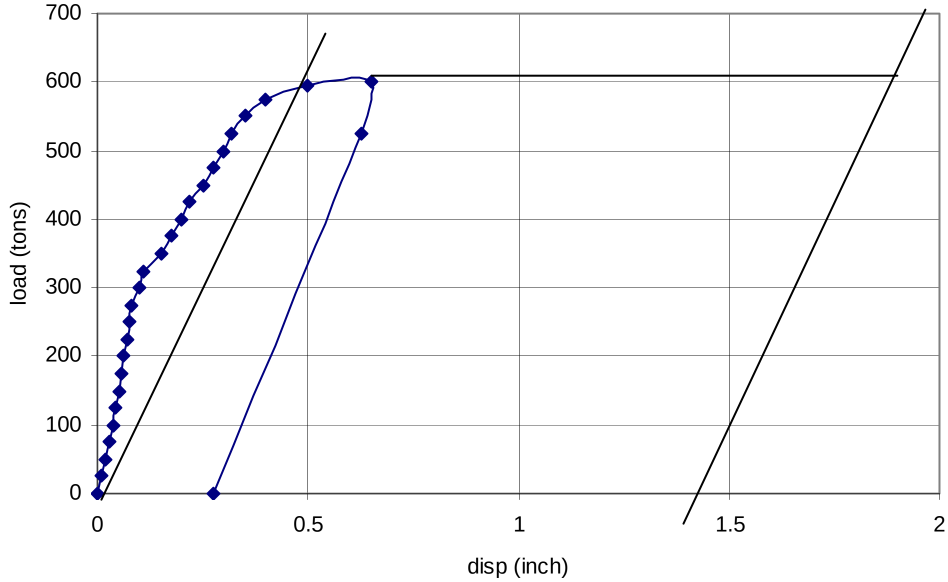

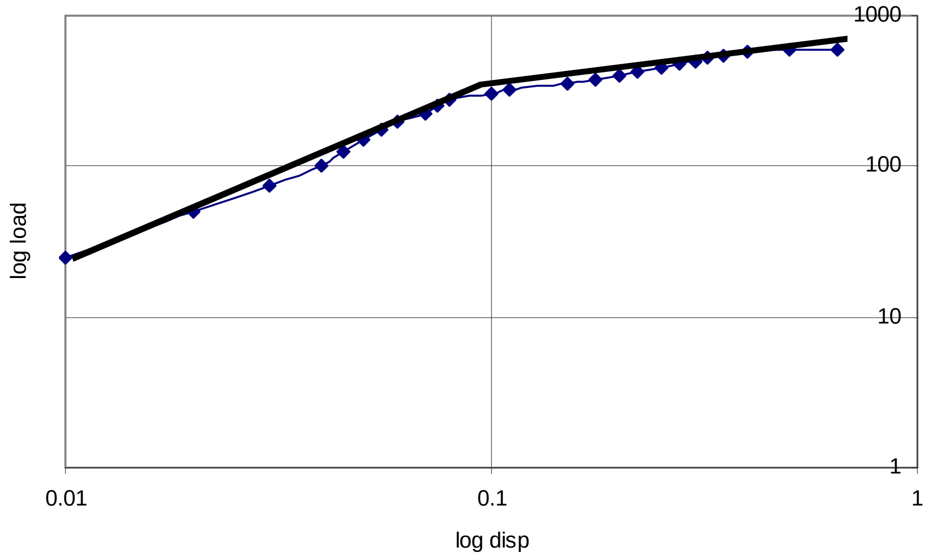

I-880 Bridge 3H.	
Skin Friction Capacity	325 Tons
End Bearing Capacity	275 Tons
FDOT Capacity	600 Tons

Figure A-18: I-880 Bridge 3H.

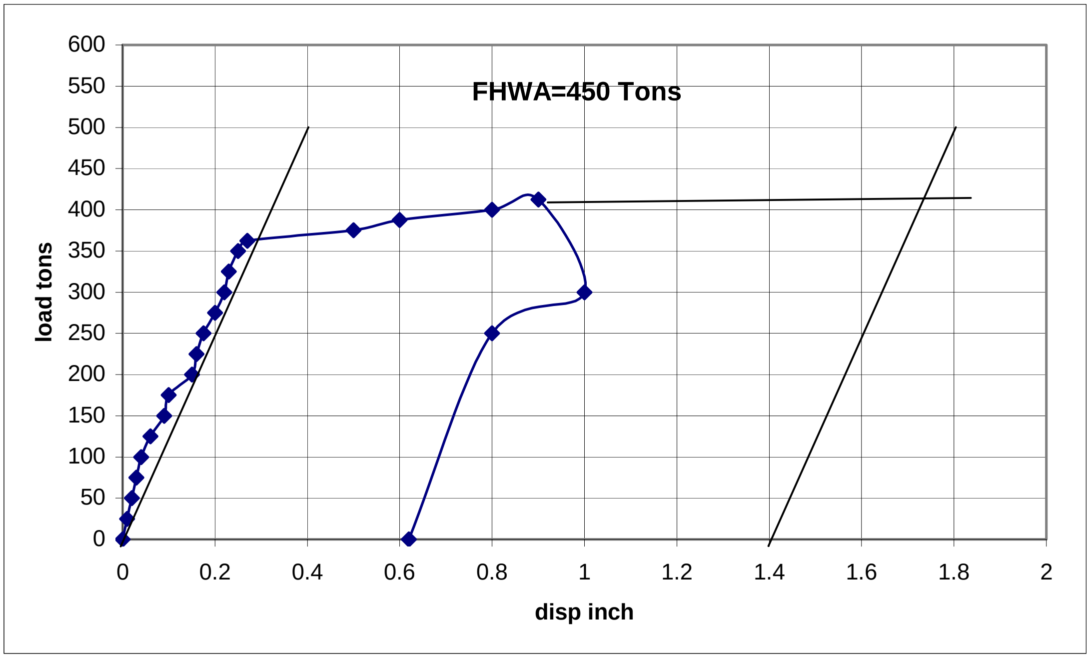

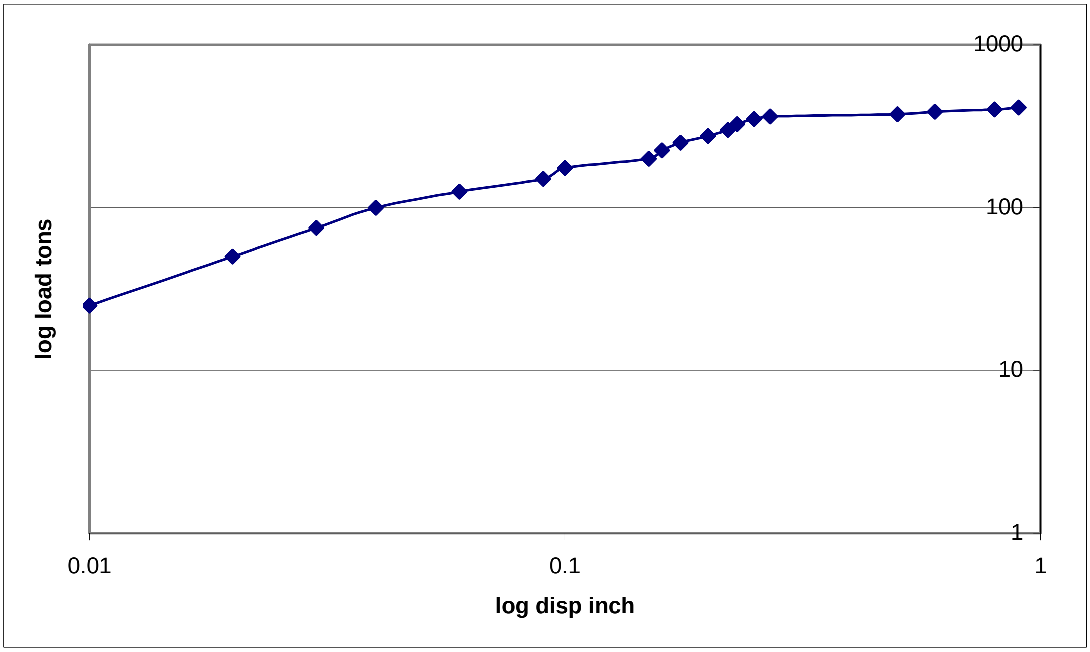

I-880 Bridge 3C.	
Skin Friction Capacity	350 Tons
End Bearing Capacity	100 Tons
FDOT Capacity	450 Tons

Figure A-19: I-880 Bridge 3C.

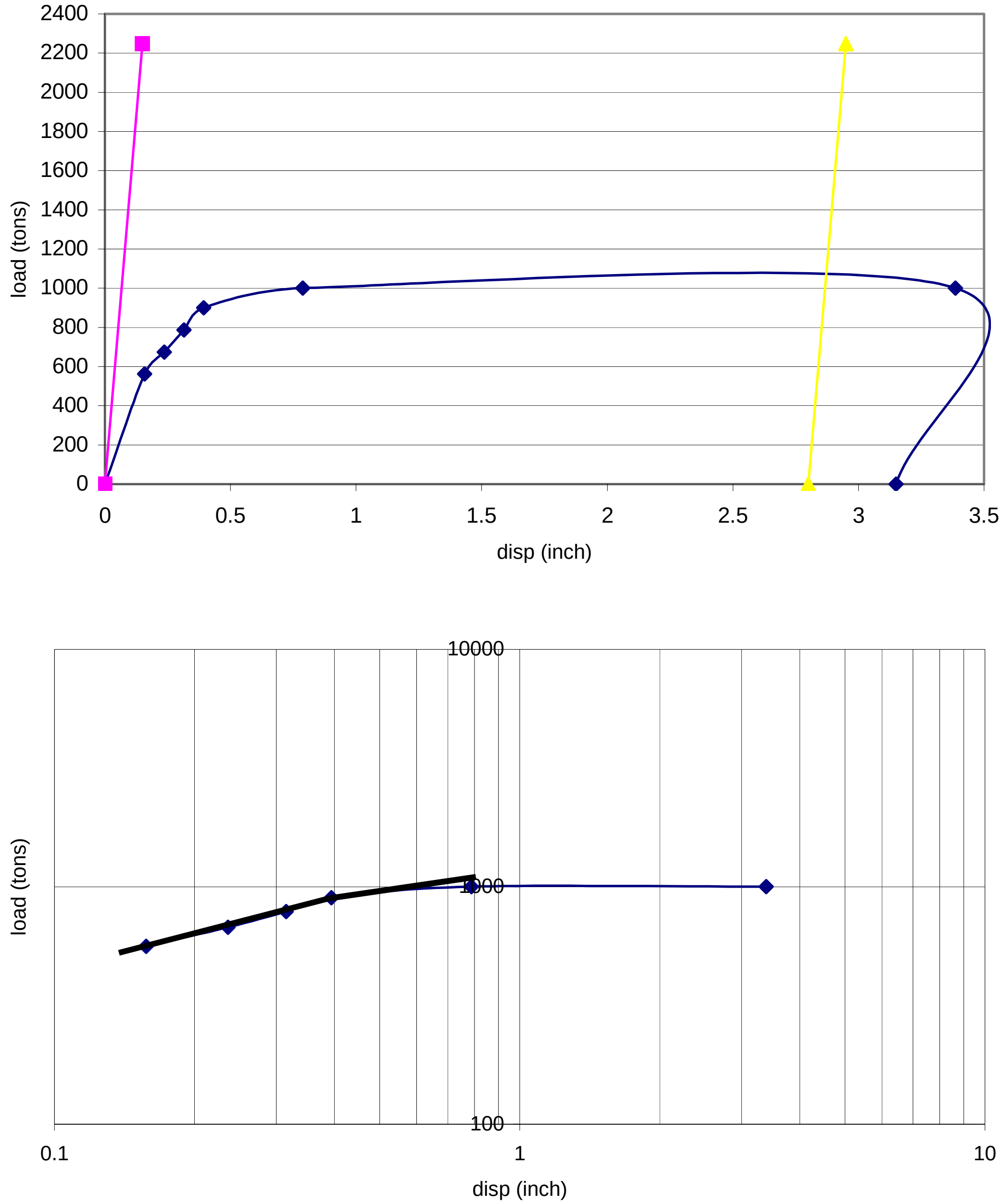

Santa Clara River Bridge Pier-7.	
Skin Friction Capacity	600 Tons
End Bearing Capacity	500 Tons
FDOT Capacity	1100 Tons

Figure A-20: Santa Clara River Bridge Pier-7.

.

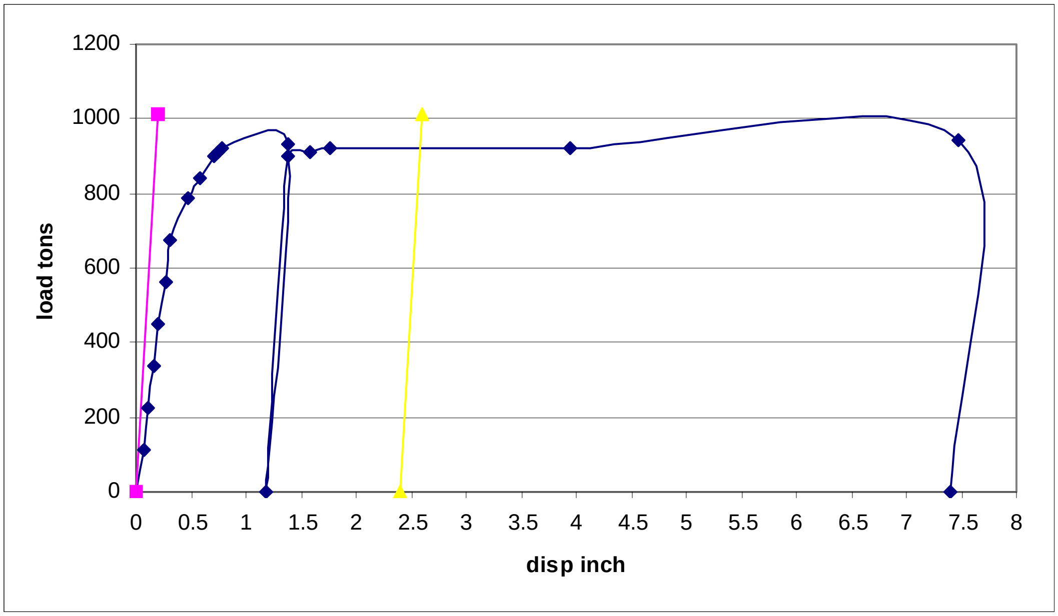

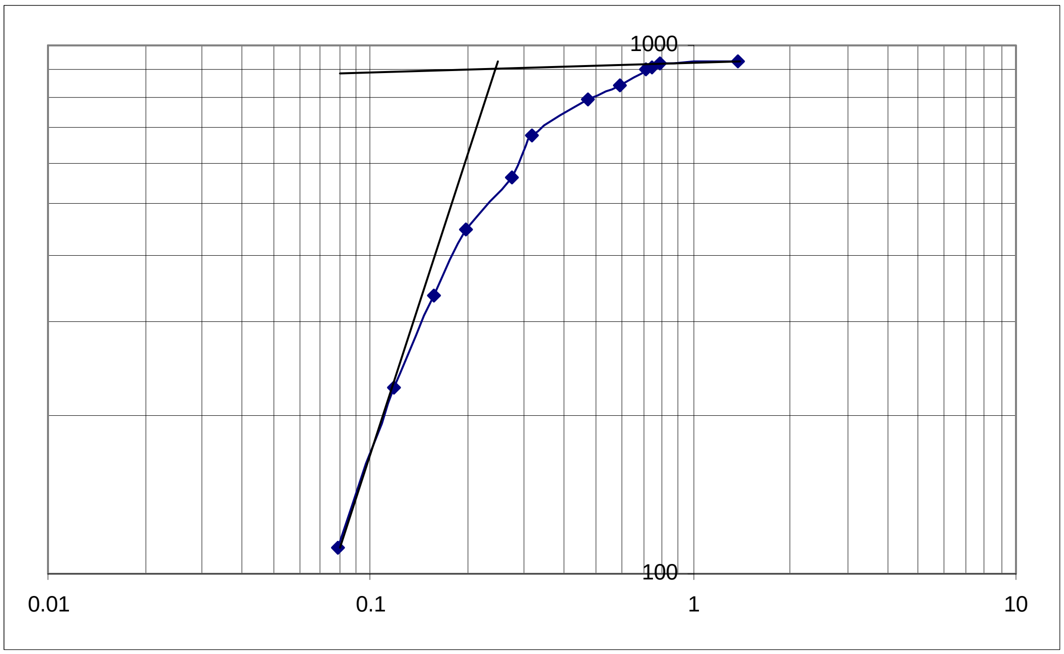

Santa Clara River Bridge Pier-13.	
Skin Friction Capacity	600 Tons
End Bearing Capacity	325 Tons

Figure A-21: Santa Clara River Bridge Pier-13.

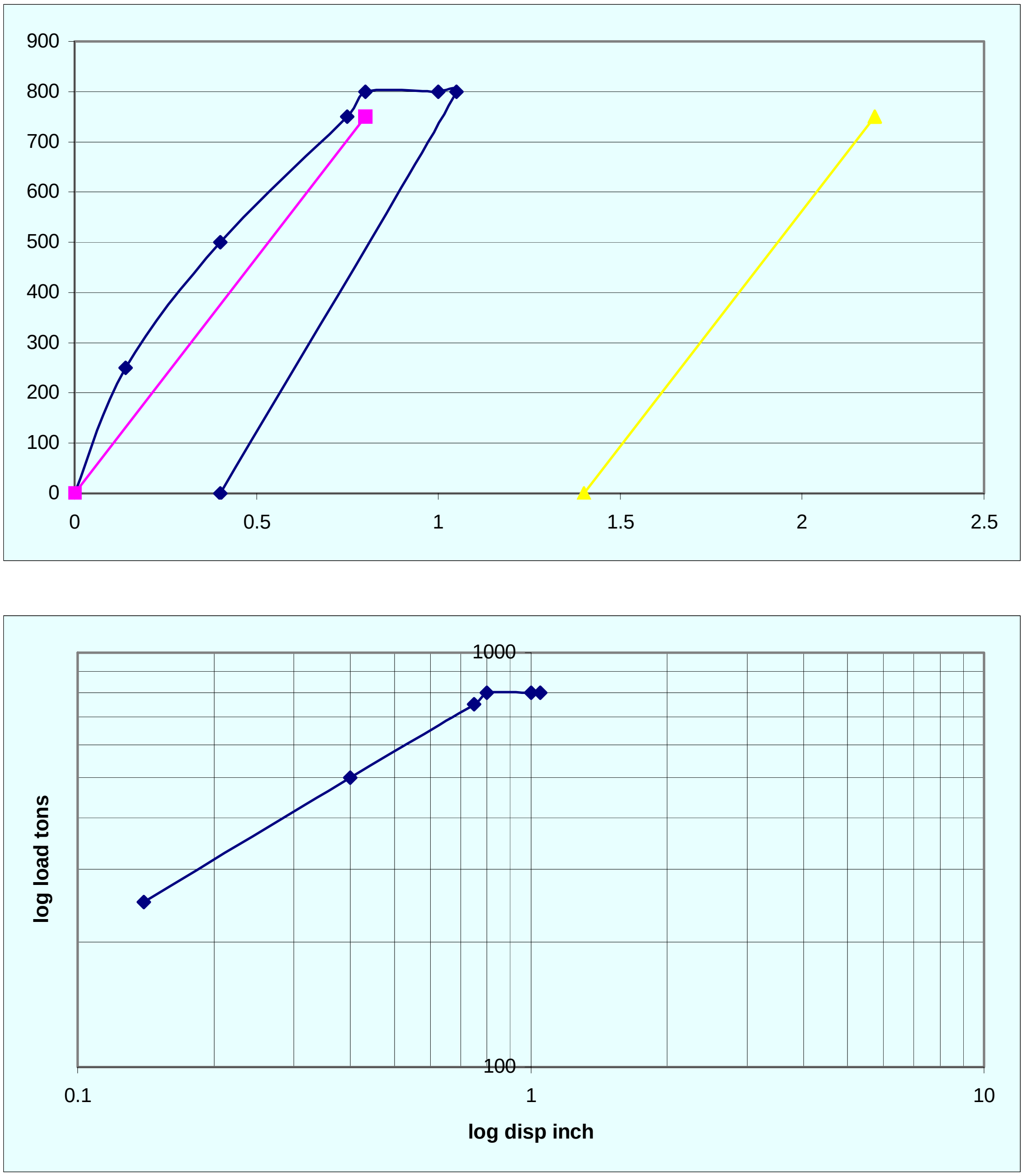

Santa Clara River Bridge Pier-13.	
Skin Friction Capacity	500 Tons
End Bearing Capacity	300 Tons

Figure A-22: Santa Clara River Bridge Pier-13.